PhD-FTSM-2020-16
The Faculty of Sciences, Technology and Medicine

DISSERTATION

Defence held on 05/06/2020 in Luxembourg

to obtain the degree of

DOCTEUR DE L'UNIVERSITÉ DU LUXEMBOURG

EN INFORMATIQUE

by

Stavros DOMOUCHTSIDIS
Born on 3 March 1992 in Lamia (Greece)

SYMBOL LEVEL PRECODING TECHNIQUES FOR HARDWARE AND POWER EFFICIENT WIRELESS TRANSCEIVERS

Dissertation defence committee

Dr Christos Tsinos, dissertation supervisor
Research Scientist, Université du Luxembourg

Dr Claude Oestges
Professor, Ecole Polytechnique de Louvain

Dr Symeon Chatzinotas, Chairman
Professor, Université du Luxembourg

Dr-Ing. Ralf Müller
Professor, Friedrich-Alexander Universität Erlangen

Dr Björn Ottersten, Vice Chairman
Professor, Université du Luxembourg

"*Thoroughly conscious ignorance is the prelude to every real advance in science.*"

-James Clerk Maxwell

ABSTRACT

Large-scale antennas are crucial for next generation wireless communication systems as they improve spectral efficiency, reliability and coverage compared to the traditional ones that are employing antenna arrays of few elements. However, the large number of antenna elements leads to a big increase in power consumption of conventional fully digital transceivers due to the one Radio Frequency (RF) chain / per antenna element requirement. The RF chains include a number of different components among which are the Digital-to-Analog Converters (DACs)/Analog-to-Digital Converters (ADCs) that their power consumption increases exponential with the resolution they support. Motivated by this, in this thesis, a number of different architectures are proposed with the view to reduce the power consumption and the hardware complexity of the transceiver. In order to optimize the transmission of data through them, corresponding symbol level precoding (SLP) techniques were developed for the proposed architectures. SLP is a technique that mitigates multi-user interference (MUI) by designing the transmitted signals using the Channel State Information and the information-bearing symbols. The cases of both frequency flat and frequency selective channels were considered.

First, three different power efficient transmitter designs for transmission over frequency flat channels and their respective SLP schemes are considered. The considered systems tackle the high hardware complexity and power consumption of existing SLP techniques by reducing or completely eliminating fully digital RF chains. The precoding design is formulated as a constrained least squares problem and efficient algorithmic solutions are developed via the Coordinate Descent method.

Next, the case of frequency selective channels is considered. To this end, Constant Envelope precoding in a Multiple Input Multiple Output Orthogonal Frequency Division Multiplexing system (CE MIMO-OFDM) is considered. In CE MIMO-OFDM the transmitted signals for each antenna are designed to have constant amplitude regardless of the channel realization and the information symbols that must be conveyed to the users. This facilitates the use of power-efficient components, such as phase shifters and non-linear power amplifiers. The precoding problem is firstly formulated as a least-squares problem with a unit-modulus constraint and solved using an algorithm based on the coordinate descent (CCD) optimization framework and then, after reformulating the problem into an unconstrained non-linear least squares problem, a more computationally efficient solution using the Gauss-Newton algorithm is presented.

Then, CE MIMO-OFDM is considered for a system with low resolution DACs. The precoding design problem is formulated as a mixed discrete- continuous least-squares optimization one which is NP-hard. An efficient low complexity solution is developed based also on the CCD optimization framework.

Finally, a precoding scheme is presented for OFDM transmission in MIMO systems based on one-bit DACs and ADCs at the transmitter's and the receiver's end, respectively, as a way to reduce the total power consumption. The objective of the precoding design is to mitigate the effects of one-bit quantization and the problem is formulated and then is split into two NP hard least squares

optimization problems. Algorithmic solutions are developed for the solution of the latter problems, based on the CCD framework.

Acknowledgements

As I submit my Doctoral Thesis I would like to express my gratitude to all the people who have helped me through this journey. The past few years at the Interdisciplinary Centre for Security, Reliability and Trust (SnT) at the University of Luxembourg have been a unique experience for me, that enabled me to significantly enhance my technical and research skills.

First of all, I would like to thank my supervisor Dr. Christos Tsinos for giving me the opportunity to pursue my Ph.D. at SnT and accepting me as a student. His guidance, his patience and his constant support were indispensable during my studies and made me a better researcher. I would also like to extend my sincere gratitude to the members of my CET committee Prof. Symeon Chatzinotas and Prof. Björn Ottersten for their invaluable support and advice throughout my studies. Additionally, I would like to thank Prof. Claude Oestges, with the Ecole Polytechnique de Louvain, and Prof. Ralf Müller, with the Friedrich-Alexander Universität Erlangen, for kindly accepting to participate in my dissertation committee.

I would also like to thank all my colleagues at SnT for the helpful discussions and for creating a great work environment.

I would like to take this opportunity to also thank my family and acknowledge the unwavering support which they have given me not only during my doctoral studies but also at every step until I got there.

Finally, I would like to gratefully acknowledge the generous funding of my Ph.D. by the Fonds National de la Recherche (FNR - Luxembourg National Research Fund) via the University of Luxembourg.

Contents

List of Figures

List of Tables

List of Abbreviations

DAC	**D**igital to **A**analog **C**onverter
ADC	**A**analog to **D**igital **C**onverter
RF	**R**adio **F**requency
SLP	**S**ymbol **L**evel **P**recoding
BLP	**B**lock **L**evel **P**recoding
MUI	**M**ulti **U**ser **I**nterference
CD	**C**oordinate **D**escent
CCD	**C**yclic **C**oordinate **D**escent
CSI	**C**hannel **S**tate **I**nformation
MIMO	**M**ultiple **I**nput **M**ultiple **O**utput
MISO	**M**ultiple **I**nput **S**ingle **O**utput
OFDM	**O**rthogonal **F**requency **D**ivision **M**ultiplexing
MRT	**M**aximum **R**ratio **T**ransmission
ZF	**Z**ero **F**orcing
CI	**C**onstructive **I**nterference
DI	**D**estructive **I**nterference
SNR	**S**signal to **N**oise **R**atio
PAR	**P**eak to **A**verage **R**atio
AS	**A**ntenna **S**election
CE	**C**onstant **E**nvelope
GN	**G**auss **N**ewton
ADMM	**A**lternating **D**irections **M**ethod of **M**ultipliers
SER	**S**ymbol **E**rror **R**ate
BER	**B**it **E**rror **R**ate
SVD	**S**ingular **V**alue **D**ecomposition
PA	**P**ower **A**mplifier

Dedicated to my family, my friends and the extraordinary educators in my life.

Preface

This Ph.D. Thesis has been carried out from March, 2017 to June, 2020 at the Interdisciplinary Centre for Security, Reliability and Trust (SnT), University of Luxembourg, Luxembourg, under the supervision of Dr. Christos Tsinos. The yearly evaluation of the Ph.D. Thesis was performed by the CET members Dr. Christos Tsinos, Prof. Symeon Chatzinotas and Prof. Björn Ottersten.

This Ph.D. Thesis has been fully supported by the Luxembourg National Research Fund under the Project ECLECTIC.

Publications

Below is a list of original publications that have been produced during the period of Ph.D. candidacy, which are referred to by J=Journal and C= Conference .

J1 S. Domouchtsidis, C. G. Tsinos, S. Chatzinotas and B. Ottersten, "Symbol-Level Precoding for Low Complexity Transmitter Architectures in Large-Scale Antenna Array Systems," in IEEE Transactions on Wireless Communications, vol. 18, no. 2, pp. 852-863, Feb. 2019.

J2 S. Domouchtsidis, C. G. Tsinos, S. Chatzinotas and B. Ottersten, "Constant Envelope MIMO-OFDM Precoding for Low Complexity Large-Scale Antenna Array Systems," in IEEE Transactions on Wireless Communications, accepted August 2020.

J3 S. Domouchtsidis, C. G. Tsinos, S. Chatzinotas and B. Ottersten, "Symbol Level Precoding For Transceiver Architectures Based on One-Bit DACs and ADCs," submitted in IEEE Transactions on Wireless Communications on May 2020, decisioned August 2020: major revisions.

C1 S. Domouchtsidis, C. Tsinos, S. Chatzinotas and B. Ottersten, "Antenna Selection Symbol-Level Precoding for Low Complexity Large-Scale Antenna Array Systems," 2018 IEEE 23rd International Workshop on Computer Aided Modeling and Design of Communication Links and Networks (CAMAD), Barcelona, 2018, pp. 1-6.

C2 S. Domouchtsidis, C. Tsinos, S. Chatzinotas and B. Ottersten, "Constant Envelope Massive MIMO-OFDM Precoding: an Improved Formulation and Solution," ICASSP 2020 - 2020 IEEE International Conference on Acoustics, Speech and Signal Processing (ICASSP), Barcelona, Spain, 2020, pp. 8956-8960.

J4 C. G. Tsinos, S. Domouchtsidis, S. Chatzinotas and B. Ottersten, "Symbol Level Precoding With Low Resolution DACs for Constant Envelope

OFDM MU-MIMO Systems," in IEEE Access, vol. 8, pp. 12856-12866, 2020.

J5 A. Li et al., "A Tutorial on Interference Exploitation via Symbol-Level Precoding: Overview, State-of-the-Art and Future Directions," in IEEE Communications Surveys & Tutorials, vol. 22, no. 2, pp. 796-839, Secondquarter 2020.

C3 S. Domouchtsidis, C. G. Tsinos, S. Chatzinotas and B. Ottersten, "Symbol Level Precoding for MIMO-OFDM systems with One-Bit quantization," under preparation.

Chapter 1

Introduction

Precoding is a signal processing technique that is generally used to enable multiple data transmissions simultaneously in multi-antenna wireless communication systems. Recently, the development of 5G increased the interest in large-scale antennas systems and by extension in precoding [1], as a means to improve spectral efficiency, reliability and coverage. Precoding techniques use the channel state information (CSI) and potentially the information symbols, to design the transmit signal in a way that directs each data stream to the intended user without inducing destructive inter-user interference.

The precoding technique known as Dirty paper coding (DPC) [2] is able to achieve theoretically the channel capacity, though its implementation is impractical in wireless communication systems. This is due to the assumption of an infinite source alphabet and the prohibitive computational complexity incurred by sequential encoding. On the other hand, in the literature low-complexity schemes which are linear combinations of the designed precoder with the information symbols and are known as linear precoding, have become increasingly popular [3]–[5]. Two of the most popular linear precoding methods in the literature are maximum ratio transmission (MRT) and Zero-forcing (ZF) precoding. The first of the two, MRT, has the lowest computational cost [3] but as it does not eliminate completely multi-user interference (MUI) it results to an error floor at the medium signal-to-noise ratio (SNR) region. ZF is able to suppress MUI even further than MRT by inverting the channel [4] but suffers from a noise amplification effect which can be mitigated by including a regularization factor as it was shown in [5].

For linear precoding methods, as in [3]–[5], the design of the precoder exploits only the CSI and all interference is considered catastrophic. However, in the literature there is also a category of non-linear precoding techniques, where both the CSI and the information symbols are used for the precoding design, such as Tomlinson-Harashima precoding (THP) [6]–[8], vector perturbation (VP) precoding [9]–[11] and convex vector precoding [12]. These schemes have challenging implementations in practical wireless communication systems, due to the complicated encoding and decoding process, which since it is symbol-by-symbol, results in high computational costs.

However, the recently proposed concept of Symbol Level Precoding (SLP), which is closely related to constructive interference (CI) precoding has been shown in survey [13] that can challenge in complexity and performance linear precoders in both unicast and multicast scenarios. Additionally, in [14] proof-of concept test-beds were presented for SLP schemes.

1.1 Preliminaries in Linear Precoding

Before moving on to SLP techniques, it would be instructive to describe how linear precoding works in the downlink transmission of a multi-antenna system. The example system that is described here uses the traditional ZF precoding which because of its computational efficiency and its optimality in minimizing MUI, is used many times in this thesis as a benchmark.

The downlink of a multi-user multiple-input single-output (MU-MISO) system is considered, where the base station (BS) is equipped with N_T transmit antennas and communicates with a total number of K single-antenna users in the same time-frequency resource. The users are located in different locations and can not cooperate. In order to manage the multi-user interference, the BS needs to apply signal processing techniques, before the transmission, on the information symbols by exploiting the CSI. This procedure explains the origins of the term precoding. The precoded signal, which is denoted by a vector $\mathbf{x} \in \mathbb{C}^{N_T \times 1}$ that is transmitted by the BS antennas is given by

$$\mathbf{x} = \sum_{k=1}^{K} \mathbf{w}_k s_k = \mathbf{W}\mathbf{s}, \tag{1.1}$$

where $\mathbf{w}_k \in \mathbb{C}^{N_T} \times 1$ is the precoding vector for the k-th user's information symbol , which is drawn from a specific signal constellation. $\mathbf{W} = [\mathbf{w}_1, \mathbf{w}_2, \ldots, \mathbf{w}_k] \in \mathbb{C}^{N_T} \times K$ is the concatenated precoding matrix and $s = [s_1, s_2, \ldots, s_K]^T \in \mathbb{C}^{K \times 1}$ is the information symbol vector. As a result, the received signal at the user k user is given by

$$y_k = \mathbf{h}_k^{\mathrm{T}}\mathbf{x} + z_k = \mathbf{h}_k^{\mathrm{T}}\mathbf{W}\mathbf{s} + z_k, \tag{1.2}$$

where y_k is the received signal for user k , $\mathbf{h}_k \in \mathbb{C}^{N_T} \times 1$ is the channel vector between the BS and the k user , and z_k is the additive Gaussian noise with zero mean and variance σ_z^2 . Equation (1.2) can also be written in a compact matrix form as

$$\mathbf{y} = \mathbf{H}\mathbf{W}\mathbf{s} + \mathbf{z}, \tag{1.3}$$

where $\mathbf{y} \in \mathbb{C}^{K \times 1}$ is the received signal vector, $\mathbf{H} \in \mathbb{C}^{K \times N_T}$ is the concatenated channel matrix, and $\mathbf{z} \in \mathbb{C}^{K \times 1}$is the additive noise vector.

Linear precoding techniques design the precoder matrix $\mathbf{W}$ in order to achieve certain targets. Here, the case of the ZF precoder is presented as an illustrative example. More specifically, the precoding matrix for ZF is given by [5]

$$\mathbf{W}_{\mathrm{ZF}} = \mathbf{H}^{\mathrm{H}}\left(\mathbf{H}\mathbf{H}^{\mathrm{H}}\right)^{-1}, \tag{1.4}$$

By substituting (1.4) into (1.3), the received signal for ZF precoding is obtained and is given by

$$\mathbf{y}_{\mathrm{ZF}} = \mathbf{H}\mathbf{H}^{\mathrm{H}}\left(\mathbf{H}\mathbf{H}^{\mathrm{H}}\right)^{-1}\mathbf{s} + \mathbf{z} = \mathbf{s} + \mathbf{z}. \tag{1.5}$$

The name of the scheme can be justified by observing that in (1.5) ZF precoding forces the MUI to be zero for all users.

1.2 Symbol Level Precoding Survey

Interference is generally considered as a factor that degrades the performance of wireless communication systems. In a multi-user system, transmit signals that are intended for different users are superimposed at the wireless channel resulting in MUI at the receivers' side. With the assumption that the CSI is available at the BS, the MUI can be predicted before the transmission. Information theoretical analysis in [2] shows that when CSI is available at the transmitter, known interference will not affect the capacity of the broadcast channel. More specifically, according to the DPC method it is optimal to code along interference, instead of attempting to cancel it. However, most linear precoding schemes still have the objective to limit MUI, [3]–[5], [15], [16]. These schemes operate on a block level as the precoder is designed based on the CSI. This means that only the power of the MUI can be controlled, which leads to the statistical view that the effect of interference is similar to noise. However, if interference is observed from an instantaneous point of view, then both the power and the direction of the interfering signals can be controlled on symbol level. Recent results in the literature have shown [17], [18] that with CI precoding MUI can be turned into an additional source of power that increases the power of the received signals and improves the performance of the multi-user system. Therefore, CI is defined as the interference that pushes away the received signals from their corresponding decision boundaries of the employed constellation, which leads to the increase of useful signal power.

It should be noted, that CI can only be exploited when the precoding operation is at symbol-level rather than at block-level. Therefore the category of SLP includes precoding schemes that exploit CI but also precoding schemes for hardware efficient architectures, as the ones that are presented in this thesis.

At first, SLP techniques for CI, focused on adapting linear precoding methods such as ZF and RZF for CI exploitation. In [19], [20], MUI is categorized as either constructive or destructive and selective precoding is proposed where the CI is retained while the destructive interference (DI) is cancelled with ZF. In [21], the DI rather than being eliminated it is instead aligned with the desired information symbols such that DI becomes CI. Additionally, there are works in the literature that achieved to adapt non-linear precoding methods to exploit CI. In [7] a complex scaling to the first user is introduced to improve the alignment of the interfering signals with the symbols of interest, and then the complex scaling factor was optimized to minimize the power of the modified transmit signals. Then, in [8] the complex scaling is expanded for a number of users, rather than just for the first as in [7].

As computational power has become more abundant recently, precoding techniques for CI exploitation have been combined with optimization to improve system performance [22]–[25]. In [22], [23], constructive regions are defined as the regions within which all the interference is constructive for PSK constellations. This new concept reveals that it is no longer necessary for the interfering

signals to be strictly aligned to the information symbols, which improves further the performance. This advanced CI metric is called non-strict phase rotation in [26], and is adopted in the precoding designs of [26]–[33]. In the majority of works for CI precoding above, [7], [8], [19]–[21], and [22]–[25], [34], [35], the precoding design was adapted only for PSK constellations. Nevertheless, CI exploitation was extended to multi-level modulations such as QAM in [36], [37] and [29]–[33], [38], where the symbol-scaling concept is introduced.

Additionally, directional modulation [39]–[41], a concept that was studied in the past, has recently gathered interest as a means to reduce hardware complexity. In directional modulation the phase and amplitude of the transmit signals are designed so that multiple interference-free symbols can be conveyed to the receivers and are applied at each antenna directly by employing analog RF components.

It becomes clear that SLP schemes have clear advantages over conventional precoding as they manage to achieve significant performance gains in terms of error rate performance and transmit power savings. By exploiting the CSI as well as the information symbols, interference can become beneficial and contribute to the increase in the useful signal power. Additionally, it exhibits a number of other significant advantages over block level precoding schemes.

First, in block level precoding the constraints are met only averaged over a transmission block. As a result, the constraints may be violated during transmission. In contrast, SLP does not have this problem and the constraint is guaranteed to be satisfied for each information symbol combination during transmission, because it operates on a symbol level and accordingly the constraints are enforced on a symbol level. This is a very crucial characteristic for the precoding schemes that are presented in this thesis, as their constrained by the hardware components that are used. Therefore, the precoding design constraints must be strictly satisfied for all transmit signals, as otherwise it will be impossible for the system to transmit a signal that violates them.

Furthermore, SLP also reduces the complexity of the receiver. When traditional block level optimization based precoding is used, receivers have to estimate and compensate the phase-rotation that is inserted by the channel, prior to decoding the symbols, [42]. In SLP all received symbols are located in the constructive area, and therefore no phase-compensation operation is necessary. This eliminates the need for CSI estimation at the receivers, as only a simple decision stage is required. This is a significant advantage in the case of downlink transmission where the receivers are mobile devices with constrained computational capabilities.

Additionally, in [23], [29], [30] was shown that SLP can support more simultaneous data streams than linear precoding. In linear precoding, the number of supported data streams is limited by the number of transmit antennas at the BS. In SLP, on the contrary, it is shown in [29], [30] that a larger number of data streams than transmit antennas can be supported with an improved BER performance. This is an observation that is verified in one of the proposed SLP schemes in this thesis.

In order to have a full picture of the SLP schemes, in addition to the advantages mentioned above the disadvantages should also be discussed. The most

major downside of SLP is the increased computational complexity. In contrast to block level precoding where the precoder is updated when the channel changes, in SLP the precoder is updated on a symbol level and thus increasing the computational costs. Furthermore, most SLP techniques in the literature, require solving an optimization problem to obtain the precoder, which can be more demanding than block level precoding designs which usually admit to closed form solutions.

Another limitation for most SLP schemes is that they are designed for uncoded communication systems and their gains can only be guaranteed for such systems. In communication systems where channel coding is employed, [39] SLP schemes with existing channel coding schemes have superior performance to conventional channel coded precoding schemes. However, the optimality of the performance cannot be guaranteed as a joint design of precoding and channel coding could lead to further performance gains. The optimal soft detector design requires the a priori probabilities of the input symbols that produce a soft output which indicates the reliability of the decision that should be taken into account, and which have not been fully addressed in the literature.

1.3 Applications of SLP

In this section, several applications that show how SLP can be adapted to different wireless communication systems are presented and the gains of exploiting interference in these scenarios is shown.

1.3.1 Cognitive Radio (CR)

CR which allows dynamic spectrum access, enables increased radio resource utilization and spectral efficiency, [43]–[46], when compared to fixed spectrum allocation strategies. Users are separated into two priorities for accessing the spectrum, primary users (PUs) and secondary users (SUs) in underlay CR networks. PUs have the highest priority for the spectrum resources and are not aware of the existence of the SUs in the network, while SUs can only access the network under the premise that their interference to PUs is below a certain threshold [46]. Subsequently, a fundamental challenge for CR networks is to enable the opportunistic spectrum access for SUs while guaranteeing PUs' quality-of-service (QoS) requirements, when the CSI of both PUs and SUs is available at the BS. The trade-off between throughput maximization and interference minimization for SUs is studied in [47] from an information-theoretic perspective, where the optimal transmission scheme that achieves the capacity of the secondary transmission as well as some sub-optimal algorithms is presented. In addition, precoding designs for CR networks are studied in [48]–[51] for both perfect CSI and imperfect CSI.

1.3.2 Simultaneous Wireless Information and Power Transfer (SWIPT)

Energy harvesting (EH) and wireless power transfer for wireless communication networks have become a new trend that can prolong the battery life of user equipments (UEs) [52], [53]. In wireless communications, the emitted RF signals carry not only the information but also energy, and SWIPT techniques allow for the simultaneous transmission of both information symbols and energy to the UEs [54], [55]. Precoding designs for MIMO SWIPT systems were considered in [56]–[59], and the joint optimization of the precoding vector and the receive power splitting ratio was investigated.

1.3.3 Physical-Layer (PHY) Security

Wireless communication systems are naturally susceptible and vulnerable to security threats due to their broadcast nature. While security issues are tackled at the network layer by employing cryptographic techniques additional measures can be taken at the PHY. PHY security techniques, which add artificially structured redundancy in the transmit signals in the physical layer so that the users can successfully decode the information while the eavesdroppers (Eves) cannot, have drawn increasing research attention in the information-theoretic society in recent years [60]–[63]. By employing PHY transmission schemes that are specifically designed for security using multiple antennas, PHY security techniques can improve the information security and act as an additional security layer on top of the traditional cryptographic approaches. One possible approach for realizing PHY security is through downlink precoding, which is able to direct the signals carrying confidential information to the legitimate users while minimizing the power leakage to the Eves, as studied in [64]–[66], where the secrecy rate maximization is discussed when the BS has either perfect or imperfect CSI of the Eves.

1.3.4 Spatio-Temporal CI: Faster-Than-Nyquist Signalling

Faster-than-Nyquist (FTN) signalling [67]–[69] is a technique that allows a significant improvement of the spectral efficiency of wireless communication systems. The key idea of FTN signalling is a reduction of the time spacing between two adjacent pulses (the symbol period) below the one satisfying the Nyquist condition. In other words, in FTN signalling the data rate is increased by accelerating the transmitted pulses in the temporal dimension (time packing), thus introducing controlled inter-symbol interference (ISI) which needs to be handled. The main problem of FTN signalling is the need to cope with the introduced ISI, which in turn results in complex receivers relying on trellis decoders as well as adhoc equalization schemes, whose computational costs are often prohibitive in practical applications. In [70]–[72], a novel transmission technique has been proposed, which merges the aggressive frequency reuse relying on precoding, in particular SLP, with FTN signalling. In a MU-MISO system, these works extend the concept of SLP at the transmitter side in order to tackle not only the interference in the spatial dimension (the multi-user

interference), but also the interference in the temporal dimension (the ISI intentionally introduced through FTN signalling). Such an extension allows FTN signaling in a MU-MISO framework and, at the same time, solves the problem of complex FTN receivers, as the ISI is completely handled at the transmitter. This transmission technique is referred to as spatio-temporal CI, as it enhances the CI both in the temporal and in the spatial dimensions, thus gleaning benefits from both the domains.

1.3.5 Hardware and Power Efficient Wireless Transceivers

Most of the SLP techniques in the literature, that were described previously, are designed with the objective to turn destructive interference into constructive by pushing the received symbols by the receivers further into the decision regions. However, these techniques usually require transmitter architectures where the signal processing is entirely implemented in the baseband domain and therefore a dedicated digital to analog converter (DAC) is required for each antenna. Furthermore, after the digital to analog conversion they require the use of highly linear RF components such as power amplifiers, which tend to have a low power-efficiency.

The problem with these power-inefficient components becomes more noticeable in large-scale antenna arrays where tens or hundreds of these components have to be used. For this reason, the feasibility of these systems depends on the use of more power efficient components and therefore the development of precoding techniques that produce transmit signals that allow the use of such power-efficient components.

One approach in the literature that aims at reducing hardware complexity and power consumption is the case of Constant Envelope (CE) precoding, where SLP techniques are designing the transmitted signals from the antennas to be of constant modulus regardless of the CSI and the information symbols that are conveyed to the users [73]–[77]. Therefore, the transmitted signals present low Peak-to-Average-Ratio (PAR) and they enable the use of power efficient nonlinear amplifiers at the transmitter's side. This characteristic is highly desirable in large-scale antenna systems since they do not need the use of highly linear power amplifiers that are necessary for the implementation of typical precoding techniques. These amplifiers may increase significantly the cost of the transmitter even if the latter is based on an antenna array of few tenths of elements [78].

In literature so far, different approaches have appeared with the view to reduce the transceivers' complexity/power consumption. Most of them are developed for the case of BLP and can be divided into two major categories, a) Hybrid analog-digital transceivers [79]–[94] that aim at the reduction of the number of RF chains via a two stage beamformer that consists of a low dimensional digital precoder applied in the BaseBand followed by an analog beamformer applied in the RF domain and b) transceivers based on low resolution DACs/ADCs since the complexity and the power consumption of the latter increases exponentially with their resolution [95]. Regarding the second category,

initial works in literature [96]–[104] proposed low complexity/power consumption solutions by developing quantized versions of well-known BLP approaches (Zero Forcing, Minimum Mean Square Error precoding), i.e. application of linear precoding followed by quantization. Despite the simplicity of such an approach, the performance is far from satisfying in several cases. To that end, SLP based approaches have been recently developed for systems with low resolution DACs [105]–[109]. It was shown that for the considered cases, these nonlinear precoders outperform the quantized versions of the BLPs. The latter result along with the power efficiency of the solutions based on constant envelope signals, as discussed above, motivate us in this work to develop Constant Envelope Symbol Level Precoding (CESLP) solutions for Multi-User Multiple Input-Multiple Output (MU-MIMO) systems with low resolution DACs at the transmitter's side. The proposed approach is tailored for multi-carrier systems functioning under the well-known Orthogonal Frequency Division Multiplexing (OFDM) technique.

In other relevant literature the efforts focused on reducing the power consumption of the multi-antenna receiver by employing low-resolution ADCs. There is a special interest in one-bit ADCs as they are the least power consuming component with the ability to convert the received analog signals into digital [110]. Additionally, since one-bit ADCs should only distinguish the sign of the signal they eliminate the need for complicated automatic gain control and can further reduce the complexity of the receiver's analog front end. Several contributions studied the uplink where multiple single antenna users employing high resolution DACs transmitted to a base station with a large number of receive antennas and one-bit ADCs. Research showed that in the case of frequency-flat channels linear detectors combined with simple linear precoding could achieve high sum rates [111]–[116] when the number of antennas was large enough. Furthermore, the authors in [117] arrived to similar results for the case of OFDM transmission over a frequency-selective channel.

On the contrary, the reduction on the number of RF chains has impact on the number of the supported streams that can be transmitted simultaneously when a BLP technique is employed (i.e., the number of the supported streams can be equal to the number of the available RF chains, at most) [118]-[121] Thus, for systems based on a few numbers of RF chains, multiuser communications, i.e. Space Division Multiple Access (SDMA), multi-carrier systems are poorly supported. Therefore, the reduction on the hardware complexity/power consumption comes at the cost of a transceiver design of limited capabilities compared to its fully digital counterpart.

1.4 Contributions of the Thesis

In this thesis, SLP schemes are considered as a means to mitigate the negative effects in the performance of hardware and power efficient transceiver architectures.

In Chapter 2 three power and hardware efficient transmitter architectures with their respective SLP schemes for frequency flat channels, are presented. The objective of the precoding design, in the proposed systems, is to minimize

the average Euclidean distance between the received signal and the desired information symbols while considering the constraints which are dependent on the employed architecture.

First, an antenna selection (AS) based SLP technique is proposed which aims at the reduction of the transmitter's complexity/power consumption via employing an architecture with much less RF chains than antennas followed by a network of switches for selecting the antenna at which each RF chain is connected. The derived optimization problem is a hard combinatorial problem which requires an exhaustive search-based solution in order to be solved. Instead, here we propose a low complexity efficient method by reformulating the problem, and replacing the $L0$-norm constraint with its convex envelope the $L1$-norm [122].

Then an architecture that uses analog only components and eliminates completely the need for DACs is proposed. In this architecture a dedicated digitally controlled analog phase shifter drives each antenna thus imposing a constant modulus constraint. The optimization problem is a non-convex one and similar problems which are refereed to as Constant Envelope precoding have been tackled in the literature [73]–[75], [123], [124] with highly complex methods.

Finally, a novel analog only architecture is presented, where each antenna is driven by two parallel connected phase shifters, in order to modify the stringent nonconvex constant modulus constraint that the single phase shifter imposes. The derived design problem is subject to a convex set of constraints and therefore it can be solved more efficiently.

We will refer to the last two architectures as RF domain SLP, since the signal processing in both cases happens in the RF domain.

Next in Chapter 3 the problem of CE precoding for MIMO-OFDM transmission over a frequency selective channel is considered. CE precoding leads to transmit signals with low peak-to-average power ratio (PAPR), a characteristic highly desirable in OFDM transmission which traditionally suffers from high PAPR and thus requires the use of highly linear amplifiers which are characterised by low power efficiency. In Chapter 3 a novel way to tackle the problem of CE precoding for MIMO-OFDM transmission over a frequency selective channel is presented.

First, a novel formulation of the MIMO-OFDM system is proposed, by creating an equivalent channel matrix which gives us the discrete Fourier transform of the noiseless received signal when multiplied with the time domain transmit signal. The advantage of the proposed formulation is that it eliminates the need for the computation of the convolution of the multipath channel with the transmit signal during the search of the solution, as required in current state of the art solutions.

Then, a mathematical formulation of the MIMO-OFDM system that enables the development of efficient algorithmic solutions is proposed. The aim of the formulation is to directly design in a nonlinear manner the time domain signal of the OFDM system such that to be of constant amplitude (CE). The improved efficiency is the result of eliminating the need for the computation of the convolution of the multipath channel with the transmit signal during the search of the solution, as required in current state of the art solutions.

The use of power efficient transmitter architectures for CE MIMO-OFDM precoding is presented. They utilize analog phase shifters and nonlinear power amplifiers and an efficient algorithmic framework to solve the precoding problem when such architectures are used is developed. Additionally, the power consumption model of these architectures for the case where CE MIMO-OFDM precoding is used is derived.

The use of a post-processing scalar factor is proposed, which changes on a per OFDM block basis, and partially compensates for the lack of amplitude control in the transmitter because of CE precoding. This scalar factor facilitates the exploitation of the array gain provided by the large-scale antenna array by scaling the signal at the receivers accordingly. Its proposed blind estimation exploits the block structure of OFDM transmission and does not introduce communication overhead or delay in the demodulation process, as would happen in single carrier systems.

Then the formulation of the CE precoding problem as a least-squares problem with a unit modulus constraint is presented and the problem is solved using an algorithm based on Coordinate Descent (CD).

Finally, a second more efficient solution is proposed using the Gauss-Newton (GN) algorithm by reformulating the problem into an unconstrained nonlinear least-squares problem.

In the following Chapter 4, CE predocing for MIMO-OFDM is extended for systems that in addition to nonlinear amplifies employ low resolution DACs as a means to reduce the power consumption of the multi-antenna transmitter. Analytically, the contributions of are the following.

A CE SLP precoding technique is developed for a MU-MIMO system constituted by a LSAA-based BS with low resolution DACs and single antenna users that are capable of linearly processing the received signal.

A novel formulation for the problem is developed for frequency selective channels, for systems that are employing the OFDM technique to deal with the frequency selectivity and the transmitter employs low resolution DACs.

The novel joint precoder-receive processing design is formulated as a constrained mixed-discrete least squares optimization problem. The formulated optimization problem is NP-hard. To that end, an efficient solution is developed via the use of the Cyclic Coordinate Descend (CCD) technique. The proposed solution is independent to the desired constellation and to the resolution of the DACs while being computationally efficient.

The power consumption of the architectures based on the low resolution DACs is modelled and used to examine the energy efficiency of the proposed techniques while comparing them to systems that employ infinite resolution DACs.

The performance of the proposed approaches is examined via simulations and compared to the state of the art solutions. The proposed solution achieves better performance compared to the one in [125] which considers also the CE SLP problem design for an OFDM based system based on low resolution DACs. The approach in [125] extends the results in [105] to a system that employs the OFDM technique to combat frequency selectivity. Furthermore, it is based on

a different problem formulation and solution to the one that is developed in the present paper.

It is also noteworthy to point out that, as it is also shown from the simulation results, the proposed approach achieves close performance to the one of a system with DACs of infinite resolution even though it is based on ones with resolution of few bits.

In Chapter 5 the case of a point-to-point MIMO system which employs OFDM transmission to mitigate the effects of the channel's frequency selectivity is studied. The considered system, is equipped with both one-bit DACs at the transmitter and one-bit ADCs at the receiver. This is a departure from the systems that have been studied so far in the literature and in the previous chapter, were one-bit DACs were considered in systems with full resolution ADCs or one-bit ADCs were considered for systems with full resolution DACs. For the first time a precoder is designed that so that it takes into account the coarse quantization both at the transmitter as well as the receiver. This kind of transceiver architecture has multiple advantages from a power consumption perspective. It achieves significant power savings which can be attributed to utilizing one-bit DACs and ADCs as well as power efficient non-linear PAs. The contributions of presented in Chapter 5 are the following.

Two novel MIMO architectures for OFDM transmission with one-bit DACs and one-bit ADCs. The first proposed system is fully digital while the second is equipped with a network of analog phase shifters at the receiver.

The study of the power consumption of such one-bit DAC/ADC transceiver architectures with the inclusion of the non-linear PA model.

An SLP scheme for OFDM transmission in a large MIMO system with one-bits DACs and ADCs. The novel precoding design is formulated as a constrained least-squares problem and is then split into two similar mixed-discrete least-squares problems that are NP hard. Then for the solution of the latter problems, an efficient algorithm that is based on Cyclic Coordinate Descent (CCD) is proposed.

A novel design for the analog post-coding matrix which is applied to the received signal by the network of analog phase shifters. The problem of the analog post-coder is decoupled from the design of the precoding design as its update is only dependent on the CSI and is formulated as a norm maximization problem with a unit-modulus constraint. A novel algorithmic solution is presented by applying the Alternating Direction Method of Multipliers (ADMM).

Numerical simulations show that the performance of the proposed schemes overcomes the shortcomings of coarse quantization both at the transmitter and at the receiver. Furthermore the proposed solutions achieve performance close to precoding schemes that based on full resolution DACs and ADCs, and even outperform them when the non-linearities of the PAs are taken into account.

Finally, in Chapter 6 the conclusions of this thesis are discussed and related open research topics for future works are presented.

Chapter 2

SLP For Frequency-Flat Low Complexity MIMO Systems

In this chapter, SLP schemes for transmission over frequency-flat channels are presented for three power and hardware efficient transmitter architectures. The objective of the precoding design, in the proposed systems, is to minimize the average Euclidean distance between the received signal and the desired information symbols while considering the constraints which are dependent on the employed architecture.

The chapter is organized in the following sections. First, in Section 2.1, the three proposed system models are described and the respective problems are formulated. In Section 2.2, the power consumption of the proposed systems is evaluated and compared to that of a fully digital architecture. In Section 2.3 the solutions to the previously formulated problems are presented. In Section 2.4, numerical results are presented in order to evaluate the performance of the proposed architectures and algorithms. The results underline the improved efficiency of the proposed systems, over the fully digital approaches and the scenarios in which each architecture is advantageous. Finally, Section 2.5 concludes this chapter.

2.1 System model

Let us consider a communication system with a Base Station (BS) equipped with M_t transmit antennas communicating with K User Terminals (UT), each of which has a single receive antenna. It is assumed that the transmitted signal is a single carrier signal and that the received signals undergo flat fading, as a result of the propagation through the wireless channel. Under these assumptions the received signal at the k-th UT, in the symbol slot n, is

$$y_k[n] = \sum_{m=1}^{M_t} h_{k,m} x_m[n] + z_k[n], \text{ for } k = 1, ..., K, \tag{2.1}$$

where $h_{k,m}$ is the channel coefficient between the m-th BS antenna and the k-th UT, $x_m[n]$ is the complex transmitted signal by the m-th antenna of the BS and $z_k[n]$ is the complex random variable that models the additive white Gaussian noise (AWGN) at the k-th UT and follows a Circularly Symmetric Complex Gaussian distribution, $z_k[n] \sim \mathcal{CN}(0, \sigma_z^2)$.

The received signals can be rewritten in a more compact form, by concatenating the transmitted complex symbols from each transmit antenna to a vector $\mathbf{x}[n] = [x_1[n], x_2[n], ..., x_{M_t}[n]]^T$ and likewise the received complex symbols at each UT to another vector $\mathbf{y}[n] = [y_1[n], y_2[n], ..., y_K[n]]^T$, as

$$\mathbf{y}[n] = \mathbf{H}\mathbf{x}[n] + \mathbf{z}[n], \tag{2.2}$$

where $\mathbf{H}$ is the $K \times M_t$ channel matrix, with each entry $h_{k,m}$ being the complex path gain between the m-th transmit antenna and the k-th UT, and $\mathbf{z}[n] = [z_1[n], z_2[n], ..., z_K[n]]^T$ is a vector formed by the concatenation of the noise components from all the UTs. Additionally, from now on in order to simplify the notation, the time index n is omitted.

As it was mentioned in the introduction, the transmitted signal vector $\mathbf{x}$ in SLP is designed by taking into account both the CSI and the data symbols that will be induced to the UTs. In the scope of this work it is assumed that the transmitter has perfect knowledge of the CSI and that it remains constant for a block of symbols.

The objective of SLP is to design the transmitted signal so that the received signal power is maximized at the intended UT while at the same time the MUI is minimized. A suitable function to quantify this objective is the sum of squared residuals

$$\mathcal{F}(\mathbf{x}) = ||\mathbf{H}\mathbf{x} - \sqrt{\gamma}\mathbf{s}||_2^2, \tag{2.3}$$

where $||\cdot||_2$ denotes the Euclidean norm, $\mathbf{s} = [s_1, s_2, ..., s_K]^T$ is a vector of information symbols and γ is the SNR of the induced symbols $\mathbf{s}$, which are drawn from a signal constellation. The goal of the communication system is to convey each complex symbol s_k to the k-th UT and it can be achieved by designing $\mathbf{x}$ so that it minimizes (2.3). The minimizer of (2.3), known as the Zero Force (ZF) precoding vector, given by [5]

$$\mathbf{x}^* = \sqrt{\gamma}\mathbf{H}^H \left(\mathbf{H}\mathbf{H}^H\right)^{-1} \mathbf{s}, \tag{2.4}$$

is the optimal solution but hard to implement in large-scale antenna systems since it requires a dedicated digital RF chain for each transmit antenna. The function in (2.3) is going to be the objective function for the problems that will be formulated and investigated here with the purpose of reducing the number of RF chains and thus reducing the hardware complexity of the transmitter while also improving its power efficiency.

2.1.1 Antenna Selection Symbol Level Precoding

Consider a system where the transmitter is equipped with a large number of antennas ($M_t \gg K$) and only a subset of N_t antennas can be activated at each transmission. This means that the number of RF chains can be reduced so that it is equal to the number of active, N_t, rather than total M_t antennas. At this point, it should be noted that a digital RF chain in the scope of this work includes two DACs, one for the I and one for the Q component, a mixer, a filter and a common local oscillator which drives all RF chains. Additionally, the

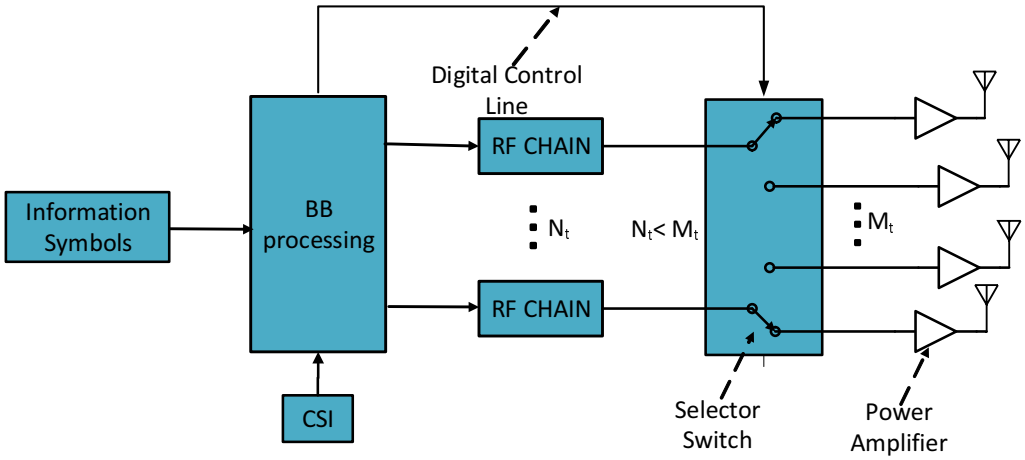

FIGURE 2.1: Block diagram of the Antenna Selection transmitter.

transmitter is equipped with a network of switches that connect the available RF chains with the antennas that are selected for transmission. The architecture of the transmitter is shown in Fig. 2.1. The motivation for this architecture is to exploit the spatial redundancy caused by the large number of available antennas at the BS in order to improve the power efficiency of the system, as fewer active antennas consume less power.

The problem now, is to find the subset of N_t antennas that will minimize $\mathcal{F}$. This can be expressed as a least squares problem by adding a constraint that limits the number of nonzero elements of $\mathbf{x}$ and can be written as

$$(\mathcal{P}_1): \min_{\mathbf{x}} \ ||\mathbf{H}\mathbf{x} - \sqrt{\gamma}\mathbf{s}||_2^2 \tag{2.5}$$

$$s.t. \quad ||\mathbf{x}||_0 = N_t, \tag{2.6}$$

where $||\cdot||_0$ denotes the $L0$-norm. The combinatorial problem $(\mathcal{P}_1)$ is NP hard [122] and later an efficient method will be presented for its solution based on the recent results in sparse estimation/ compressed sensing literature [126].

2.1.2 RF Domain SLP With One Phase Shifter Per Antenna

In this section an analog only transmitter architecture will be considered, shown in Fig. 2.2 which eliminates the need for baseband processing and can be implemented by simple phase shifter modules which drive the transmitter's antennas. The purpose of the system is to communicate K independent data streams to K UTs from a large-scale array antenna of M_t elements, by minimizing the MUI. The processing is done in the RF domain, by mapping the output of a single variable gain amplifier (VGA) onto the antennas using the phase shifter at each antenna. If α is the amplitude of the output signal of the VGA and θ_m is the angle shift that the m-th phase shifter inserts, then the transmitted signal by

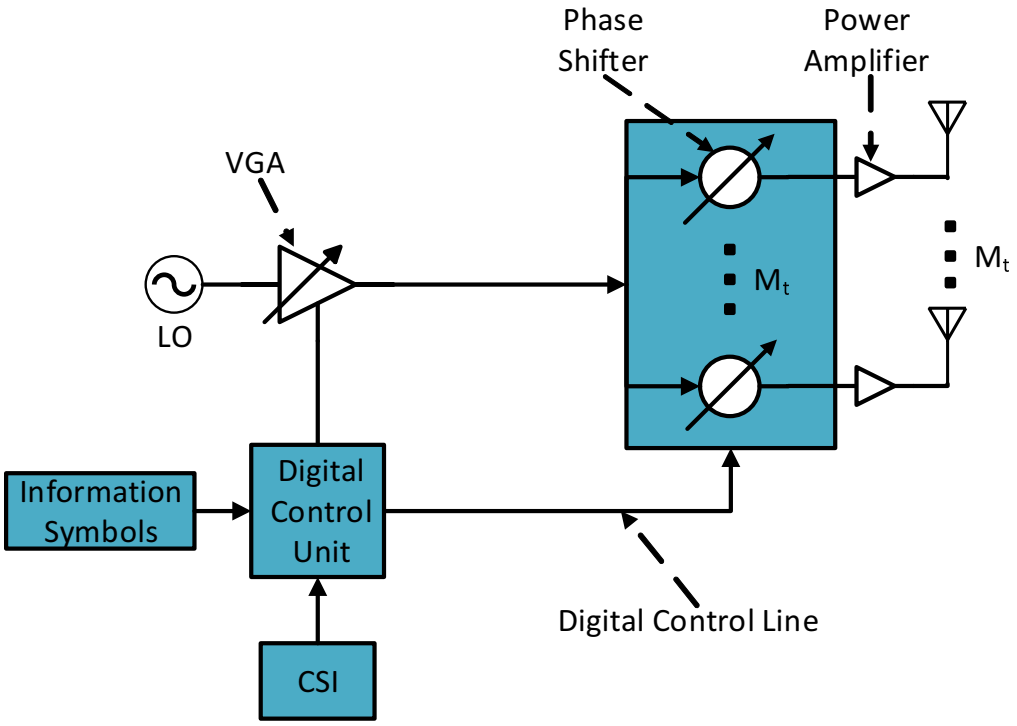

FIGURE 2.2: Block diagram of the RF domain SLP with 1-PS per antenna transmitter.

the m-th antenna can be written as

$$x_m = \alpha e^{j\theta_m}, \ m = 1, 2, ..., M_t. \tag{2.7}$$

The objective of SLP here is to design the amplitude α of the VGA that drives the phase shifters and the angles $\boldsymbol{\theta} = [\theta_1, \theta_2, ..., \theta_{M_t}]$ of the phase shifters, in a way that minimizes the euclidean distance between the received signal and the desired information symbols $\mathbf{s}$ at each UT. In other words, the problem at hand is to determine the vector $\mathbf{x} = \alpha e^{j\boldsymbol{\theta}}$ that minimizes $\mathcal{F}$ and can be written as an optimization problem of the form

$$(\mathcal{P}_2) : \min_{\mathbf{v},\alpha} \ ||\mathbf{H}\alpha\mathbf{v} - \sqrt{\gamma}\mathbf{s}||_2^2 \tag{2.8}$$

$$s.t. \quad |v_m| = 1 \quad m = 1, ..., M_t \tag{2.9}$$

where $\mathbf{v}$ is an auxiliary variable so that $\mathbf{x} = \alpha\mathbf{v}$. Although the problem above is non convex, a solution was derived, based on coordinate descent, that converges to minima which the numerical results show that are sufficiently small to guarantee a reliable communication.

It should be mentioned that the same transmitter architecture shown in Fig. 2.2, can also be used to implement Constant Envelope (CE) precoding [73], [74], by keeping the amplitude α fixed regardless of the information symbols $\mathbf{s}$ and the channel matrix $\mathbf{H}$. However, the additional degree of freedom provided by designing the output amplitude α of the VGA, greatly improves the performance

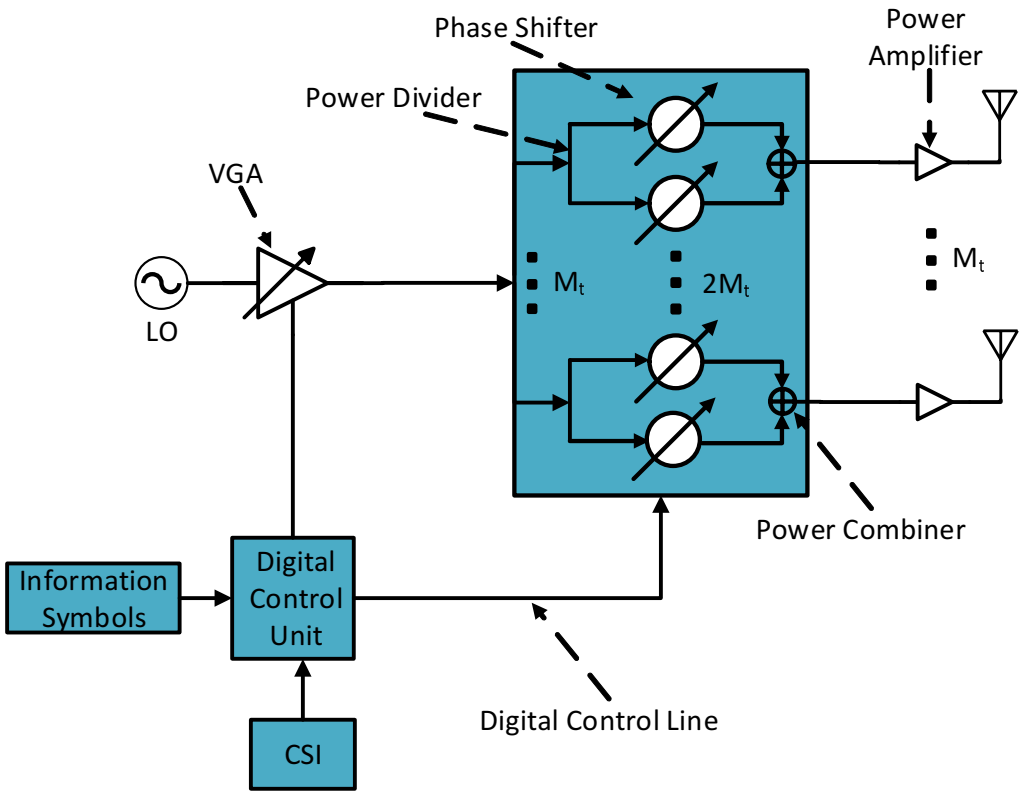

FIGURE 2.3: Block diagram of the RF domain SLP with 2-PS per antenna transmitter.

of the system as the numerical results show.

2.1.3 RF Domain SLP With Two Phase Shifters Per Antenna

Let us now propose an alteration of the architecture proposed in the previous section which relaxes the unit modulus constraint imposed by the single phase shifter per antenna. In order to achieve this the transmitter has to be equipped with two phase shifters, instead of one, at each antenna as it is shown in Fig. 2.3. Adding a second parallel connected phase shifter provides the flexibility to design complex signals that lie inside the complex disk enclosed by the circle of radius 2 ($|v_i| \leq 2$) rather than on the unit circle ($|v_i| = 1$).

The output signal from the VGA is equally divided into $2M_t$ signals and each signal is driven to a phase shifter. Each phase shifter imposes a unit amplitude constraint, as before, but the addition of the signal from the second phase shifter means that the amplitude of the signal that drives each antenna can be modified by selecting appropriately the phases of the two superimposing unit modulus signals. Therefore, the complex symbol x_m transmitted by the m-th antenna is the sum of two phase shifters and is of the form

$$x_m = \alpha \left(e^{j\phi_{m,1}} + e^{j\phi_{m,2}} \right), \quad m = 1, 2, ..., M_t. \tag{2.10}$$

Since the objective of the precoder is the same as before and by considering the relaxed constraint imposed by the two parallel connected phase shifters the problem can be formulated as

$$(\mathcal{P}_3): \min_{\mathbf{v},\alpha} \ ||\mathbf{H}\alpha\mathbf{v} - \sqrt{\gamma}\mathbf{s}||_2^2 \tag{2.11}$$

$$s.t. \quad |v_m| \leq 2 \quad m = 1, ..., M_t \tag{2.12}$$

where $\mathbf{v}$ is an auxiliary variable so that $\mathbf{x} = \alpha\mathbf{v}$.

One can observe, that when the element of $\mathbf{x}$ with the largest modulus is bounded, the same is true for all the elements of $\mathbf{v}$. Therefore, the component wise inequality constraint,$|v_m| \leq 2$, can be replaced with the uniform norm constraint, $||\mathbf{v}||_\infty \leq 2$. Now the problem can be rewritten as,

$$(\mathcal{P}_4): \min_{\mathbf{v},\alpha} \ ||\mathbf{H}\alpha\mathbf{v} - \sqrt{\gamma}\mathbf{s}||_2^2 \tag{2.13}$$

$$s.t. \, ||\mathbf{v}||_\infty \leq 2 \tag{2.14}$$

In Section 2.3 the problem is solved by an efficient alternating optimization algorithm , based on coordinate descent.

2.2 Power Consumption Analysis

One of the main reasons for researching techniques that reduce the number of RF chains, is to improve the power efficiency of large-scale antenna array systems. Therefore, it is critical to include in our study an analysis of the power that is consumed by each of the different architectures. In this analysis both the power of the transmitted signal and also the power that is consumed by the different components of each system is taken into account. For the analysis below the models that are developed in [127] are used.

First, let us examine the fully digital ZF transmitter, which employs a dedicated RF chain for each antenna and the processing is done in the baseband domain. Its consumed power can be approximated by

$$P_{ZF} \approx \frac{\mathbb{E}\left[||\mathbf{x}||_2^2\right]}{\eta} + M_t P_{RF}, \tag{2.15}$$

where η is the efficiency of the power amplifier and P_{RF} is the power consumed by a single RF chain. As it was noted in Section II, an RF chain includes a DAC, a local oscillator, a mixer, and a filter, which consume P_{DAC}, P_{LO}, P_{mix}, P_{fil} respectively. The consumed power by an RF chain therefore is $P_{RF} = P_{DAC} + P_{LO} + P_{mix} + P_{fil}$.

The transmitter of the Antenna Selection scheme is equipped with M_t transmit antennas and N_t RF chains, with $N_t < M_t$. Additionally, in this case power is also consumed on the N_t selector switches that connect the available RF chains with the active antennas. By taking this into account the consumed

power at the transmitter is given by,

$$P_{AS} \approx \frac{\mathbb{E}\left[||\mathbf{x}||_2^2\right]}{\eta} + N_t P_{RF} + N_t P_{sw}, \tag{2.16}$$

where P_{sw} is the power consumed by a switch.

For the two proposed RF domain precoding schemes the transmitter utilizes a LO and a single VGA that feed the network of phase shifters, and consume P_{LO} and P_{VGA} respectively. Assuming that each phase shifter consumes P_{PS} power, the consumed power by the transmitter with one phase shifter module per antenna is given by,

$$P_{\text{RF SLP 1-PS}} \approx \frac{\mathbb{E}\left[||\mathbf{x}||_2^2\right]}{\eta} + P_{LO} + P_{VGA} + M_t P_{PS}, \tag{2.17}$$

while the consumed power by the transmitter with two phase shifters per antenna is given by,

$$P_{\text{RF SLP 2-PS}} \approx \frac{\mathbb{E}\left[||\mathbf{x}||_2^2\right]}{\eta} + P_{LO} + P_{VGA} + 2M_t P_{PS}. \tag{2.18}$$

2.3 Symbol Level Precoding Design

2.3.1 Antenna Selection SLP

A straightforward approach to solve problem $(\mathcal{P}_1)$ would be, to compute the precoding vector for every possible sparsity pattern and then find which one minimizes $\mathcal{F}$. If we denote with $\tilde{\mathbf{H}}$ the channel matrix that is acquired from $\mathbf{H}$ after replacing $M_t - N_t$ of its M_t columns with null $K \times 1$ vectors, the precoding vector can be computed by

$$\mathbf{x}^* = \sqrt{\gamma}\tilde{\mathbf{H}}^H \left(\tilde{\mathbf{H}}\tilde{\mathbf{H}}^H\right)^{-1} \mathbf{s} \tag{2.19}$$

for the given subset of N_t active antennas. However, for a system with M_t available antennas there are $\binom{M_t}{N_t}$ possible subsets of N_t active antennas and in order to find the subset that minimizes $\mathcal{F}$, (2.19) has to be computed for every possible subset. This approach becomes computationally inefficient for large-scale antenna array systems, as the number of possible subsets increases, and therefore a less complex method is needed in order to find the optimal subset of active antennas.

Let us now show an efficient heuristic method for solving problem $(\mathcal{P}_1)$. The first step towards a solution is to reformulate the constrained problem into an unconstrained one

$$\min_{\mathbf{x}} \; ||\mathbf{H}\mathbf{x} - \sqrt{\gamma}\mathbf{s}||_2^2 + \lambda \, ||\mathbf{x}||_1 \tag{2.20}$$

where the $L1$-norm replaces the $L0$-norm as its convex envelope. The problem (2.20) is a regularized Least Squares regression problem known as LASSO and it has been proposed in [122] as a heuristic in order to find a sparse $\mathbf{x}$ that

Algorithm 1 Antenna Selection SLP

Input: H, s
Initialize λ with a random small value, $\mathbf{x}$ with zeros
while $||\mathbf{x}||_0 \neq N_t$ **do**
  while $\left|\mathbf{x}^{(j)} - \mathbf{x}^{(j-1)}\right| \leq \epsilon$ **do**
    for $i = 1$ to M_t **do**
      Update x_i with (2.21)
    end for
  end while
  Update the value of λ
end while
fix the sparsity pattern
$\mathbf{x}^* = \sqrt{\gamma}\tilde{\mathbf{H}}^H \left(\tilde{\mathbf{H}}\tilde{\mathbf{H}}^H\right)^{-1} \mathbf{s}$
Output: $\mathbf{x}^*$

minimizes $\mathcal{F}$. The parameter λ provides a trade off between $\mathcal{F}$ and the sparsity of $\mathbf{x}$ which in this case is the number of active antennas. Increasing the value of λ leads to a vector $\mathbf{x}$ with more zero elements while decreasing it results in a less sparse $\mathbf{x}$. In order to find a vector $\mathbf{x}$ with exactly N_t non zero elements, which correspond to the antennas that will be activated, we need to solve the problem (2.20) for different values of λ until we find the one that leads to the desired sparsity ($||x||_0 = N_t$). The value of λ in each iteration is updated by using a simple line search algorithm. For the solution of the LASSO problem there are many available methods in the literature. Here an efficient and easily implementable algorithm known as Coordinate Descent (CD) [128] is proposed.

The CD algorithm is based on the idea of minimizing the coordinate x_i of $\mathbf{x}$ while keeping the rest of them fixed. This means that each iteration of the CD updates one of the coordinates of $\mathbf{x}$.

Minimizing the objective function of the problem (2.20) over x_i results to

$$x_i = S_{\lambda/||\mathbf{H}_i||^2}\left(\frac{\mathbf{H}_i^H\left(\mathbf{s} - \mathbf{H}_{-i}\mathbf{x}_{-i}\right)}{\mathbf{H}_i^H\mathbf{H}_i}\right), \tag{2.21}$$

where $\mathbf{H}_i$ is the i-th column of $\mathbf{H}$, $\mathbf{H}_{-i}$ is the matrix $\mathbf{H}$ after removing its i-th column, $\mathbf{x}_{-i}$ is the vector $\mathbf{x}$ after removing its i-th component and $S_{\lambda/||\mathbf{H}_i||^2}$ is the soft thresholding operator given by [129]

$$S_\gamma\left(\mathbf{u}\right) = \frac{\max\{|\mathbf{u}| - \gamma, 0\}}{\max\{|\mathbf{u}| - \gamma, 0\} + \gamma}\mathbf{u} \tag{2.22}$$

The algorithm is terminated when a predefined tolerance ϵ is reached so that

$$\left|\left|\mathbf{x}^{(j)} - \mathbf{x}^{(j-1)}\right|\right| \leq \epsilon \tag{2.23}$$

Once the CD algorithm is terminated the number of nonzero elements of $\mathbf{x}$ is checked and if it is found equal to N_t, the ZF precoding vector is calculated, $\mathbf{x}^* = \tilde{\mathbf{H}}^{\mathbf{H}}\left(\tilde{\mathbf{H}}\tilde{\mathbf{H}}^{\mathbf{H}}\right)^{-\mathbf{1}}\mathbf{s}$, by fixing the sparsity pattern of $\mathbf{x}$. This means that the

columns of the channel matrix $\mathbf{H}$, which correspond to the zero elements of $\mathbf{x}$, are replaced by null $K \times 1$ vectors and this results to the new $K \times N_t$ channel matrix $\tilde{\mathbf{H}}$. In case the number of nonzero elements of $\mathbf{x}$ is not N_t, the value of λ is increased by a predefined value if $||\mathbf{x}_0|| > N_t$ or decreased by the same value if $||\mathbf{x}||_0 < N_t$ and the CD algorithm is repeated for the updated value of λ.

A good way to estimate the computational complexity of the proposed solution is to calculate the number of FLOPS (floating point operations per second) carried out by the algorithm as a function of the size of the matrices and vectors that are involved. The computational complexity in FLOPS of a single iteration of Algorithm 1 is given by [130]

$$C_{ASSLP} = (2K\,(M_t - 1) - K) + K + 2\,(2K - 1) + 8, \tag{2.24}$$

or in big $\mathcal{O}$ notation, $\mathcal{O}(K \times M_t)$. On the other hand the computational complexity of the straightforward combinatorial approach is known to be exponential and thus it becomes obvious that the running time of the proposed algorithm will be significantly shorter than the straightforward approach especially as the number of UTs, K, and available transmit antennas, M_t increases.

2.3.2 RF Domain SLP With One Phase Shifter Per Antenna

In this system architecture, the digitally controlled analog phase shifters that are employed for the signal processing, impose a unit modulus constraint across all the transmit antennas, thus making the problem of designing the precoding vector non convex. Here an alternating optimization method based on Coordinate Descent for finding a minimizer to the problem, is proposed.

First, α is initialized and its value is fixed while the CD algorithm runs in order to find the unit modulus vector $\mathbf{v}$. The CD algorithm finds the minimizer by minimizing over one coordinate at a time, while keeping the rest fixed. The solution for the problem $(\mathcal{P}_2)$ with $v_j, j \neq i$ fixed is given by

$$v_i = Pr\left(\frac{\mathbf{H}_i^H\,(\mathbf{s} - \mathbf{H}_{-i}\mathbf{x}_{-i})}{\mathbf{H}_i^H\mathbf{H}_i}\right), \tag{2.25}$$

where $Pr\,(\mathbf{u})$ is the projection of $\mathbf{u}$ onto the unit circle, given by

$$Pr\,(u) = \begin{cases} u & |u| = 0 \\ u/\,|u| & |u| \neq 0 \end{cases}$$

The algorithm repeats this update for $i = 1, 2, ..., M_t, 1, 2, ...$ until a predefined convergence criterion of the form $\left|\left|\mathbf{v}^{(j)} - \mathbf{v}^{(j-1)}\right|\right| \leq \epsilon_2$ is met.

In the next step, the output of the CD algorithm, $\mathbf{v}$, is kept fixed and the objective function is minimized over α which yields

$$\alpha = \frac{\mathcal{R}e\{\mathbf{s}^H\mathbf{H}\mathbf{v}\}}{||\mathbf{H}\mathbf{v}||_2^2}, \tag{2.26}$$

where $\mathcal{R}e\{\cdot\}$ denotes the real part of a complex number.

Algorithm 2 RF Domain SLP

Input: H, s
Initialize α , **v**
while $\left|\alpha^{(n)} - \alpha^{(n-1)}\right| \leq \epsilon_1$ **do**
    while $\left|\mathbf{v}^{(j)} - \mathbf{v}^{(j-1)}\right| \leq \epsilon_2$ **do**
        for $i = 1$ to M_t **do**
            Update v_i
        end for
    end while
    Update the value of α
end while
Output: v, α

After α is updated, the CD algorithm repeats for the new value of α. Finally, the alternating optimization algorithm is terminated when α converges to a predefined tolerance ϵ_1, so that $\left|\alpha^{(n)} - \alpha^{(n-1)}\right| \leq \epsilon_1$. The optimal angles of the phase shifters can be calculated simply as

$$\theta^* = Arg(\mathbf{v}^*). \tag{2.27}$$

where $Arg(\cdot)$ is the principal value of a complex number.

At this point, it should also be noted that if the value of α is fixed to $\alpha = 1$ and the step that updates the value of α is skipped, the Coordinate Descent algorithm becomes an efficient algorithm for solving the Constant Envelope (CE) precoding problem [73]–[75], since the modulus of $\mathbf{x}$ will be constant regardless of the channel realization and the transmitted information symbols.

While the problem that is tackled here is non-convex and therefore the derived solution is not necessarily optimal, numerical results in Section V show that the derived solutions are good enough in order to achieve low SER, when the number of transmit antennas are at least twice as many as the UTs ($K \leq 2M_t$).

The computational complexity of one iteration of the proposed algorithm is very similar with that of AS-SLP, since both algorithms are based on Coordinate Descent and it is given by

$$C_{RF\,SLP} = (2K(M_t - 1) - K) + K + 2(2K - 1) + 6, \tag{2.28}$$

or in big $\mathcal{O}$ notation, $\mathcal{O}(K \times M_t)$.

2.3.3 RF Domain SLP With Two Phase Shifters Per Antenna

The addition of a second phase shifter connected in parallel with the first changes the stringent modulus constraint, $|v_i| = 1$, of the problem $(\mathcal{P}_2)$ to a constraint of the form $||v_1| \leq 2$. To solve the precoding design problem with the new constraint, the same alternating optimization algorithm that was used

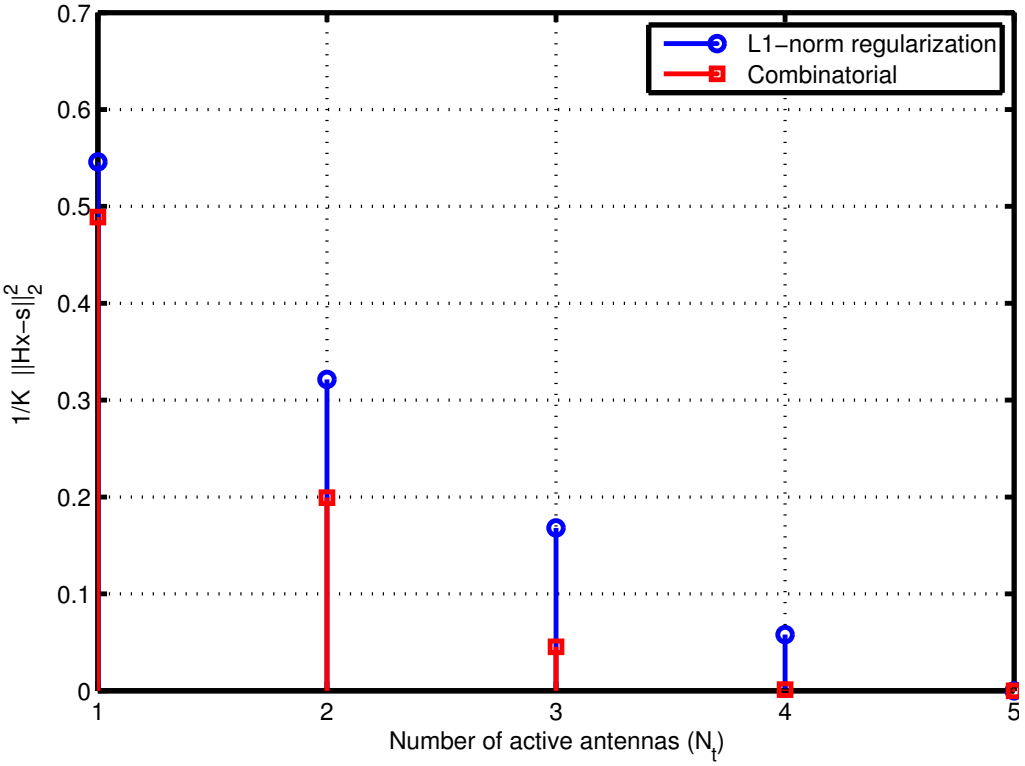

FIGURE 2.4: Trade-off between the average MUI energy and the number of active antennas N_t, for an AS system with $M_t = 10$ antennas, $K = 5$ UTs and QPSK modulation.

in the previous problem, will be used again. However, since the constraint is different here, the update step will also have to be different.

Minimizing the objective function over v_i while keeping the other components, $v_j, j \neq i$ and α fixed, we get

$$v_i = T\left(\frac{\mathbf{H}_i^H\left(\mathbf{s} - \mathbf{H}_{-i}\mathbf{x}_{-i}\right)}{\mathbf{H}_i^H\mathbf{H}_i}\right), \tag{2.29}$$

where $T(u)$ denotes the truncating operator

$$T(u) = \begin{cases} -2u/|u| & u < -2 \\ u & |u| \leq 2 \\ 2u/|u| & u > 2 \end{cases}$$

Once the optimal precoding vector $\mathbf{x}^*$, compliant with the constraint, is computed, the transmitter needs to determine the phases $\phi_{m,1}$ and $\phi_{m,2}$ of the phase shifters. To that end we need to solve the equation

$$x_m^* = \alpha\left(e^{j\phi_{m,1}} + e^{j\phi_{m,2}}\right), \quad m = 1, 2, ..., M_t \tag{2.30}$$

which yields the results

$$\phi_{i,1} = \theta_i + \cos^{-1}\frac{z_i}{2} \tag{2.31}$$

$$\phi_{i,2} = \theta_i - \cos^{-1}\frac{z_i}{2} \tag{2.32}$$

where $z_i = |x_i^*|$ and $\theta_i = Arg\,(x_i^*)$.

Finally, the computational complexity in FLOPS and the time complexity of one iteration of the proposed algorithm is identical with the previous one, (2.28). However, as the unit modulus constraint is here is replaced by a uniform constraint the problem is more efficiently solved, which is confirmed by the simulations results.

2.4 Numerical Results

In this section, simulation results and a discussion on the performance of the proposed approach is presented. The channel coefficients follow an i.i.d. Circularly Symmetric Complex Gaussian distribution with zero mean and unit variance, $\mathcal{CN}\,(0,1)$. The power consumption values for the different components are $P_{DAC} = 200mW$, $P_{LO} = 5mW$ $P_{mix} = 19mW$, $P_{fil} = 14mW$, $P_{SW} = 5mW$, $P_{PS} = 30mW$, $P_{VGA} = 9.5mW$ while the energy efficiency of the power amplifier is set to $\eta = 0.39$, [82], [127]. The consumed power in the following results is given by (2.15)-(2.18) depending on the precoding scheme and architecture that is employed. The transmit power is the average transmit power of the employed precoding scheme given by $\mathbb{E}\left[||\mathbf{x}||_2^2\right]$ where $\mathbf{x}$ is the precoded vector. The results were averaged over 1000 independent channel realizations and over 100 symbols which were transmitted over a fixed channel realization.

We will begin with some results for the proposed AS-SLP scheme. Figure 2.4 illustrates the trade-off between the number of active antennas N_t and the average of the multiuser interference energy defined as $(1/K\,||\mathbf{Hx} - \mathbf{s}||_2^2)$, in a system with $K = 5$ UTs and $M_t = 10$ available transmit antennas, in order to explore the performance gap between the proposed heuristic approach and the optimal solution. The red squares were obtained by solving the combinatorial sparsity problem with the inefficient exhaustive search-based approach of evaluating the precoding vector $\mathbf{x}$ for every possible sparsity pattern and selecting the one that minimizes the objective function. The blue circles were obtained by the proposed antenna selection algorithm which is based on CD. We observe that the proposed heuristic approach shows, as it is expected, a slightly worse performance than the straightforward approach, when the number of active antennas is smaller than the number of UTs. However, when the number of active antennas is equal to the number of UTs the two methods yield the same performance. If we take a closer look at the cases where the number of active antennas is less than the number of UTs, we observe that for $N_t = 1, 2, 3$ the average MUI of the proposed heuristic solution is rather large and therefore it is expected that such systems would have a low throughput, making them impractical for modern communications. However, for $N_t = 4$ active antennas and $K = 5$ UTs the average MUI is greatly reduced and the gap between the

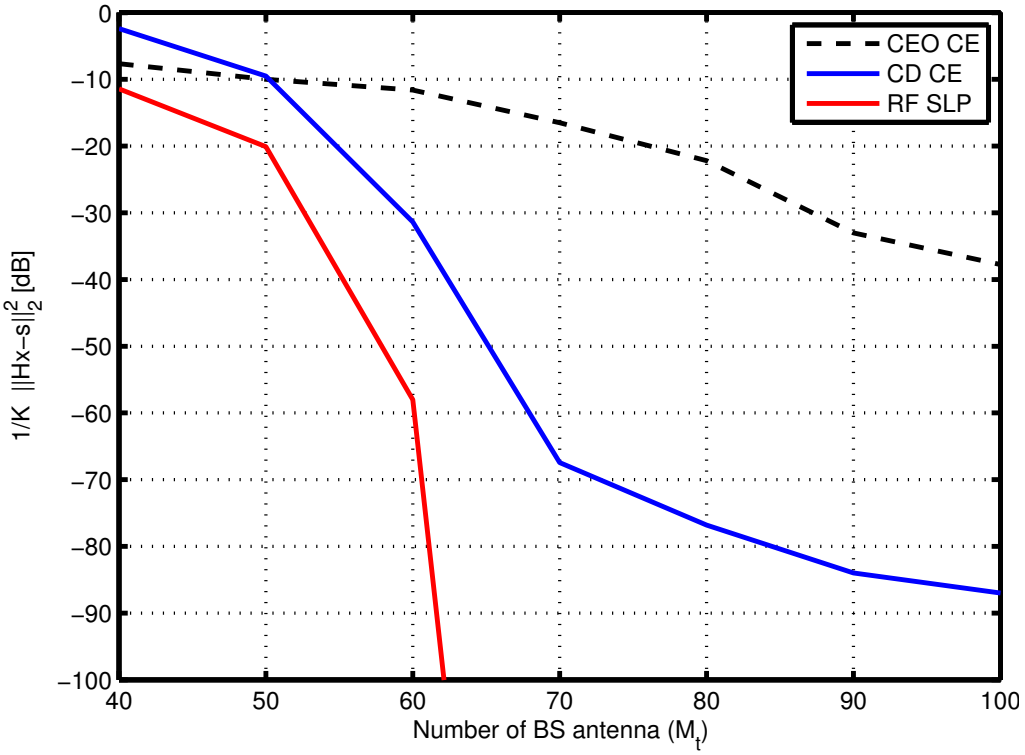

FIGURE 2.5: Trade-off between the average MUI energy and the number of transmit antennas M_t, for a system with $K = 30$ UTs and QPSK modulation.

proposed heuristic solution and the optimal solution is smaller than in the previous cases. This suggests that when the number of active antennas is slightly less than the number of UTs (e.g $N_t = 9$, $K = 10$) the system performance is not going to be limited by MUI, a find that is also supported by the SER performance results that follow.

The performance of the proposed algorithm for RF domain SLP with one phase shifter per antenna is compared, in Figure 2.5 with the performance of CE precoding schemes for an increasing number of BS transmit antennas and a fixed number of $K = 30$ UTs. The two CE precoding schemes used here, are the CD based CE which we discussed in a previous section and the Cross Entropy Optimization (CEO) based CE [131]. Firstly, it is observed that the CD based CE outperforms the CEO based CE precoding as the number of transmit antennas increases. Additionally, the proposed RF-SLP outperforms both CE schemes which is expected since it does not have a stringent constant envelope constraint, that keeps its amplitude fixed for each transmission. For example an average MUI energy of $-30dB$, which was used as a benchmark value in [131] and numerical results also show that can guarantee a reliable communication, can be achieved for $M_t = 55$ by RF SLP while it requires $M_t = 60$ and $M_t = 88$ for CD based CE precoding and CEO based CE precoding respectively. This shows that the added degree of freedom of changing the amplitude α of the single VGA gives a significant performance advantage to the RF SLP over the CE precoding schemes.

In Fig. 2.6, the average symbol error rate performance of various antenna

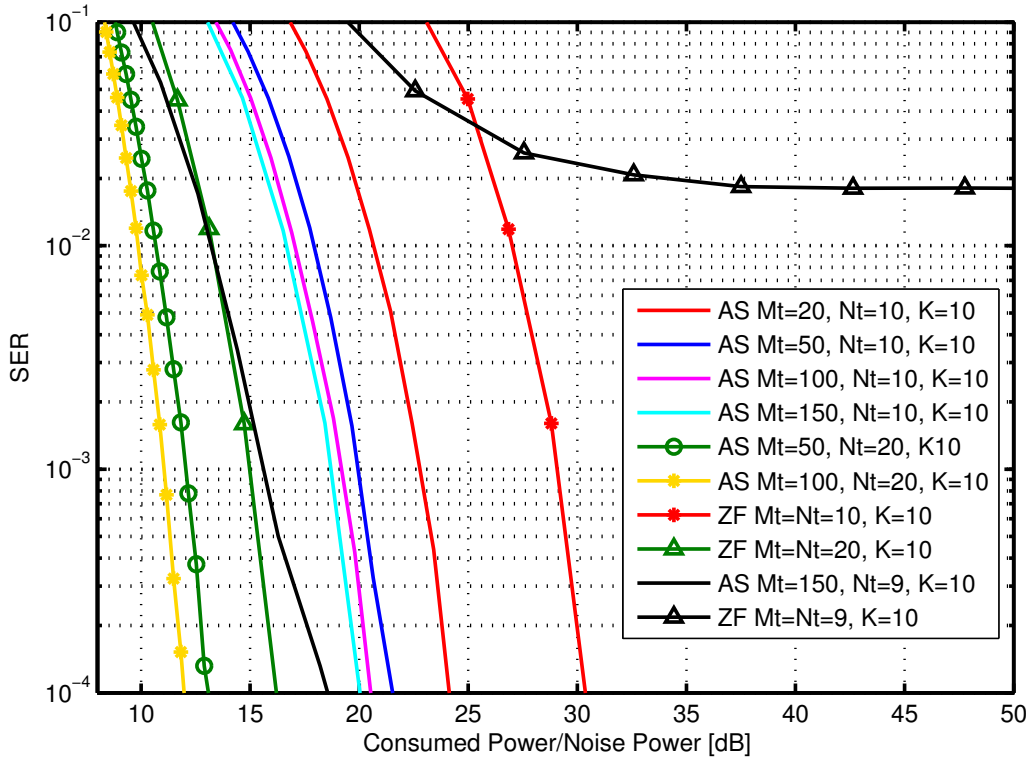

FIGURE 2.6: SER of various configurations of the AS scheme with QPSK modulation.

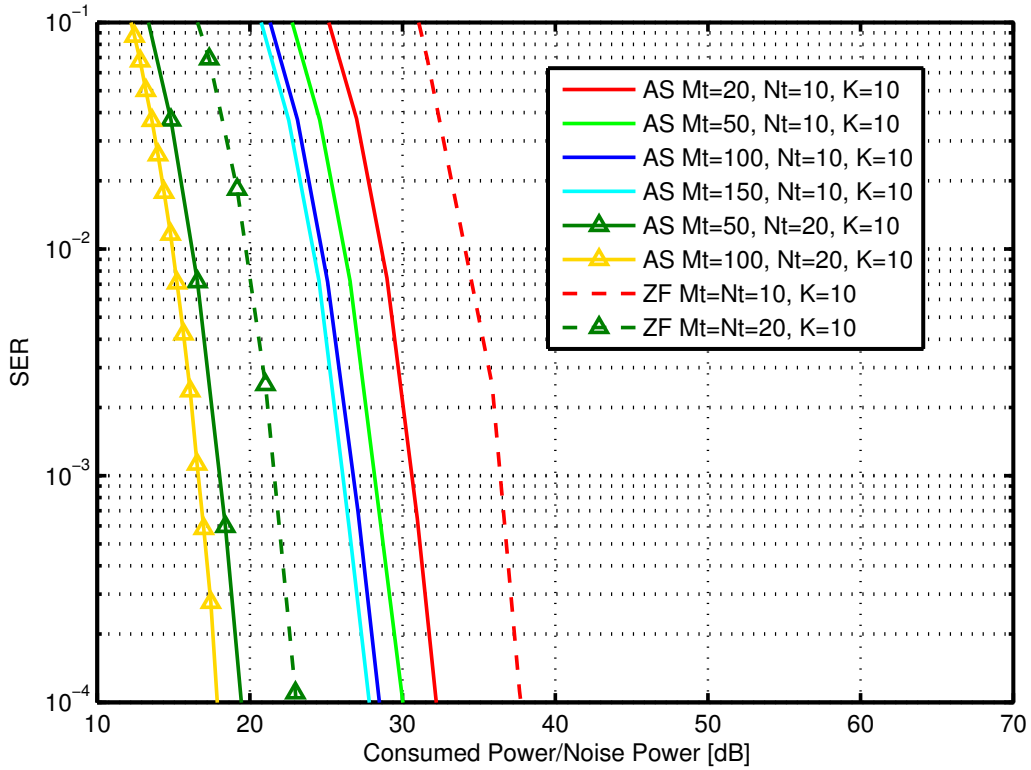

FIGURE 2.7: SER of various configurations of the AS scheme with 16-QAM modulation.

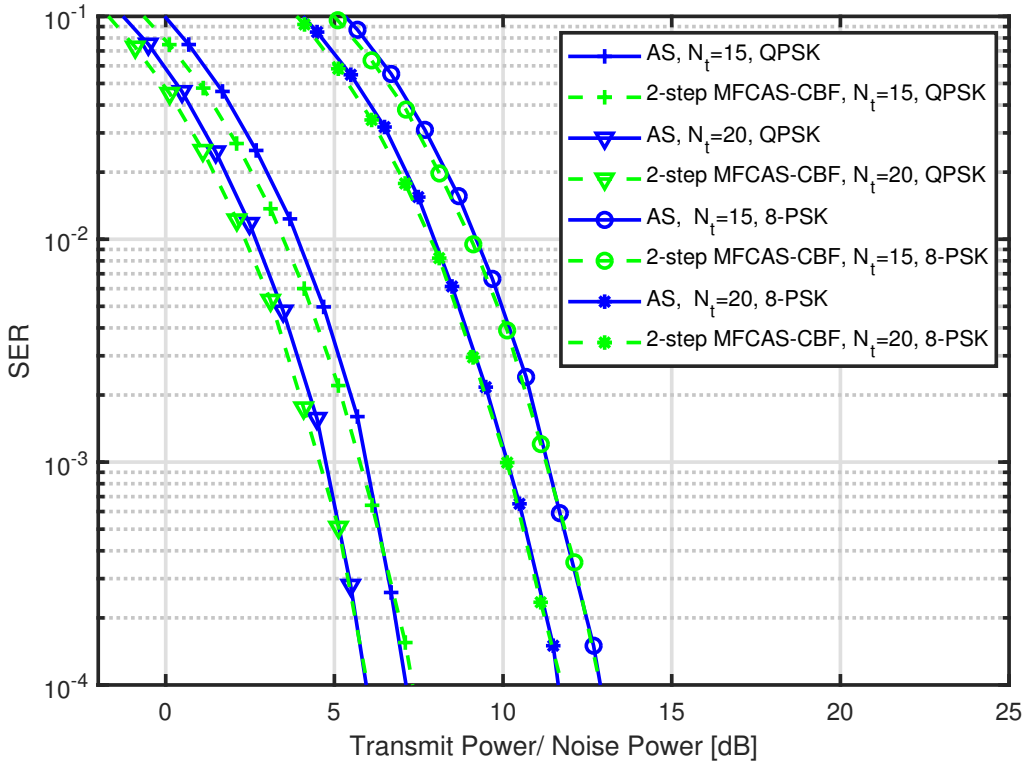

FIGURE 2.8: SER of various configurations of the proposed AS-SLP scheme compared with the 2-Step MFCAS-CBF in [132] with $M_t = 100$ and $K = 10$.

selection configurations with QPSK modulation and for a different number of transmit antennas M_t and RF chains N_t, is shown. The ZF precoding, a technique which requires a transmitter with as many RF chains as its transmit antennas, is used as a benchmark. The consumed power for AS-SLP and ZF is given by (2.16) and (2.15), respectively. One may observe that for the same number of $N_t = 10$ RF chains the AS-SLP scheme significantly outperforms the ZF scheme, by exploiting the large number of available antennas. Increasing the number of transmit antennas improves the performance, but after some point the gains are incremental. For example the performance gap between the two schemes, when QPSK modulation is employed, is approximately $7dB$ for $M_t = 20$, $9dB$ for $M_t = 50$ and $10dB$ for $M_t = 100$, and $N_t = 10$ RF chains. When the number of RF chains and active antennas becomes much larger than that of the UTs ($N_t = 20, K = 10$), AS-SLP still outperforms ZF ($3dB$ gain), while the increase of transmit antennas, in this scenario, seems to slightly improve the performance of AS-SLP. Similar observations can be made when 16-QAM modulation is employed in Fig. 2.7. Finally, returning to Fig.2.6, one can observe that the AS-SLP allows more users to be served than the number of RF chains and active antennas ($N_t = 9, K = 10$) when the number of available transmit antennas is large enough. In fact it outperforms, all the schemes that have $N_t = 10$ RF chains. At the same time, ZF precoding cannot reliably serve more users than the number of its RF chains, as its SER curve shows.

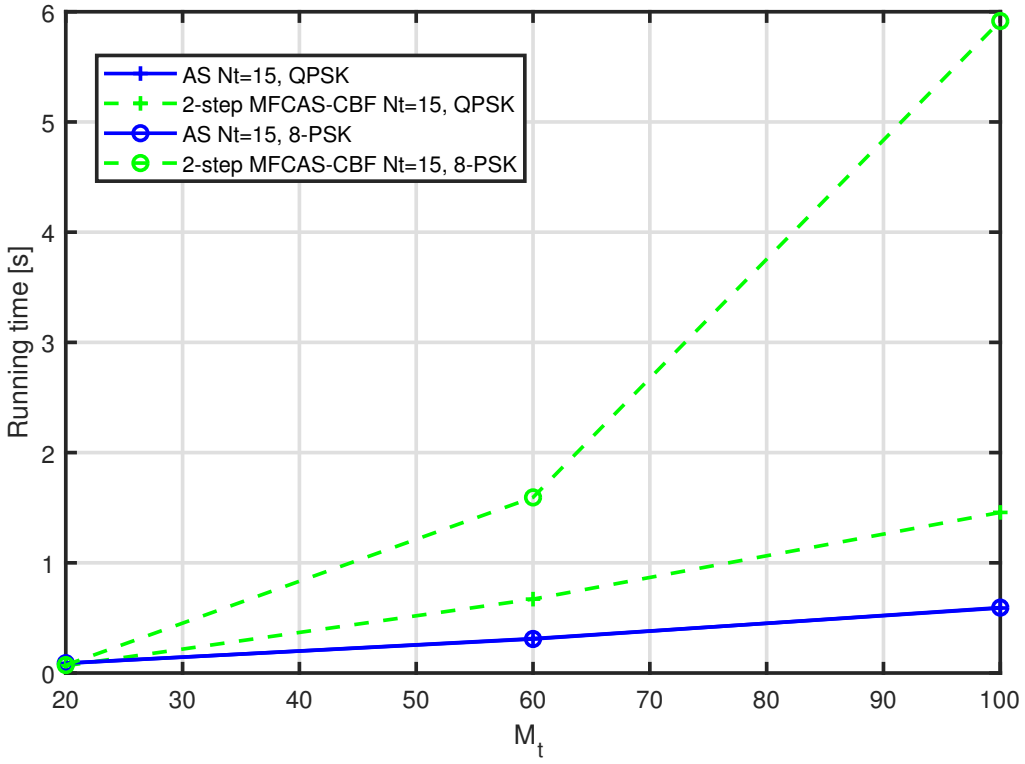

FIGURE 2.9: Running time of various configurations of the proposed AS scheme compared with the 2-step MFCAS-CBF, [132], for $K = 10$.

Furthermore, in Figures 2.8 and 2.9 a comparison of the SER performance and the running time respectively for a single transmit symbol $\mathbf{x}$, between the proposed AS-SLP scheme and the AS scheme for interference exploitation that is introduced in [132], referred to as 2-Step MFCAS-CBF, is presented. The compared schemes are both symbol level precoders, utilize the same transmitter architecture and therefore have the same power consumption. However, contrary to the AS-SLP scheme which works with any given symbol constellation, the scheme in [132] supports only PSK constellations with the objective to turn the harmful MUI into constructive interference, [17]. Additionally, the precoding problem that is formulated in [132] is solved using commercially available tools such as MoSek, which usually have higher computational complexity than algorithms who are tailored for a specific problem. The two schemes show almost identical SER performance, for a different number of active antennas, N_t and for different modulation orders. The advantages of the proposed scheme can be seen in Fig. 2.9, which shows that the proposed algorithm for AS-SLP results in significantly reduced running times compared to 2-Step MFCAS-CBF, as the number of transmit antennas, M_t, increases. The use of a higher order modulation such as 8-PSK leads to a significant increase of the running time for the 2-Step MFCAS-CBF scheme while it does not affect at all the running time of the proposed AS-SLP scheme whose running time remains the same and is independent from the order of the modulation.

In Figures 2.10 and 2.11 the average SER performance of the two proposed

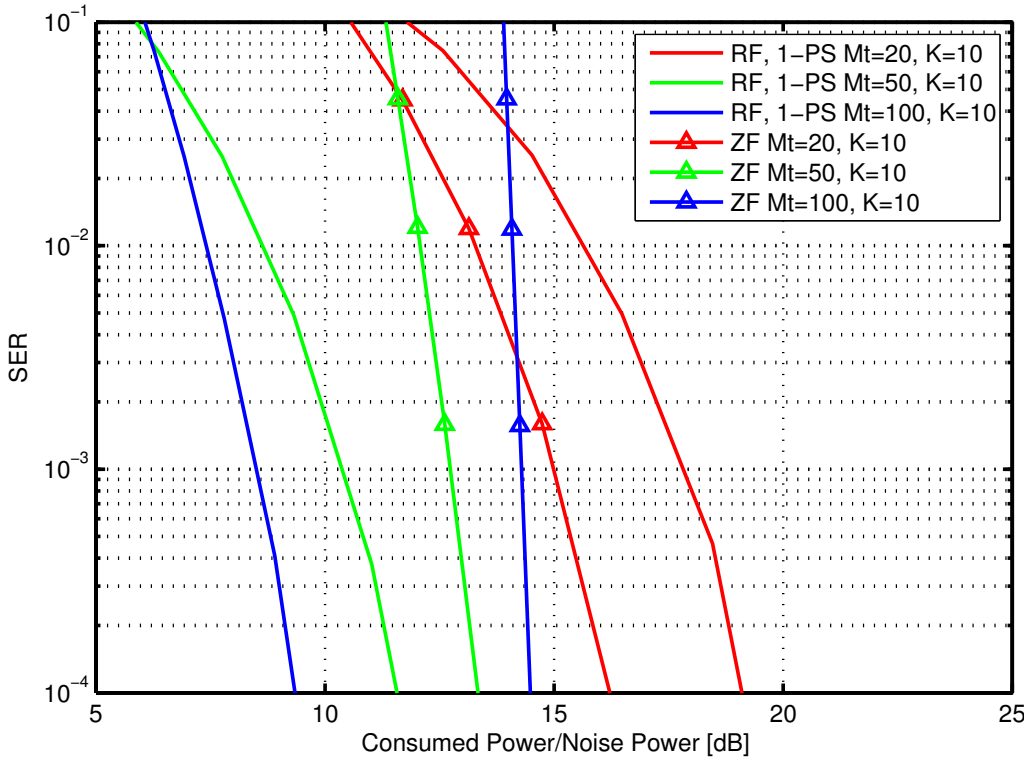

FIGURE 2.10: SER of various configurations of the RF domain SLP with one phase shifter scheme with QPSK modulation.

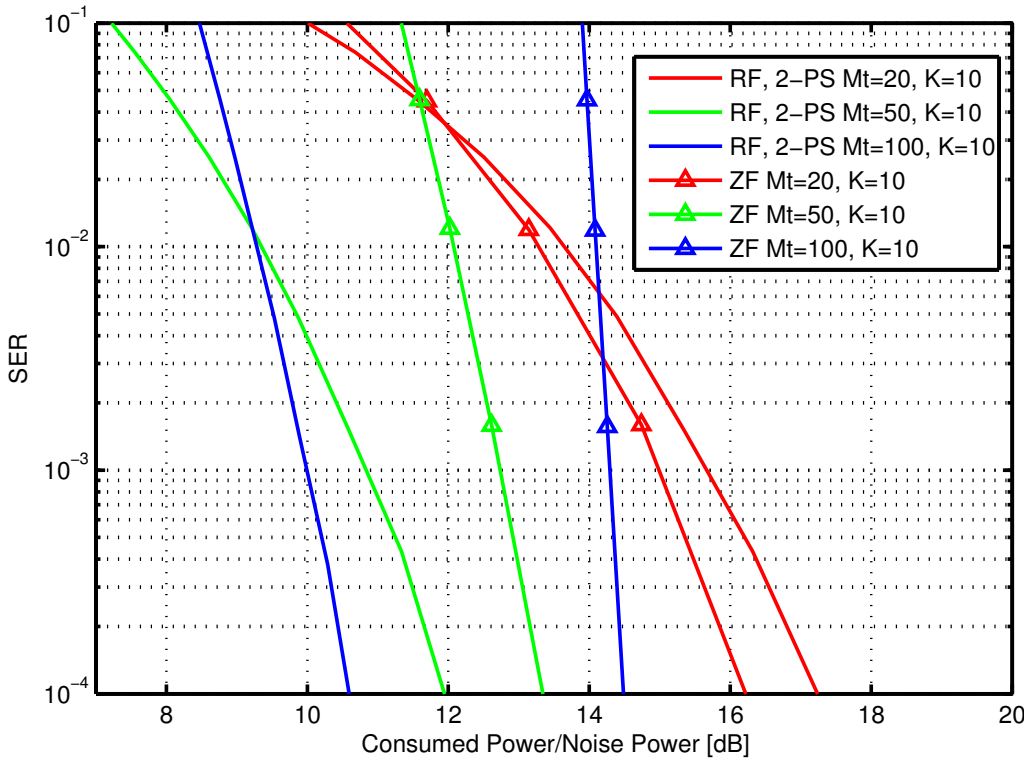

FIGURE 2.11: SER of various configurations of the RF domain SLP with two phase shifters scheme with QPSK modulation.

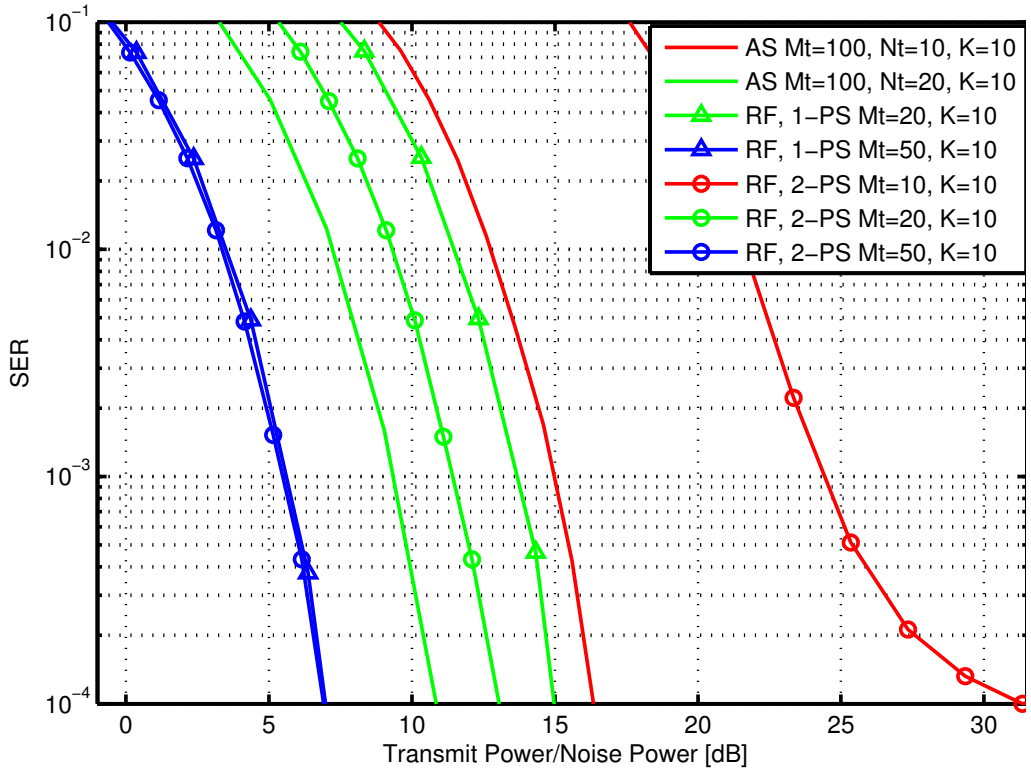

FIGURE 2.12: SER performance comparison of the different proposed schemes with QPSK modulation.

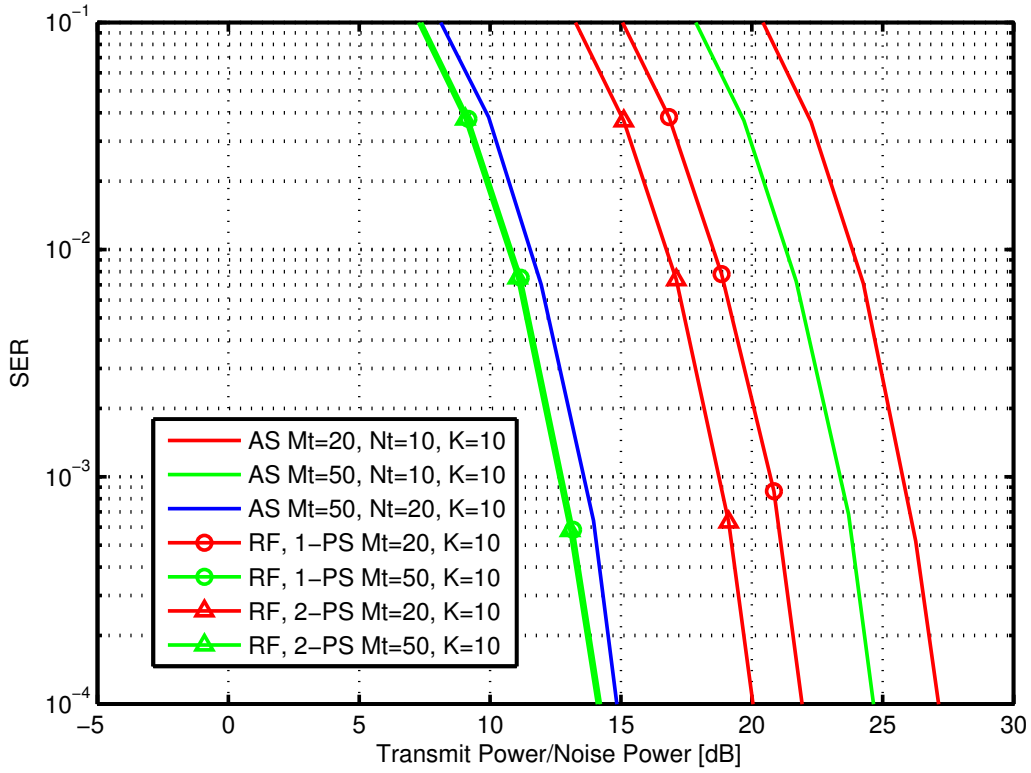

FIGURE 2.13: SER performance comparison of the different proposed schemes with 16-QAM modulation.

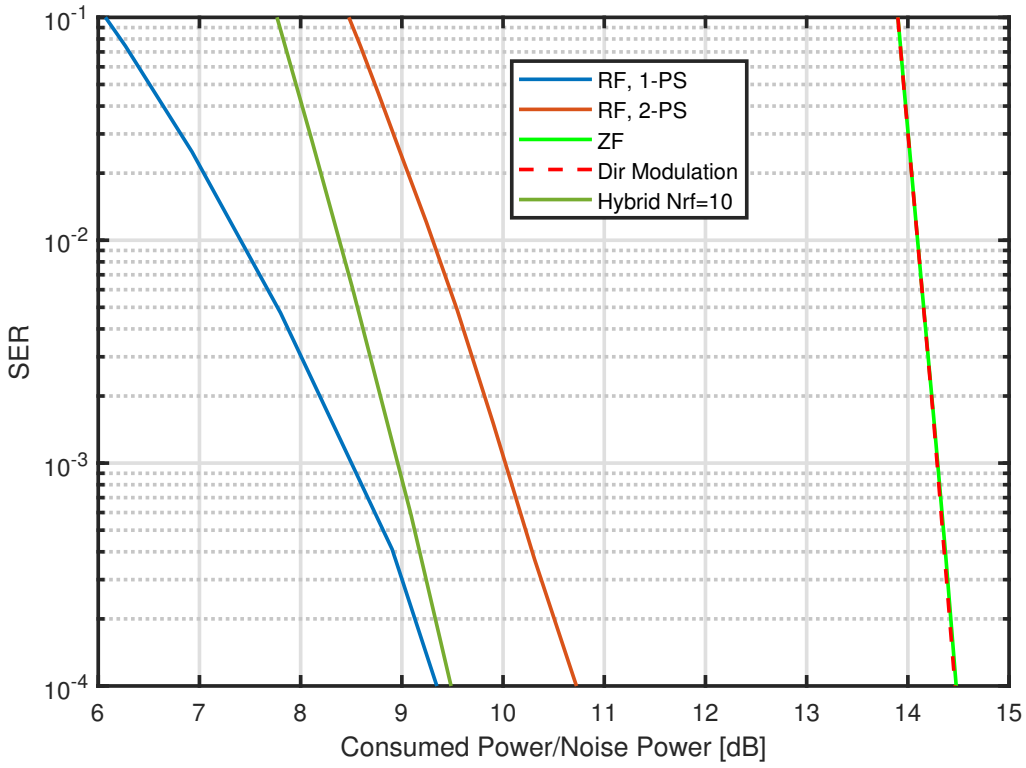

FIGURE 2.14: SER performance comparison of the different proposed and benchmark schemes for a system with $M_t = 100$, $K = 10$ and QPSK modulation.

RF SLP schemes is examined as a function of the consumed power at the BS over the noise power at the UTs. The power consumed by the transmitter of the system with one phase shifter per antenna and two phase shifters per antenna is given respectively by (2.17) and (2.18). Firstly, it is observed that both schemes outperform the fully digital ZF precoder as the ratio of transmit antennas M_t over the number of UTs K, while the opposite is true when the ratio is smaller. For example for a SER value of 10^{-4}, $M_t = 100$ and $K = 10$ the RF SLP scheme with one phase shifter per antenna outperforms the ZF scheme for $5dB$ while the scheme with two phase shifters per antenna outperforms it for nearly $4dB$, when QPSK modulation is used. On the other hand for a different scenario where the number of transmit antennas is significantly smaller $M_t = 20$ and the number of UTs remain the same $K = 10$ and for the same SER, the RF SLP scheme with one phase shifter per antenna shows a $3dB$ worse performance than the ZF precoder, while the RF SLP scheme with two phase shifters per antenna shows a $1dB$ worse performance than the ZF precoder.

These observations underline that the RF SLP schemes show a much improved performance over as the number of transmit antennas increases when compared to a fully digital approach. This is because the power consumption of the analog phase shifters is significantly less than that of the DACs which are required in fully digital architectures. As a result, the diversity gains of the increased number of antennas diminish in fully digital architectures, when you take into account the power consumption of the components of the dedicated

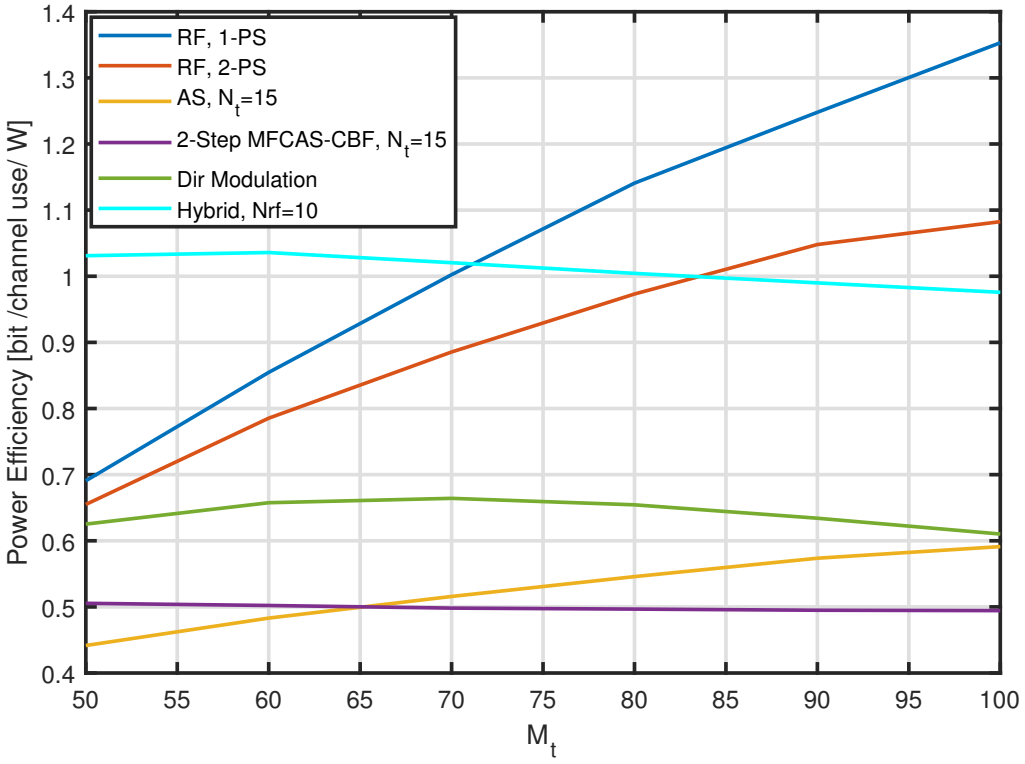

FIGURE 2.15: QPSK Power Efficiency for a system with $K = 10$ and $SNR = 15dB$.

RF chains, while RF SLP schemes are better suited to exploit the advantages of the large number of transmit antennas because of their power efficient analog components.

In Fig. 2.12 different SER curves for the three proposed SLP schemes with QPSK modulation are illustrated. The average transmit power for all schemes is defined here as $\mathbb{E}_{\mathbf{H},\mathbf{s}}\left[||\mathbf{x}||_2^2\right]$. The AS-SLP schemes perform better than the RF domain SLP schemes when the compared schemes have the same number of active transmit antennas. On the contrary, if we compare schemes with the same number of available transmit antennas the performance of AS-SLP falls behind the two proposed RF domain SLP schemes. One can observe, that when the number of active transmit antennas is the same as the number of users, 10, AS-SLP significantly outperforms SLP with two phase shifters per antenna. Lastly, it is observed that the SLP with two phase shifters per antenna outperforms the SLP with one phase shifter per antenna when the number of transmit antennas is relatively small, $M_t = 20$, while the two schemes have an identical performance as the number of transmit antennas increases, $M_t = 50$. When 16-QAM modulation is employed as it is shown in Fig. 2.13 we observe that the SER performance of the different SLP configurations is similar to the SER performance when QPSK is used. This shows that the proposed SLP schemes can operate with various higher-order modulations.

In Fig. 2.14 a SER performance comparison of the two proposed RF-SLP schemes, with two competing schemes from the literature, is presented. The first one is a directional modulation via symbol level precoding scheme presented in

TABLE 2.1: Runtime in [s] for a for a frame of 10 symbols

	$M_t = 50$	$M_t = 60$	$M_t = 70$	$M_t = 80$	$M_t = 90$	$M_t = 100$
RF-SLP 1-PS	0.27	0.28	0.32	0.42	0.45	0.65
RF-SLP 2-PS	0.11	0.15	0.18	0.21	0.22	0.24
AS-SLP	0.77	0.81	1.54	1.58	1.64	3.29
Hybrid	0.46	0.51	0.57	0.61	0.64	0.70
2-Step MFCAS-CBF	2.20	4.45	6.92	7.26	8.00	9.22
Dir. Modulation SLP	0.06	0.023	0.024	0.026	0.030	0.031

[133] and the objective of its precoder is to minimize the transmit power. The second one is the hybrid Analog-Digital precoder presented in [82] and is a block level precoder designed with the view to reduce the hardware complexity and the power consumption of the transceiver. The precoder in [133] employs a fully digital architecture and thus, its power consumption is given by (2.15). On the other hand the hybrid scheme is based on a transmitter architecture with a reduced number of N_{RF} DACs and RF chains that are connected to the antennas via a network of M_t phase shifters and its power consumption, [82]

$$P_{HY} \approx \frac{\mathbb{E}\left[||\mathbf{F}||_F^2\right]}{\eta} + N_{RF}P_{RF} + M_t P_{PS}, \tag{2.33}$$

where $\mathbf{F}$ is the precoding matrix and $||\cdot||_F$ is the Frobenius norm. We observe that the SLP technique from the literature shows exactly the same performance as the ZF precoder and far worse than the proposed RF-SLP schemes, while the hybrid precoder outperforms RF-SLP with 2-PS. The scheme that shows the best SER performance in this scenario is the proposed RF-SLP with 1-PS per antenna. It should be noted that the hybrid precoder employs a more complex receiver which requires a postcoding matrix in order to successfully detect the received symbols while the other schemes in this comparison require only a simple demodulator at the receiver.

In order to better highlight the advantages of the proposed RF-SLP schemes for large-scale antenna array systems over the existing techniques in the literature we compare the proposed schemes with the SLP scheme in [133] with the Hybrid precoding scheme in [82] and with the AS-SLP in [132] using a Power Efficiency metric η_T as it was introduced in [132]

$$\eta_T = \frac{T}{P} \tag{2.34}$$

where T is the throughput defined as $T = (1-BLER)*m*K$ where BLER is the Block Error Rate, $m = log2(M)$ is the number of bits per constellation symbol, K is the number of UTs and P is the consumed power given by (2.15)-(2.18) and (2.33). We can observe in Fig. 2.15 that the two AS schemes show the worst performance and justifiably so as they only transmit through $N_t = 15$ antennas. However, the proposed AS-SLP outperforms the current state of the art AS-SLP, 2-Step MFCAS-CBF, as the number of available transmit antennas increases and manages to achieve almost the same power efficiency as the directional

modulation SLP when $M_t = 100$. The two RF-SLP schemes outperform all the other schemes as the number of transmit antennas increases above $M_t = 85$. It is worth noting that the power efficiency of the proposed schemes increases as the number of transmit antennas increases while it decreases for the schemes from the literature. This highlights that the proposed techniques here are appropriate for systems with large antenna arrays, mainly as a result of their simplified analog only architecture, as compared to the fully digital architectures that have large number of RF chains and the Hybrid one that involve in general more RF chains than our proposed solutions.

Finally, to complete this comparison we need to discuss the complexity of the proposed solutions. To that end, the average runtimes of each precoder are compared for a frame of 10 symbols, which is a realistic value, as stated in [132] , for a fast fading channel where SLP techniques are suitable. By observing Table 2.1, it becomes obvious that the AS schemes are the most complex and have much higher runtimes than the rest, though our proposed algorithm for AS manages to drastically reduce the runtime when compared to the current state of the art AS-SLP, 2-Step MFCAS-CBF, which use an optimization toolbox. RF-SLP with 2-PS has faster runtimes than RF-SLP with 1-PS but as we have already seen the later has a better power efficiency and SER performance. This shows that the addition of a second PS provides an interesting trade-off between complexity and performance. It is also worth noting that the RF-SLP schemes have a faster runtime than the hybrid precoder, which is a block level precoder, though it is expected that this would change for the same comparison with a larger frame, e.g 100 symbols. For this reason SLP techniques are generally better suited for fast-fading scenarios where the channel coherence time is relatively small. Finally, directional modulation SLP has the fastest runtimes when compared to the other schemes, but as we have already seen it also has the worse SER performance for the scenarios that have been tested.

2.5 Summary

In this chapter, SLP schemes were developed for the three proposed power efficient transmitter architectures, when single-carrier transmission is assumed over a frequency flat channel. SLP design problems were formulated by taking into account the shortcomings of the power efficient components that were employed in the transmitter architectures. Then, novel computationally efficient algorithmic solutions were developed for the optimization problems. Finally, extensive simulation results showed the improved system performance of the proposed SLP schemes when compared with existing solutions in the literature and showed the scenarios in which each of the proposed SLP schemes is advantageous.

Chapter 3

SLP For CE MIMO-OFDM Systems

In this chapter the problem of CE precoding for MIMO-OFDM transmission over a frequency selective channel is presented. The design problem is formulated with the view to minimize the Euclidean distance between the Fourier Transform of the received signal and the desired information symbols. Two efficient algorithmic solutions are then presented for solving this problem.

The remainder of the chapter is structured in the following way. In Section 3.1 the system model of a classic MIMO-OFDM system is presented followed by the description of the system model of CE MIMO-OFDM and the formulation of the CE MIMO-OFDM precoding problem. The section ends by a presentation of power-efficient transmitter architectures for CE MIMO-OFDM precoding. In Section 3.2, two different solutions for the precoding problem are presented, first, a solution based on the CDD algorithmic framework and then a solution using the Gauss-Newton method. In Section 3.3 numerical results of simulations of the proposed system are presented as well as comparisons with Zero Forcing precoding and CEP techniques from the literature ([124], [123]), that show the advantages that the proposed solutions provide. Finally, in Section 3.4 the summary of this chapter is presented.

3.1 System Model

Before describing the system model of the proposed CE MIMO-OFDM scheme, let us first briefly consider the downlink of a classic multiuser MIMO-OFDM, using a linear precoding scheme (i.e. Zero Forcing precoding), system operating over a frequency selective channel.

3.1.1 MIMO-OFDM

In the considered wireless communication system a BS equipped with a large array of M antennas serves K single-antenna UTs over a bandwidth W using OFDM.

Generally in OFDM, the channel, of bandwidth W, that is assigned for transmission is divided into N sub-channels with equal width of $\Delta f = W/N$, because it is assumed that a signal of bandwidth W will suffer from frequency selective fading as a result of the multipath propagation. The width Δf of the

sub-channels is chosen so that it will be smaller than the coherence bandwidth of the channel so that the frequency response of the channel will be flat over each sub-channel. Each sub-carrier that corresponds to one of the N sub-channels is modulated forming the $M \times N$ OFDM block in the frequency domain

$$\mathbf{X}_F = [\mathbf{x}_F(1),\ \mathbf{x}_F(2),\ \ldots,\ \mathbf{x}_F(N)]\,, \tag{3.1}$$

where $\mathbf{x}_F(n)$ is an $M \times 1$ column vector that is loaded on the n_{th} sub-carrier and which contains the M precoded symbols, one for each transmit antenna of the BS.

In order to produce the OFDM signal in the time domain the N-point inverse FFT (IFFT) is applied on each row of the frequency domain signal $\mathbf{X}_F$ and the result is the time domain signal

$$\mathbf{X}_T = \sqrt{N}\ \mathrm{IFFT}(\mathbf{X}_F, 2) = \left(\frac{\mathbf{W}^*}{\sqrt{N}}\mathbf{X}_F^T\right)^T, \tag{3.2}$$

where $\mathrm{IFFT}(\cdot, 2)$ denotes the row wise IFFT and $\mathbf{W}_N$ is the $N \times N$ Discrete Fourier Transform (DFT) matrix. which can be defined as

$$\mathbf{W}_N = \begin{bmatrix} 1 & 1 & 1 & \ldots & 1 \\ 1 & w^1 & w^2 & \ldots & w^{N-1} \\ 1 & w^2 & w^4 & \ldots & w^{2(N-1)} \\ \vdots & \vdots & \vdots & \ddots & \vdots \\ 1 & w^{N-1} & w^{2(N-1)} & \ldots & w^{(N-1)(N-1)} \end{bmatrix},$$

where $w = e^{-\imath 2\pi/N}$ with $\mathbf{W}_N^H\mathbf{W}_N = N\mathbf{I}_N$. The utility of $\mathbf{W}_N$ is that it allows to express the N-point DFT (or IDFT) as a multiplication, as in (3.2). The term $1/\sqrt{N}$ is a normalization factor which is used so that $||\mathbf{X}_F||_F = ||\mathbf{X}_T||_F$.

After the IFFT computation, the Cyclic Prefix is added at the beginning of the OFDM block $\mathbf{X}_T$. The CP has a length, which must be larger or at least equal to the multipath channel's length, of L samples, and is comprised by the last L samples of $\mathbf{X}_T$,

$$\mathbf{CP} = [\mathbf{x}_T(N - L + 1),\ \ldots,\ \mathbf{x}_T(N-1),\ \mathbf{x}_T(N)]\,, \tag{3.3}$$

where $\mathbf{x}_T(n)$, is the n-th $M \times 1$ column of $\mathbf{X}_T$, and represents the n-th time domain symbol which is transmitted from the M transmit antennas. The cyclic prefix is crucial for the transmission over multipath channels, [134], because it serves as a guard interval protecting the received signal from intersymbol interference but also because it allows for frequency domain processing. The latter is due to the fact that the cyclic prefix makes the linear convolution of the transmitted signal with the multipath channel equivalent to the circular convolution, which can easily be transformed in the frequency domain by the DFT.

After prepending the cyclic prefix the signal is transmitted over a channel with ν resolvable multipath components which is expressed as

$$\mathbf{h}_T(m,k) = [h(m,k,1),\ h(m,k,2),\ \ldots.\ h(m,k,\nu)]\,, \tag{3.4}$$

where $h(m,k,n)$ is the n-th path gain from the m-th transmit antenna of the BS to the k-th UT. Additionally, Rayleigh fading is assumed and therefore the channel coefficients are modelled as circularly symmetric complex Gaussian random variables with $h(m,k,n) \sim \mathcal{CN}(0, \frac{1}{\nu})$. The received time domain signal at the k-th receiver is denoted by

$$y_T(k,n) = \sum_{m=1}^{M} \sum_{l=0}^{v-1} h(m,k,l) x_T(m, n-l) + z_T(k,n), \tag{3.5}$$

where $z_T(k,n)$ is the n-th noise sample which is modeled as a circularly symmetric complex Gaussian random variable with distribution $z_T(k,n) \sim \mathcal{CN}(0, N_0)$, where N_0 is the noise variance. Additionally, in the scope of this work it is assumed that the receiver has perfect knowledge of the CSI in order to calculate the precoded symbols accordingly.

The k-th receiver performs an FFT on the received signal after removing the CP which is equivalent to discarding the first L samples of $\mathbf{y}_T(k)$. The output of the N point FFT at the k-th UT is given by

$$y_F(k,n) = \sum_{m=1}^{M} h_F(k,m,n) x_F(m,n) + z_F(k,n), \tag{3.6}$$

with $n = 1, 2, \ldots, N$ where $h_F(m,k,n)$ and $z_F(k,n)$ are the frequency domain channel coefficients and AWGN noise samples, respectively. Finally, a simple Maximum Likelihood detector is employed in order to detect the information symbols that have been transmitted.

3.1.2 CE MIMO-OFDM

Now that we have a basic understanding of the MIMO-OFDM system let us continue with the CE MIMO-OFDM. Here the transmit signal in the time domain is constrained to have a per antenna constant amplitude regardless of the transmitted symbols and channel realization, which is expressed by

$$|x_T(m,n)| = \sqrt{\frac{\gamma}{M}} \tag{3.7}$$

where $\frac{\gamma}{M}$ is the per antenna constant power constraint and γ is the total transmit power. The problem with (3.7) is that it constrains the signal in the time domain and there is not an easy way to transform the constraint in the frequency domain where the processing happens in OFDM transmission.

Before formulating the CE MIMO-OFDM precoding problem, it is important to show how the frequency domain channel coefficients are formulated appropriately into a $KN \times MN$ matrix $\tilde{\mathbf{H}}_F$, the DFT matrix $\mathbf{W}_N$ into a $MN \times MN$ matrix $\tilde{\mathbf{W}}_N$ that helps us compute the N-point DFT of a $MN \times 1$ vector $\tilde{\mathbf{x}}_T$, which is comprised not only from symbols of different time slots but also of different antennas and it is structured as

$$\tilde{\mathbf{x}}_T = \begin{bmatrix} \mathbf{x}_T(1) \\ \mathbf{x}_T(2) \\ \vdots \\ \mathbf{x}_T(N) \end{bmatrix},$$

where $\mathbf{x}_T(n)$, is an $M \times 1$ vector, and represents the n-th time domain sample which is transmitted from the M transmit antennas. In other words, $\tilde{\mathbf{x}}_T$ is $\mathbf{X}_T$ written in a vector form.

Now, the frequency selective MIMO channel can be reshaped into a $KN \times MN$ block matrix as

$$\tilde{\mathbf{H}}_F = \begin{bmatrix} \tilde{\mathbf{H}}_{F1} & 0 & \dots & 0 \\ 0 & \tilde{\mathbf{H}}_{F2} & \dots & 0 \\ \vdots & \vdots & \ddots & \vdots \\ 0 & 0 & \dots & \tilde{\mathbf{H}}_{FN} \end{bmatrix},$$

where $\tilde{\mathbf{H}}_{Fn}$ is a $K \times M$ matrix that denotes the channel frequency response over the n-th sub-carrier, with $n = 1, 2, \dots, N$ and its elements $\tilde{H}_{Fn}(k, m)$ denoting the fading coefficient from the m-th transmit antenna to the k-th UT.

Finally, the DFT matrix $\tilde{\mathbf{W}}_N$, that is used to compute the N-point DFT by multiplying it with $\tilde{\mathbf{x}}_T$, needs to be constructed. This matrix is the Kronecker product, $\tilde{\mathbf{W}}_N = \mathbf{W}_N \otimes \mathbf{I}_M$ defined as

$$\tilde{\mathbf{W}}_N = \begin{bmatrix} W_N(1,1)\mathbf{I}_M & W_N(1,2)\mathbf{I}_M & \dots & W_N(1,N)\mathbf{I}_M \\ W_N(2,1)\mathbf{I}_M & W_N(2,2)\mathbf{I}_M & \dots & W_N(2,N)\mathbf{I}_M \\ \vdots & \vdots & \ddots & \vdots \\ W_N(N,1)\mathbf{I}_M & W_N(N,2)\mathbf{I}_M & \dots & W_N(N,N)\mathbf{I}_M \end{bmatrix},$$

where $\mathbf{I}_M$ is the $M \times M$ identity matrix.

The problem of minimizing the MUI across all users in CE precoding MIMO-OFDM can now be formulated as a constrained least squares problem,

$$(\mathcal{P}_1) : \min_{\tilde{\mathbf{x}}_T, \beta} \; ||\tilde{\mathbf{s}} - \beta \tilde{\mathbf{H}}_F \tilde{\mathbf{W}}_N \tilde{\mathbf{x}}_T||_2^2 \tag{3.8}$$

$$s.t. \quad |\tilde{\mathbf{x}}_T(m)| = \sqrt{\frac{\gamma}{M}} \quad m = 1, ..., MN \tag{3.9}$$

$$\text{and } \beta \in \mathbb{R}, \tag{3.10}$$

where $\tilde{\mathbf{s}}$ is an $KN \times 1$ vector containing the information symbols that must be conveyed to the K UTs over the N sub-carriers. The N information symbols corresponding to the k-th UT are drawn from a constellation which is assumed to have average power equal to the target received power for this UT. Here, β is also introduced, a scalar which is applied at the receivers' side, and allows the exploitation of the array gain of the multiple BS transmit antennas, and depends on the transmitted symbols and the channel realization [105]. This factor remains constant for the whole OFDM block in order to enable its blind

estimation at the UTs. Additionally, it is kept common across all users in order to decrease the computational complexity and achieve performance fairness among the UTs.

The problem formulation $\mathcal{P}_1$ means that we are searching for the vector $\tilde{\mathbf{x}}_T$ with elements of constant amplitude equal to $\sqrt{\gamma/M}$, as well as the factor β that minimize the distance between the vector of information symbols $\tilde{\mathbf{s}}$ and the FFT of the received noiseless signal $\tilde{\mathbf{H}}_F\tilde{\mathbf{W}}\tilde{\mathbf{x}}_T$. Additionally, it is assumed that the UTs rescale the received signal by β before using an ML detector to estimate the transmitted signal. The choice to address the case of the noiseless received signals was made in order to achieve a solution that is as computationally efficient as possible since the problem of CE MIMO-OFDM is already a hard problem to tackle.

Once the optimal vector $\tilde{\mathbf{x}}_T^*$ is computed, the IFFT does not have to be computed as in classic OFDM because our signal is already in the time domain. However, the cyclic prefix with length of LM samples still has to be prepended at the beginning of $\tilde{\mathbf{x}}_T^*$. After that, the signal is transmitted by loading to the M antennas during the n-th time slot the symbols $[\tilde{\mathbf{x}}_T^*((n-1)M+1),\ \tilde{\mathbf{x}}_T^*((n-1)M+2),\ \ldots,\ \tilde{\mathbf{x}}_T^*(nM)]$.

At each UT, after the removal of the first L samples of the received signal which correspond to the cyclic prefix, the N-point FFT of the received signal is computed. By concatenating the outputs of the FFT from all the UTs we get

$$\tilde{\mathbf{y}}_F = \tilde{\mathbf{H}}_F\tilde{\mathbf{W}}_N\tilde{\mathbf{x}}_T + \tilde{\mathbf{z}}_F \tag{3.11}$$

where $\tilde{\mathbf{y}}_F$ is a $KN \times 1$ vector and $\tilde{\mathbf{z}}_F$ a $KN \times 1$ vector formed by the noise samples in the frequency domain. Each receiver must estimate the factor β and scale the signal accordingly before making a decision on the transmitted symbols. The factor can be estimated blindly or using pilot symbols as it was proposed in [105]. Here, $\hat{\beta}_k$ is estimated blindly at the receiver according to the equation

$$\hat{\beta}_k = \sqrt{\frac{||\mathcal{Q}||^2/M_Q + N_0}{||\mathbf{y}_F^{(k)}||^2/N}}, \tag{3.12}$$

where $\mathcal{Q}$ is the employed constellation, M_Q is the order of the constellation and $\mathbf{y}_F^{(k)}$ is the $N \times 1$ output of the FFT at the k-th receiver. It should be noted that although β is common for all UTs, the estimated $\hat{\beta}_k$ may have small variations among the UTs since each UT uses only $\mathbf{y}_F^{(k)}$ to estimate it. Finally, each UT employs a simple ML detector on the scaled signal $\hat{\beta}_k\mathbf{y}_F^{(k)}$ to estimate the symbols that have been sent.

3.1.3 CE Transmitter Architecture

gh In a transmitter operating with a conventional precoder, such as a Zero-Forcing precoder, the large envelope fluctuations of the signal would lead to significant non-linear distortions by the power amplifiers. In order to mitigate the distortion each amplifier has to work in its linear region, but this leads to a low power efficiency, [78]. On the other hand, a system that uses CE signals

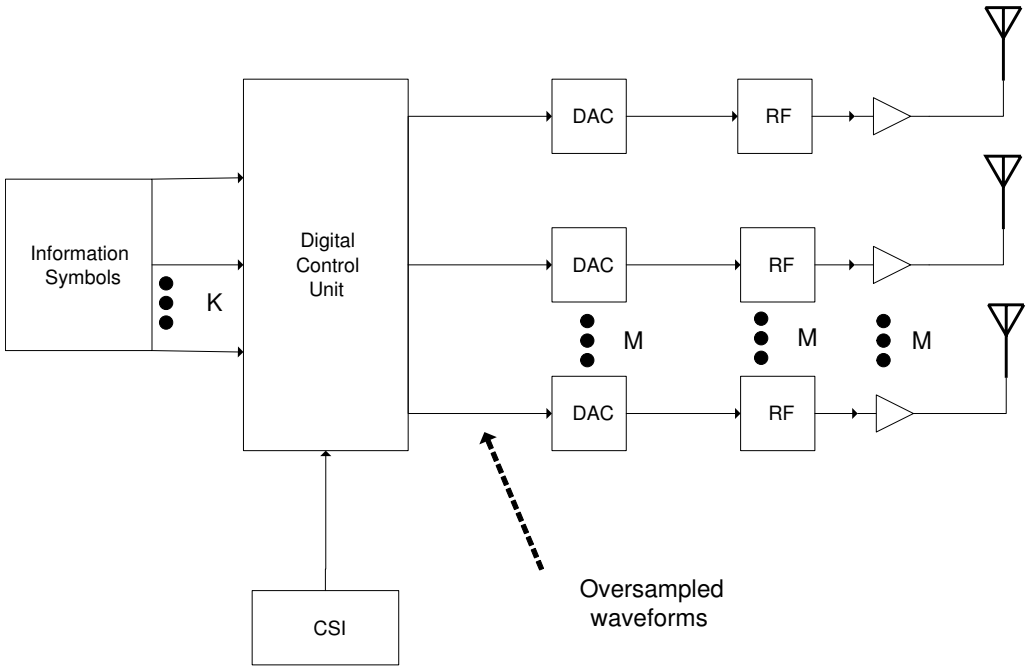

FIGURE 3.1: Block diagram of the CE MIMO-OFDM transmitter with a DAC per antenna.

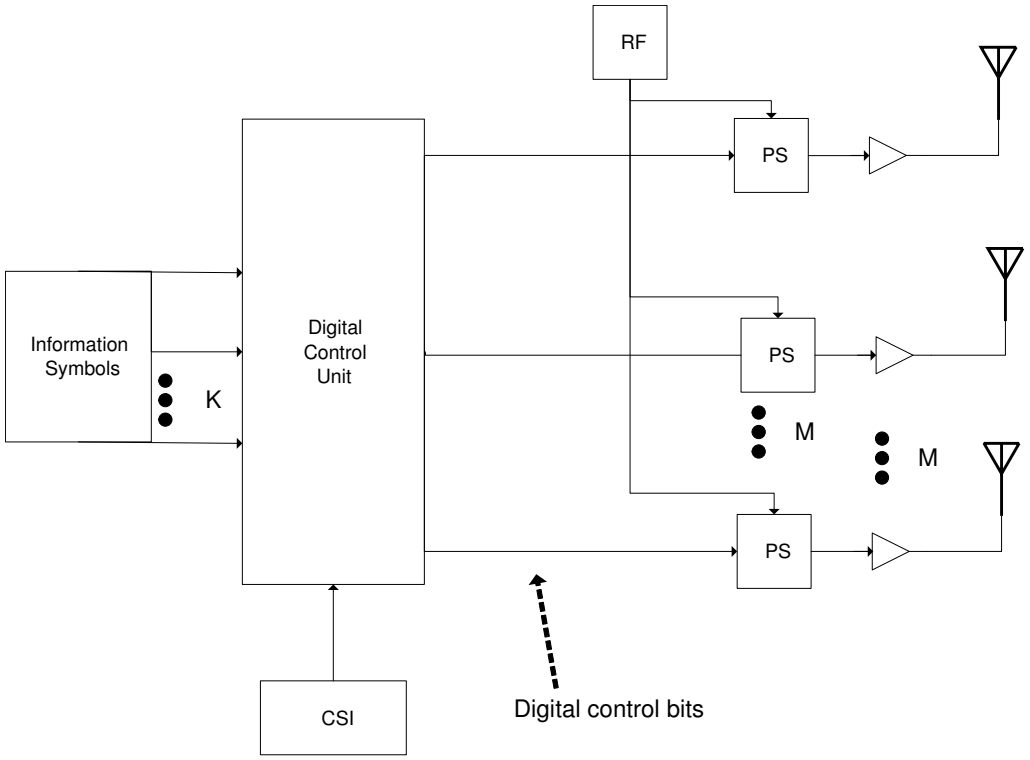

FIGURE 3.2: Block diagram of the CE MIMO-OFDM transmitter with 1-PS per antenna.

such as the one proposed here is not affected by the distortions produced by amplitude non-linearities when appropriate filtering is used, [135].

In order to quantify the effects of the power amplifier on the transmitted

signal the model for a solid state power amplifier (SSPA) presented in [78] is going to be used, in which the time domain envelope response also referred to as AM/AM characteristic is given by

$$g(A) = A_{o,max} \frac{A/A_{max}}{\left[1 + (A/A_{max})^{2p}\right]^{\frac{1}{2p}}}, \tag{3.13}$$

where A is the envelope of the input signal given by

$$A = |\tilde{\mathbf{x}}_T|, \tag{3.14}$$

$A_{o.max}$ is the maximum amplitude of the output signal given by

$$A_{o,max} = \upsilon A_{max}, \tag{3.15}$$

with υ denoting the signal gain of the amplifier and A_{max} is the input reference amplitude. Finally, p is a positive parameter that controls the smoothness of the transition from the linear region to the limiting region. According to [78] the AM/PM conversion of an SSPA is assumed to be very small and therefore can be neglected.

The average power amplifier efficiency of such an amplifier, according to [78], is given by

$$\eta = \frac{\pi}{4} \frac{E[A_o^2]}{A_{o,max} E[A_o]}, \tag{3.16}$$

where A_o is the envelope of the output signal.

A classic large-scale antenna array BS would require a dedicated RF chain and DAC for each transmit antenna, as it is shown in Fig.3.1, which makes the system very inefficient as the power consumption greatly increases when a large-scale antenna with hundreds of elements is used. The proposed per antenna CE precoding means that the power consumption of the transmitter can be reduced because it facilitates the operation of the PAs in their non-linear region where they are more power efficient. However, there can be further gains in power efficiency by altering the transmitter's architecture so that it fully exploits the CE nature of the signal.

The proposed system transmits signals from each antenna that do not change in amplitude but only in phase, since the CE signal can be written as

$$\tilde{\mathbf{x}}_T = \sqrt{\frac{\gamma}{M}} e^{\imath\tilde{\theta}}, \tag{3.17}$$

where $\tilde{\theta}$ is an $MN \times 1$ vector which contains the phase shifts of the transmit signal for one OFDM block of N sub-carriers across the M transmit antennas of the BS. Additionally, contrary to classic OFDM systems where each sub-carrier is modulated separately before computing the IFFT, here the CE time domain signal is computed in a digital processing unit so that the N-point FFT at each UT will be as close as possible to the information symbols that we want to convey. Therefore, it is not necessary to use a DAC at each transmit antenna,

which would consume power, to produce the baseband signal. Motivated by these reasons, it is proposed to use in place of the M DACs, M digitally controlled PSs as shown in Fig.3.2, which will alter the phase of the sinusoidal carrier wave according to $\tilde{\theta}$ at each antenna in order to produce the transmit signal $\tilde{\mathbf{x}}_T$.

To underline the gains from using PSs to modulate the RF signal instead of DACs the approximation of the power consumption of a transmitter utilizing DACs and of one utilizing PSs is provided, using the models developed in [82], [127]. The consumed power of the fully digital architectures shown in Fig.3.1 is given by

$$P_{FD} = \frac{E[||\tilde{\mathbf{x}}_T||_2^2]}{\eta} + M(P_{DAC} + P_{LO} + P_{mix} + P_{fil}), \tag{3.18}$$

where P_{DAC}, P_{LO}, P_{mix}, P_{fil} is the power consumed by a DAC, a local oscillator, a mixer, and a filter of the transmitter respectively, while the consumed power of the CE transmitter that uses PSs shown in Fig.3.2 is given by

$$P_{RF-CE} = \frac{E[||\tilde{\mathbf{x}}_T||_2^2]}{\eta} + M(P_{PS} + P_{LO} + P_{mix} + P_{fil}), \tag{3.19}$$

where P_{PS} is the power consumed by a phase shifter. Since the consumed power by the PSs is significantly smaller than the one by the DACs the gains become very significant as the number of transmit antennas M increase.

3.2 CE MIMO-OFDM precoding design

In this section, two iterative algorithms for solving the precoding problem $(\mathcal{P}_1)$ are presented. The first is an alternating minimization algorithm based on CD. In the following subsection problem $(\mathcal{P}_1)$ will reformulated into an unconstrained non-linear least-squares problem and will be solved using the Gauss-Newton algorithm.

3.2.1 Coordinate Descent

CD is an easily implementable and efficient method where the cost function is minimized at each iteration over one coordinate direction [128] and CD based methods have been successfully used in the past to solve similar type optimization problems. This practically means that when we minimize over the i-th coordinate, $\tilde{x}_{Ti}$, the rest, $\tilde{x}_{Tr}$ for $r \neq i$, are kept fixed to their previous values. As a result a full iteration of CD includes as many sub-iterations as the number of coordinates, in our problem MN. Additionally, apart from minimizing the cost function of $(\mathcal{P}_1)$ over $\tilde{\mathbf{x}}_T$ we also have the factor β, and therefore we have to resort to alternating optimization. Finally, before we move on with a more detailed explanation of the iterative solution, let us slightly reformulate $(\mathcal{P}_1)$ by replacing the matrix multiplication in the cost function with an equivalent

Algorithm 3 CD CE MIMO-OFDM

Input: $\tilde{\mathbf{Q}}$, $\tilde{\mathbf{s}}$
Initialize β , $\tilde{\mathbf{x}}_T$
while $\left|\beta^{(n)} - \beta^{(n-1)}\right| \leq \epsilon_1$ **do**
    while $\left|\tilde{\mathbf{x}}_T(j) - \tilde{\mathbf{x}}_T^{(j-1)}\right| \leq \epsilon_2$ **do**
        for $i = 1$ to MN **do**
            Update x_{Ti}, according to (3.23)
        end for
    end while
    Update the value of β, according to (3.25)
end while
Output: $\tilde{\mathbf{x}}_T$, β

$KN \times MN$ matrix $\tilde{\mathbf{Q}} = \tilde{\mathbf{H}}_F \tilde{\mathbf{W}}_N$ we obtain

$$(\mathcal{P}_2) : \min_{\tilde{\mathbf{x}}_T, \beta} ||\tilde{\mathbf{s}} - \beta \tilde{\mathbf{Q}} \tilde{\mathbf{x}}_T||_2^2 \tag{3.20}$$

$$s.t. \quad |\tilde{\mathbf{x}}_{\mathbf{T}m}| = \sqrt{\frac{\gamma}{M}} \quad m = 1, ..., MN \tag{3.21}$$

$$\text{and } \beta \in \mathbb{R}. \tag{3.22}$$

Algorithm 3 presents the CD based solution in pseudocode. The algorithm is initialized by providing as inputs $\tilde{\mathbf{Q}}$ and the vector of information symbols $\tilde{\mathbf{s}}$ that must be conveyed to the UT. The algorithm at the i-th sub-iteration minimizes the objective function over $\tilde{x}_{Ti}$ while keeping all the other coordinates, including β, fixed. This results to the update step

$$\tilde{x}_{Ti} = \Pr\left(\frac{\beta \tilde{\mathbf{Q}}_{\mathbf{i}}{}^H (\tilde{\mathbf{s}} - \beta \tilde{\mathbf{Q}}_{-i} \tilde{\mathbf{x}}_{\mathbf{T}-i})}{\beta \tilde{\mathbf{Q}}_i^H \beta \tilde{\mathbf{Q}}_i} \right), \tag{3.23}$$

where $\tilde{\mathbf{Q}}_i$ is the i-th column of $\tilde{\mathbf{Q}}$, $\tilde{\mathbf{x}}_{\mathbf{T}-i}$ is the vector produced after removing the i-th element of $\tilde{\mathbf{x}}_T$, $\tilde{\mathbf{Q}}_{-i}$ is the matrix produced after removing the i-th column of $\tilde{\mathbf{Q}}$ and $\Pr(u)$ is the projection of u onto the circle with radius $\sqrt{\gamma/M}$ given by

$$Pr\,(u) = \begin{cases} u & |u| = 0 \\ \sqrt{\dfrac{\gamma}{M}} \dfrac{u}{|u|} & |u| \neq 0. \end{cases}$$

The convergence criterion for $\tilde{\mathbf{x}}_T$ is

$$\left|\tilde{\mathbf{x}}_T^{(j)} - \tilde{\mathbf{x}}_T^{(j-1)}\right| \leq \epsilon_2, \tag{3.24}$$

where $\tilde{\mathbf{x}}_T^{(j)}$ is the result of the j-th update and ϵ_2 is a predefined tolerance. After this criterion is met the algorithm moves to minimize the objective function over

β which results to the update step

$$\beta = \frac{\Re\{\tilde{\mathbf{s}}^H \tilde{\mathbf{Q}} \tilde{\mathbf{x}}_T\}}{||\tilde{\mathbf{Q}} \tilde{\mathbf{x}}_T||_2^2}. \tag{3.25}$$

Following the update of β the CD algorithm repeats the same update steps until the termination criterion, which is defined as

$$\left|\beta^{(n)} - \beta^{(n-1)}\right| \leq \epsilon_1, \tag{3.26}$$

is reached. Then, the algorithm outputs the optimal $\tilde{\mathbf{x}}_T$ which is of constant amplitude equal to $\sqrt{\gamma/M}$ and β. The transmitter has no further use for β, since the UTs will blindly estimate it using (3.12) before detecting the transmitted symbols.

Finally, $\tilde{\mathbf{x}}_T$ has to be converted from a single $MN \times 1$ column to N parallel $M \times 1$ vectors corresponding to the N time slots of the OFDM block. As a result at the n-th time slot the signal

$$\begin{bmatrix} \tilde{x}_T((n-1)M+1) \\ \tilde{x}_T((n-1)M+2) \\ \vdots \\ \tilde{x}_T((n-1)M+M) \end{bmatrix}$$

is transmitted from the M antennas of the BS. In case the transmitter uses digitally controlled analog phase shifters, as in Fig.3.1 then we need the phase shifts that the PSs will impose on the RF signal. These angles can be easily extracted from $\tilde{\mathbf{x}}_T$ by calculating

$$\tilde{\theta} = \mathrm{Arg}(\tilde{\mathbf{x}}_T), \tag{3.27}$$

where Arg is the principal value of a complex number.

The problem $(\mathcal{P}_2)$ that is tackled here is non-convex and therefore the solutions are not guaranteed to be optimal. However, as the numerical results show in section V. the solution is sufficient for reliable communications as it reduces sufficiently the average MUI energy, and achieves low SER.

Finally, let us briefly discuss the computational complexity of the proposed CD based algorithm. In order to estimate the complexity of the proposed solution, the number of FLOPS (floating point operations per second) per iteration of the algorithm as a function of the size of the matrices and vectors that are involved, were computed. The computational complexity in FLOPS of an iteration which updates one coordinate is given by

$$C_{CE,CDperiter} = 4KN^2M + 8KN + 6, \tag{3.28}$$

or in big $\mathcal{O}$ notation, $\mathcal{O}(KN^2M)$. However, in order to update all the coordinates the CD algorithm needs to perform MN updates. Therefore for a full iteration of the algorithm, the complexity is given by

$$C_{CE,CD} = MN(4KN^2M + 8KN + 6), \tag{3.29}$$

or in big $\mathcal{O}$ notation, $\mathcal{O}(KN^3M^2)$. The computation costs that were used to calculate the expressions above can be found in [130]. While it was observed that the algorithm converges after a few dozens of full iterations, a theoretical analysis of its convergence is an open problem. Even for cases where the addressed problem is convex [128] the convergence analysis is extremely challenging. Therefore, the convergence analysis of the non-convex problem that is tackled here cannot be addressed within the scope of this work.

3.2.2 Gauss-Newton

The proposed CD based method becomes computationally inefficient as the number of sub-carriers and the number of antennas increases, as (3.29) shows. As a reminder, a full iteration of the algorithm proposed in the previous section consists of MN, the number of optimization variables, sub-iterations and therefore an increase in the number of sub-carriers or antennas by ΔN or ΔM translates to $M\Delta N$ and $M\Delta M$ respectively, increase of sub-iterations in each full iteration. Here, the reformulation of the problem $(\mathcal{P}_2)$ into an unconstrained non-linear least squares problem is presented and solved using the simple and efficient Gauss-Newton (GN) method. GN minimizes a sum of squared functions and does so in a computational efficient way because it does not require the analytic expression for the Hessian matrix as other competing iterative methods [136]. Additionally, it has a quadratic convergence when the initial guess is relatively close to the optimal value [136].

The CE transmit signal in (3.17) can also be written as

$$\tilde{\mathbf{x}}_T = \sqrt{\frac{\gamma}{M}}(\cos\tilde{\theta} + \imath \sin\tilde{\theta}). \tag{3.30}$$

As a result we can rewrite $\mathcal{P}_3$ as

$$(\mathcal{P}_3): \min_{\mathbf{v}} \ ||\tilde{\mathbf{s}} - \beta\tilde{\mathbf{Q}}\sqrt{\frac{\gamma}{M}}(\cos\tilde{\theta} + \imath \sin\tilde{\theta})||_2^2, \tag{3.31}$$

where $\mathbf{v} = [\tilde{\theta}^T \ \ \beta]^T$. Finally, in order to eliminate the imaginary unit, the residual vector $\mathbf{r}(\mathbf{v})$, $2KN \times 1$, is defined by separating the real and imaginary parts of the cost function of $(\mathcal{P}_3)$ as

$$\mathbf{r}(\mathbf{v}) = \begin{bmatrix} \Re\{\tilde{\mathbf{s}}\} - \beta\sqrt{\frac{\gamma}{M}}(\Re\{\tilde{\mathbf{Q}}\}\cos\tilde{\theta} - \Im\{\tilde{\mathbf{Q}}\}\sin\tilde{\theta}) \\ \Im\{\tilde{\mathbf{s}}\} - \beta\sqrt{\frac{\gamma}{M}}(\Re\{\tilde{\mathbf{Q}}\}\sin\tilde{\theta} + \Im\{\tilde{\mathbf{Q}}\}\cos\tilde{\theta}) \end{bmatrix}.$$

Now, the CE MIMO-OFDM problem can be expressed in a form that can be solved using the GN method for under-determined non-linear least squares [136], as

Algorithm 4 GN CE MIMO-OFDM

1: **Input:** $\tilde{\mathbf{Q}}$, $\tilde{\mathbf{s}}$
2: **Initialize** $\mathbf{v}$
3: **while** $\left|\mathbf{v}^{(j)} - \mathbf{v}^{(j-1)}\right| \leq \epsilon$ or $j \leq$ maxIter **do**
4: Calculate $\mathbf{r}(\mathbf{v}^{(j-1)})$, according to (3.38)
5: Calculate $\mathbf{J}_r(\mathbf{v}^{(j-1)})$, according to (3.39)
6: Calculate $\mathbf{v}^{(j)}$, according to (3.36)
7: **end while**
8: **Output:** $\mathbf{v}$

$$(\mathcal{P}_4): \min_{\mathbf{v}\in\mathbb{R}^{MN+1}} f(\mathbf{v}) := \frac{1}{2}\sum_{i=1}^{2KN} \mathbf{r}_i(\mathbf{v})^2 = \frac{1}{2}||\mathbf{r}(\mathbf{v})||_2^2. \tag{3.32}$$

GN is an alternation of the Newton's method where we use an approximation of the Hessian that does not require information about the second order derivative. In Newton's method in order to find the search direction $\mathbf{p}_N$ we must solve the system $\nabla^2 f(\mathbf{v})\mathbf{p}_N = -\nabla f(\mathbf{x})$. In GN the Hessian is approximated as

$$\nabla^2 f(\mathbf{v}) \approx \mathbf{J}_r^T \mathbf{J}_r, \tag{3.33}$$

where $\mathbf{J}_r$ is the Jacobian matrix with its (i, j)-element defined as

$$\mathbf{J}_{\mathbf{r}ij} = \frac{\partial r_i(\mathbf{v})}{\partial \mathrm{v}_j}. \tag{3.34}$$

We arrive at the approximation (3.33) by setting $\mathbf{D}(\mathbf{v}) = \sum_{i=1}^{2KN} r_i(\mathbf{v})\nabla^2 r_i(\mathbf{v})$ to zero, since $\nabla^2 f(\mathbf{v}) = \mathbf{J}_r^T\mathbf{J}_r + \mathbf{D}(\mathbf{v})$. The approximation $\mathbf{D}(\mathbf{v}) = 0$ is valid either when $\mathbf{v}$ is close to the solution $\mathbf{v}^*$ because the residuals $\mathbf{r}$ there are close to affine [136] (therefore $\nabla^2 r_i(\mathbf{v})$ is relatively small) or $\mathbf{v}$ leads to small residuals ($r_i(\mathbf{v})$ is relatively small). As a consequence, in order for the assumption to be valid and for the algorithm to quickly converge, it needs to be initialized with a $\mathbf{v}$ that results to a small residual $\mathbf{r}(\mathbf{v})$.

As a result, in order to obtain the search direction $\mathbf{p}_{GN}$ of GN we must solve

$$\mathbf{J}_r^T\mathbf{J}_r\mathbf{p}_{GN} = -\mathbf{J}_r^T\mathbf{r}(\mathbf{v}). \tag{3.35}$$

Finally, by solving the system above [136], the update step for the $j+1$-th iteration of the method is derived and is given by,

$$\mathbf{v}^{(j+1)} = \mathbf{v}^{(j)} - \mathbf{J_r}^T(\mathbf{J_r}\mathbf{J_r}^T)^{-1}\mathbf{r}(\mathbf{v}^{(j)}). \tag{3.36}$$

Let us now take a closer look at the details of the implementation of the proposed algorithm, shown in pseudocode in Algorithm 4. For the first step of the algorithm, which is to initialize $\mathbf{v}^{(0)} = [\tilde{\theta}^{(0)T}\beta^{(0)}]^T$, the Zero Forcing

precoding vector is computed, as

$$\tilde{\mathbf{x}}_{TZF} = \tilde{\mathbf{Q}}^H(\tilde{\mathbf{Q}}\tilde{\mathbf{Q}}^H)^{-1}\tilde{\mathbf{s}}, \tag{3.37}$$

the initial angles are calculated, as $\tilde{\theta}^{(\mathbf{0})} = \text{Arg}(\tilde{\mathbf{x}}_{TZF})$ and the initial $\beta^{(0)}$ as in (3.25). Next, the j-th, with $j = 1, 2, ..., maxIter$ iteration of the algorithm begins by computing the residuals as

$$\mathbf{r}(\mathbf{v}^{(\mathbf{j-1})}) = \begin{bmatrix} \Re\{\tilde{\mathbf{s}} - \beta^{(j-1)}\tilde{\mathbf{Q}}\frac{e^{\imath\tilde{\theta}^{(\mathbf{j-1})}}}{\sqrt{M}}\} \\ \Im\{\tilde{\mathbf{s}} - \beta^{(j-1)}\tilde{\mathbf{Q}}\frac{e^{\imath\tilde{\theta}^{(\mathbf{j-1})}}}{\sqrt{M}}\} \end{bmatrix}. \tag{3.38}$$

After that, the Jacobian $\mathbf{J}_r(\mathbf{v}^{(j-1)})$ is constructed in the following way

1. we create a $KN \times MN$ matrix $\boldsymbol{\Theta}$ by repeating KN times the vector $[\tilde{\theta}^{(j-1)}]^T$
2. we compute the element wise multiplication $\mathbf{A} = \left[\imath\beta\tilde{\mathbf{Q}}. * \frac{e^{\imath\boldsymbol{\Theta}}}{\sqrt{M}}\right]$
3. we compute the multiplication $\mathbf{B} = \tilde{\mathbf{Q}}\frac{e^{\imath\tilde{\theta}^{(j-1)}}}{\sqrt{M}}$
4. Finally, we get $\mathbf{J}_r$ as

$$\mathbf{J}_r(\mathbf{v}^{(j-1)}) = -\begin{bmatrix} \Re\{[\mathbf{A}\ \mathbf{B}]\} \\ \Im\{[\mathbf{A}\ \mathbf{B}]\} \end{bmatrix} \tag{3.39}$$

Each iteration is completed by updating the value of $\mathbf{v}$ according to (3.36). The algorithm is terminated either when the termination criterion, $\left|\mathbf{v}^{(j)} - \mathbf{v}^{(j-1)}\right| \leq \epsilon$, is met or when the number of maximum iterations, $maxIter$, is reached.

GN method can be improved in order to avoid divergence if the cost function does not decrease in every update step. Since $\mathbf{p}_{GN}$ is a descent direction it is true that $f(\mathbf{v} + \alpha\mathbf{p}_{GN}) < f(\mathbf{v})$ for a sufficiently small $\alpha \in (0, 1)$. The update step is changed to accordingly to

$$\mathbf{v}^{(j+1)} = \mathbf{v}^{(j)} - \alpha\mathbf{J_r}^T(\mathbf{J_r}\mathbf{J_r}^T)^{-1}\mathbf{r}(\mathbf{v}^{(j)}). \tag{3.40}$$

and the value of α can be determined by employing a line search algorithm such as Armijo-line search. In our numerical simulations the algorithm always converged without the need for a step size control and therefore the additional complexity that it would introduce is omitted from the computation of the computational complexity of the algorithm.

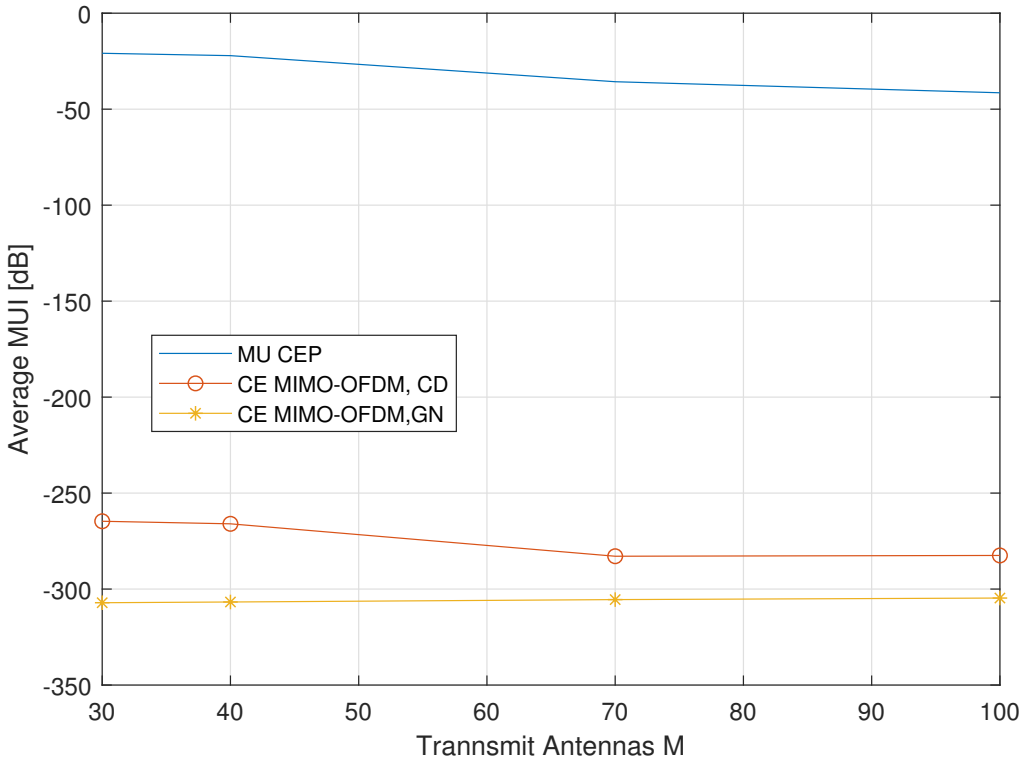

FIGURE 3.3: Average MUI of different CE MIMO-OFDM algorithms for $N = 64$ sub-carriers and $K = 10$ UTs.

Finally, the computational complexity of one iteration of the GN algorithm in FLOPS, using the computation costs found in [130], is given by

$$C_{CE,GN} = 8K^3N^3M + 64K^3N^3 + 12K^2N^2 \tag{3.41}$$
$$+4KN^2M - 2KN - MN, \tag{3.42}$$

or in big $\mathcal{O}$ notation, $\mathcal{O}(K^3N^3M)$. It is observed that the proposed algorithm reaches convergence in less than 10 iterations.

3.3 Numerical Results

In this section various simulation results of the CE MIMO-OFDM system will be presented and will be compared with the performance of the two proposed algorithms in this chapter as well as the algorithm that was proposed in [124] for single carrier CE precoding in frequency selective channels and was then proposed again in [123] for CE precoding in OFDM systems. ZF precoding, as was described in (3.37), is also going to be used as a benchmark scheme. In the results that follow a multipath MIMO channel with $\nu = 8$ resolvable taps, that follow an i.i.d Circularly Symmetric Complex Gaussian distribution with zero mean and variance equal to $1/\nu$, $\mathcal{CN}(0, 1/\nu)$, was assumed. The PAs are assumed to have unit gain and their input reference amplitude A_{max} is chosen so that for a CE signal of a given amplitude they operate at 1dB backoff. The termination criteria for the algorithms are chosen to be $\epsilon = \epsilon_1 = \epsilon_2 = 10^{-15}$.

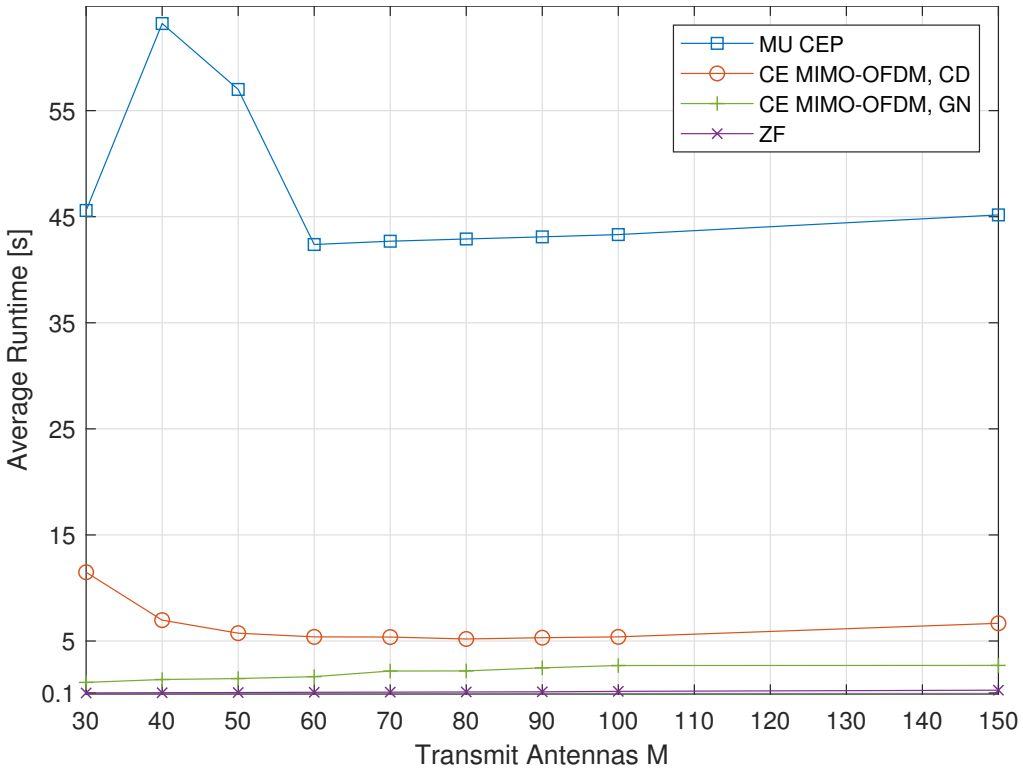

FIGURE 3.4: Average runtime of the different CE MIMO-OFDM algorithms and ZF precoding for $N = 64$ sub-carriers and $K = 10$ UTs.

Additionally, the QAM constellations that are employed are normalized to have average unit power. Finally, in the simulations below β is estimated blindly at the receiver unless it is stated otherwise.

In Fig. 3.3,the average MUI energy is presented, which is defined as

$$\frac{1}{KN} E_{\tilde{\mathbf{H}}_F, \tilde{\mathbf{x}}_T}[||\tilde{\mathbf{s}} - \tilde{\mathbf{H}}_F \tilde{\mathbf{W}} \tilde{\mathbf{x}}_T||_2^2], \tag{3.43}$$

of a system with $K = 10$ UTs, $N = 64$ sub-carriers and 16-QAM modulation of the two proposed algorithms for CE MIMO-OFDM in addition to the algorithm presented in [123], [124] for CE precoding over frequency selective channels. The algorithm in the literature rather than transforming the CE problem in the frequency domain as the algorithms here, attempts to find the CE precoding vector in the time domain by calculating the convolution of the channel and the transmit signal at each iteration of the algorithm thus leading to a solution with a higher complexity than the ones proposed here. Additionally, in the competing solution a heuristic splitting of the transmit angles into blocks is performed that can lead to an increased interference. Indeed, it is observed that the algorithm for CEP in [124] produces an MUI of about -20 dB when the BS is equipped with 30 transmit antennas and decreases down to about -45 dB as the number of transmit antennas reaches 100. On the other hand, the solutions that were proposed here show an excellent performance by reducing the MUI to less than -250 dB even when the number of transmit antennas is

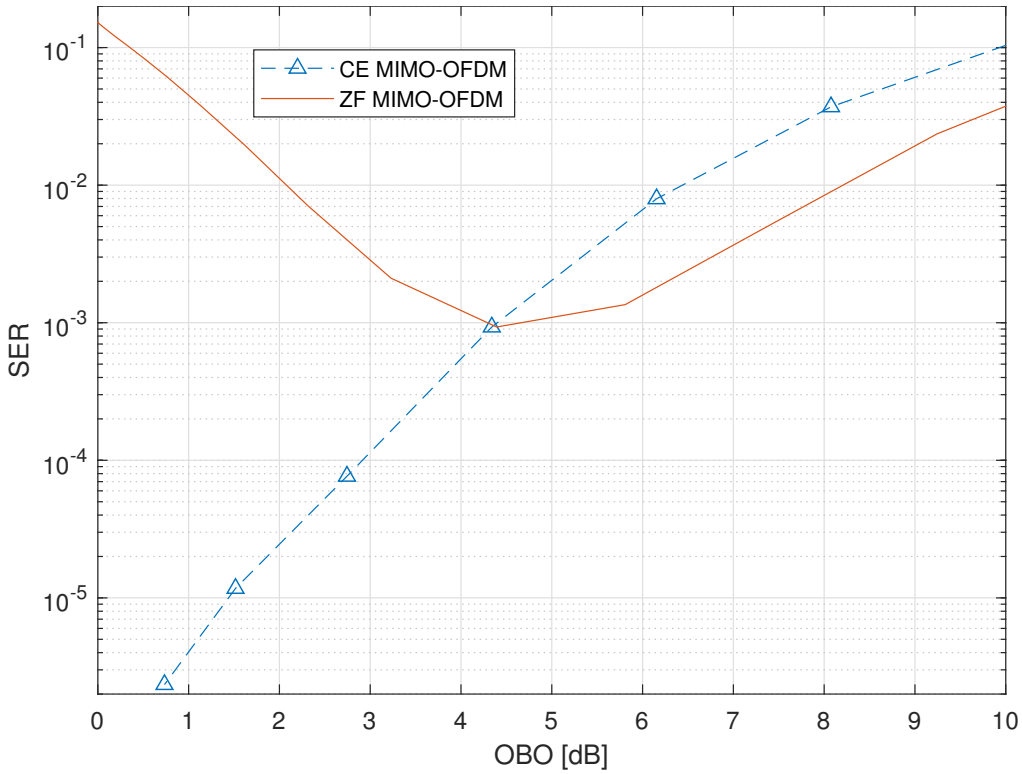

FIGURE 3.5: SER as a function of OBO for a system with $K = 10$ UTs, $M = 50$ BS antennas, $N = 64$ sub-carriers and $16 - QAM$.

30. This is a result of the efficient proposed model where a heuristic splitting is not necessary, as in [124], and also of the introduction of β which partially compensates for the lack of amplitude control at the transmitter. Finally, we observe that of the two studied algorithms, the Gauss-Newton solution yields the best results when it comes to reducing the average MUI, as it manages to reach solutions closer to better minima.

Next, in Fig. 3.4, the average runtimes, on a system equipped with an intel core i7 $-$ 8750H CPU, 16 GB RAM and 256 GB SSD, of the GN, CD algorithms as well as the one proposed in [124] for a system with $K = 10$ UTs, $N = 64$ sub-carriers and 16-QAM modulation, are presented. It can be observed that the proposed solutions for CE MIMO-OFDM precoding take significantly less time to converge than the competing algorithm in the literature, and as it was shown in Fig. 3.3 they also converge to better solutions. The peak in runtime that is observed for the MU CEP when the number of transmit antennas is between 30-50 is due to the fact that the maximum number of iterations is reached without reaching convergence. This shows us that this solution is not suitable when the ratio of UTs to transmit antennas K/M is relatively large. On the other hand, the results show that the most computationally efficient algorithm is the proposed GN as its runtime is less than 5 seconds when $M = 100$ while CD needs about 6 seconds to converge for the same number of transmit antennas. The gap between the two is much larger for a small number of transmit antennas and this is because CD needs a few hundreds of iterations to converge in such

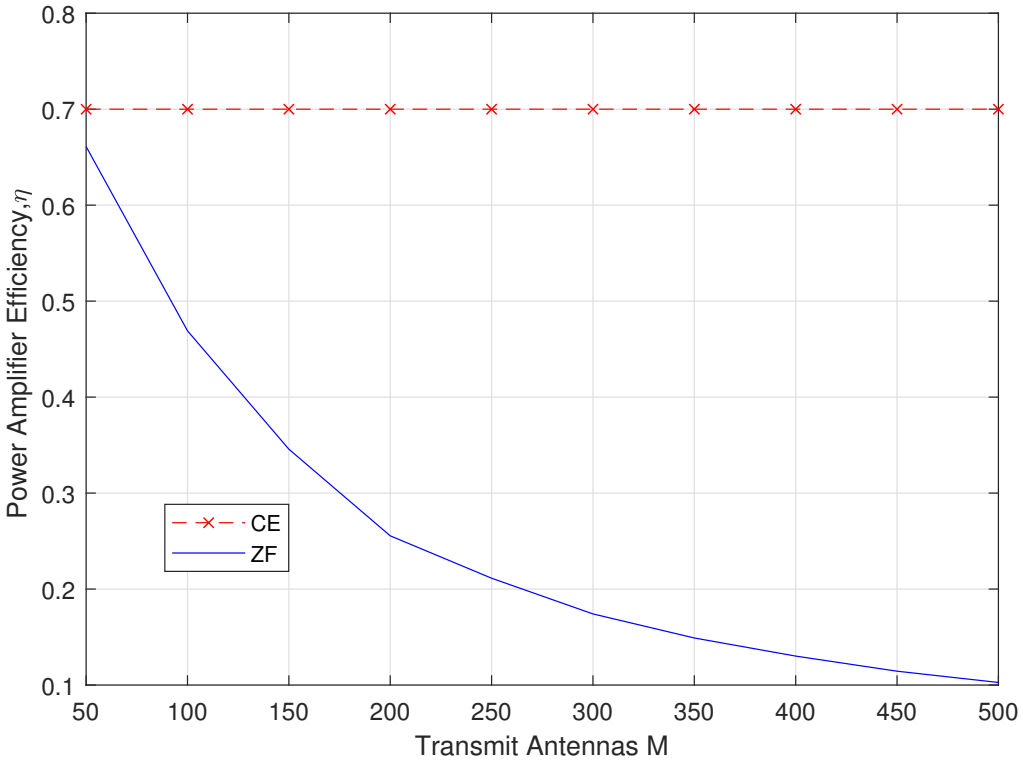

FIGURE 3.6: Average power amplifier efficiency, given by (3.16), for a system with $M = 100$, $N = 64$, $K = 10$ and 16-QAM.

scenarios while GN always converges in less than ten iterations. However, as the number of antennas increases the number of iterations for CD decreases almost proportional to $1/(M^2)$ and this justifies the observed average runtime of the algorithm. Finally, the average runtime of ZF precoding for MIMO-OFDM is almost ten times smaller than the runtime of GN ranging from 0.1 seconds when is $M = 30$ to 0.36 seconds when $M = 150$. This gap in computational complexity is expected as ZF precoding does not need an iterative algorithm to run but rather a simple matrix inversion. However, the following results are going to show that CE MIMO-OFDM makes up for the increased complexity with gains in SER performance as well as energy efficiency.

In Fig. 3.5, the SER performance of CE and ZF precoding is presented in MIMO-OFDM systems for different output backoff values of the PAs. The output backoff (OBO) of an amplifier is given by [78]

$$OBO = 10log\frac{P_o}{P_x}dB, \tag{3.44}$$

where P_o denotes the maximum output power of the amplifier and P_x is the average output power of the transmitted signal $\mathbf{x}_T$. Additionally the following values have been used for the PAs, $A_{max} = \upsilon = A_{o,max} = 1$ and $p = 2$. We observe that as the OBO decreases the SER performance of CE precoding constantly improves, while on the other hand the performance of ZF precoding reaches its best performance at $4.2dB$ OBO and after that it deteriorates significantly. In order to decrease the OBO of a given PA the average power of the

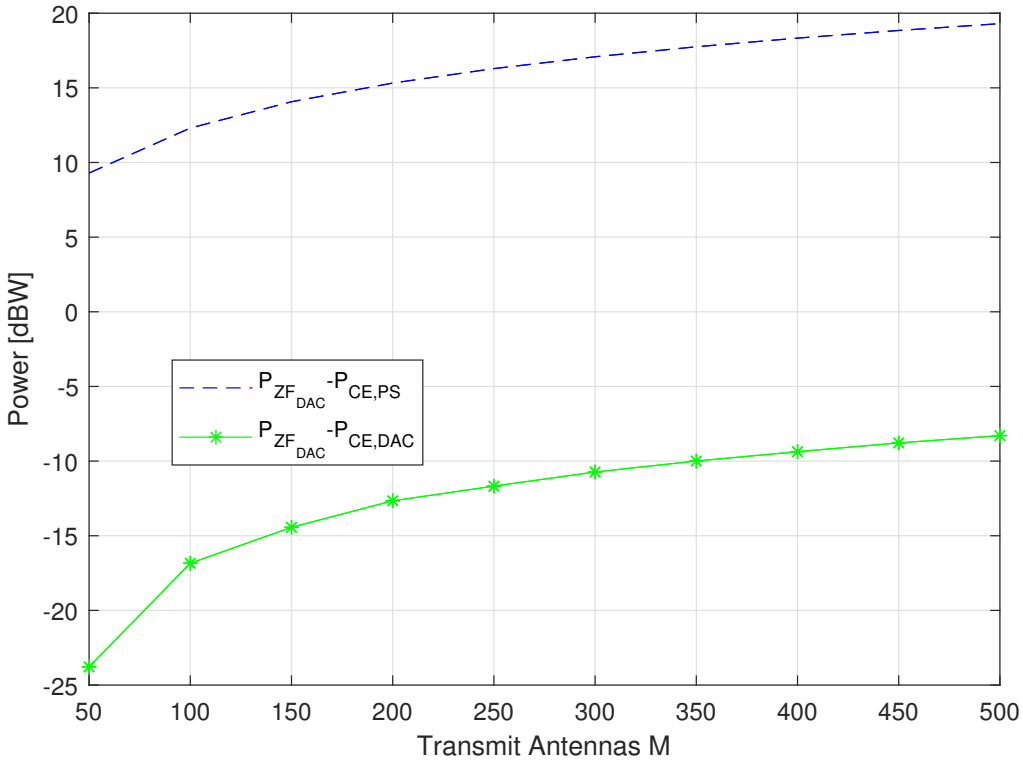

FIGURE 3.7: Power consumption gains of the proposed CE precoding architectures over a fully-digital architecture for ZF precoding, for a system with $M = 100$, $N = 64$, $K = 10$ and 16-QAM.

transmit signal $\mathbf{x}_T$ has to be increased. By doing so we also increase the value of the envelope of the signal A. Increasing the envelope of the signal results to significant non-linear effects which are modelled by the denominator in Eq. (3.13). Therefore the increase of transmit power which leads to the decrease of OBO drives the PA into its non-linear region. This induces significant harm to the ZF signal but does not affect the CE signal.

In Fig. 3.6, the average power amplifier efficiency , given by (3.16), is compared in the cases that CE and ZF precoding is employed. It is observed that when CE precoding is used, η remains constant and equal to 0.7 regardless of the number of transmit antennas while when ZF precoding is employed the efficiency falls from about 0.66 to 0.1 as the number of transmit antennas increases from $M = 30$ to $M = 100$. This is the result of the high PAR of the ZF MIMO-OFDM signal and it demonstrates why low PAR techniques such as CE MIMO-OFDM are necessary for large scale antenna systems.

In Fig. 3.7 the power consumption difference between the architectures for CE MIMO-OFDM and the fully digital architecture for ZF MIMO-OFDM is plotted. The difference between CE and ZF precoding when it comes to power consumption is that the power amplifiers have a different average power efficiency as we discussed in the previous paragraph. Additionally, as it was mentioned in a previous section CE precoding can be implemented in a system that uses power-efficient PSs instead of DACs. We acquire the plots by assuming the following power consumption values for the components $P_{DAC} = 200$mW,

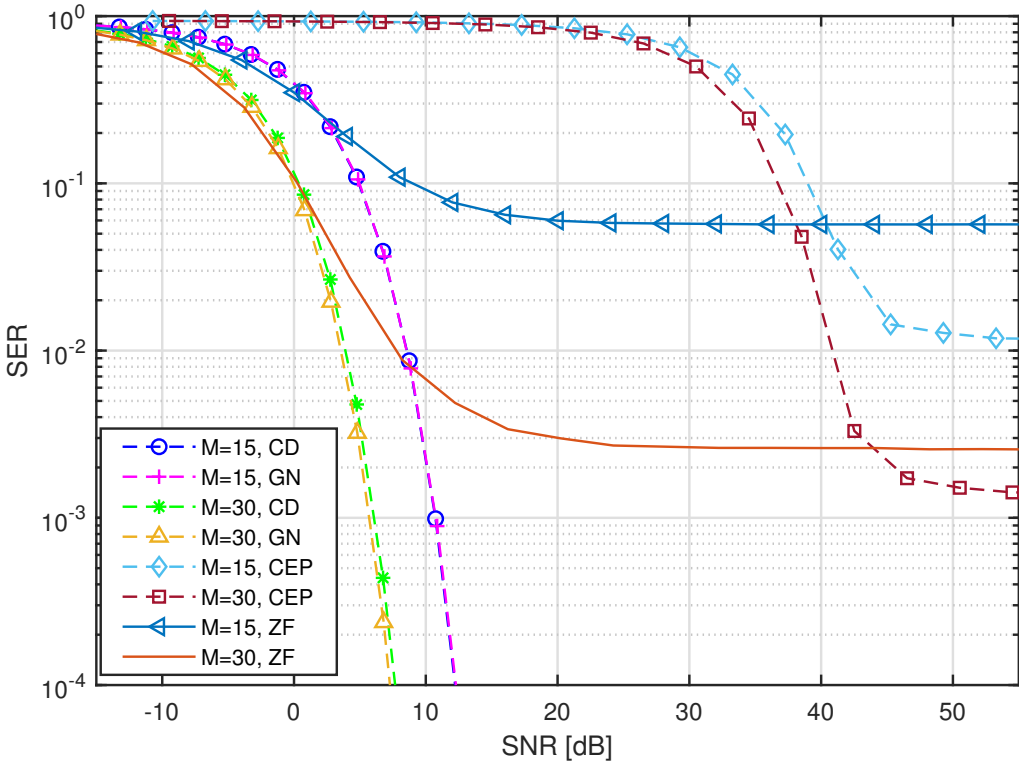

FIGURE 3.8: SER performance of ZF, the two proposed CE MIMO-OFDM algorithms and the algorithm for CEP in [124] for a system with $K = 5$ UTs and $N = 32$ sub-carriers and 16-QAM modulation.

$P_{LO} = 5$mW, $P_{mix} = 19$mW, $P_{fil} = 14$mW, $P_{PS} = 30$mW, [82], [127] and using the power consumption approximations given by (3.18) and (3.19). We observe that both architectures for CE precoding have increasing gains in power consumption over the fully digital architecture for ZF precoding as the number of transmit antennas increases. Additionally, a further decrease in the power consumption is achieved by about 30 dBW when using the analog architecture with phase shifters rather than DACs. These results show that these architectures, and especially the analog one, are suitable candidates for large MIMO systems when the objective is to reduce the power consumption.

In Fig. 3.8, the SER performance of different configurations of the two proposed algorithms will now be presented and compared with the ZF precoder as well as the algorithm that is proposed for CEP in [124] and is used in [123] for OFDM transmission. All systems have PAs which operate at the same point in order to have comparable efficiency. The first thing to observe is that the SER performance of the two algorithms is almost identical and so it becomes evident that when taking into account their computational efficiency, as was shown in Fig. 3.4, the GN algorithm is far more suitable for the CE MIMO-OFDM system. Furthermore, we observe that in both cases when $M = 15$ and $M = 30$ the CE precoding shows better performance than ZF precoding. The bad performance of the ZF precoder and the observed error floor is a result of the in band distortion that is introduced by the non-linear power amplifier. On the other hand CE MIMO-OFDM does not suffer from this because of its

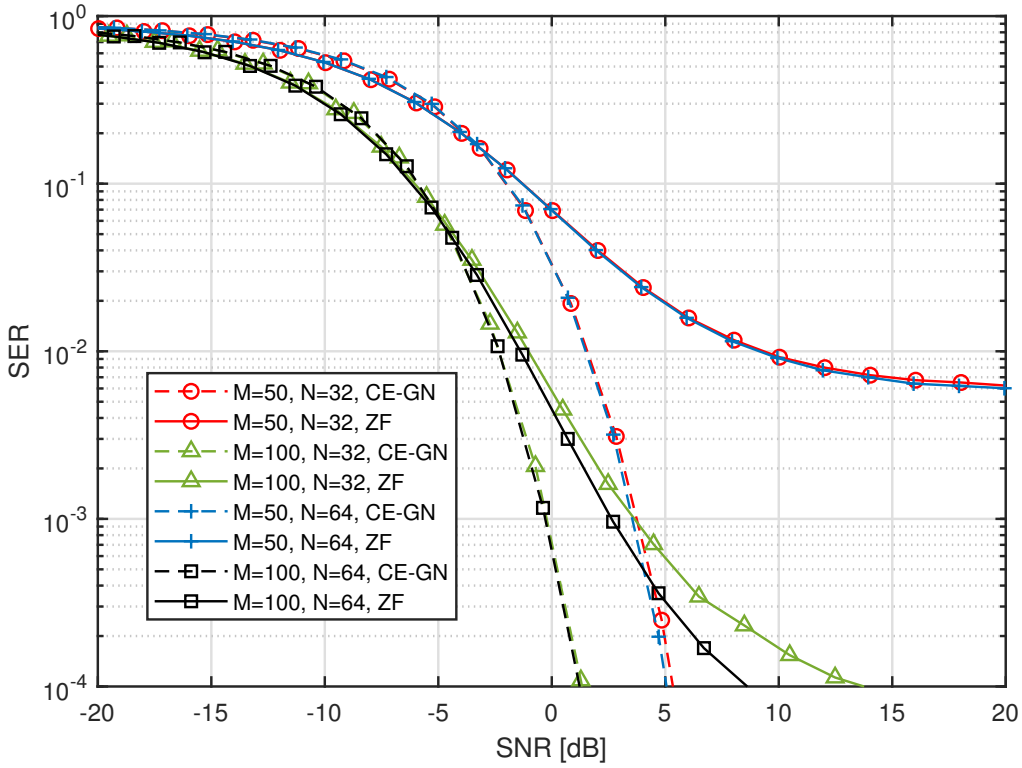

FIGURE 3.9: SER performance of the GN algorithm CE MIMO-OFDM algorithms for a system with $K = 10$ UTs and 16-QAM modulation.

constant envelope nature. Finally, when compared to prior art CE precoding for OFDM systems [123],[124], the advantage of our system model and algorithmic solutions becomes apparent as it outperforms the prior art scheme by more than $30dB$. This is a result that highlights the importance of the improved formulation which enables efficient algorithmic solutions as well as the different system model which scales the signal at the UTs by β.

In Fig. 3.9, the SER performance of the GN algorithm for a different number of sub-carriers N and transmit antennas M is presented and compared with the ZF precoding scheme. Firstly, it is observed that the performance of CE MIMO-OFDM remains identical when the number of sub-carriers is increased from 32 to 64. This is not true for ZF precoding as we observe that when $M = 100$ there is a widening gap between the SER curves that correspond to $N = 64$ and $N = 32$ sub-carriers. The reason for this gap is that a different number of sub-carriers leads to a different PAR in the case of ZF precoding, which results to an increased distortion by non-linear amplification. Although, CE MIMO-OFDM precoding performs significantly better than ZF precoding in every scenario it is observed that the performance gap becomes smaller as the number of transmit antennas increases from 50 to 100. However, it should also be taken into account that as the number of transmit antennas increases the efficiency of the power amplifiers decreases as it was shown in Fig. 3.6. Therefore, ZF precoding, or any other precoding with high PAR, forces the designer of the system to choose the best trade off between power efficiency and error rate performance, while

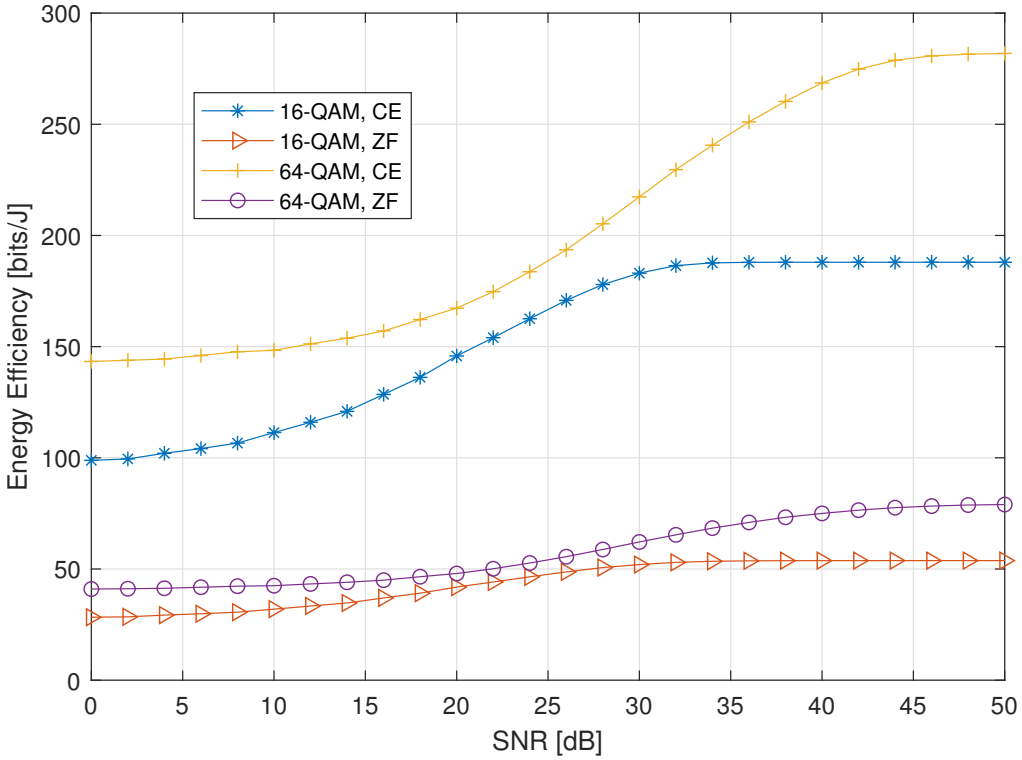

FIGURE 3.10: Energy efficiency of systems equipped with $M = 100$ transmit antennas, $K = 10$ UTs and $N = 32$ subcarriers.

CE precoding has always high power amplifier efficiency without impeding the performance of the system.

In the figures above while the superiority in SER performance of the proposed CE MIMO-OFDM precoding is clearly shown there is not a clear connection with the power consumption gains of the proposed architecture for CE MIMO-OFDM precoding. To this end, the metric of energy efficiency as defined in [88] is used,

$$EE(P_{kn}^e, b, K, N) = \frac{\sum_{n=1}^{N}\sum_{k=1}^{K}(1 - P_{kn}^e)b}{P}, \tag{3.45}$$

where P_{kn}^e is the bit error probability per UT and per subcarrier, b is the number of bits per constellation symbol and P denotes the power that is consumed by the transmitter and is given by (3.18) or (3.19). In Fig. 3.10 it is shown that the power efficient components that are used by the transmitter of CE MIMO-OFDM result in a significantly better energy efficiency when compared to ZF precoding. What is more, it is proved that CE MIMO-OFDM precoding can employ higher order modulations such as $64-QAM$ that result in a significantly better rate and overall energy efficiency. On the other hand ZF precoding, does not only have poorer SER performance as it was discussed above, but its overall power consumption drives its energy efficiency down. Finally, the increase of the modulation order to $64-QAM$ does not yield the same improvement in rate and energy efficiency as it does for CE precoding because of the harm induced by the non-linear distortion which is becomes more damaging as the modulation

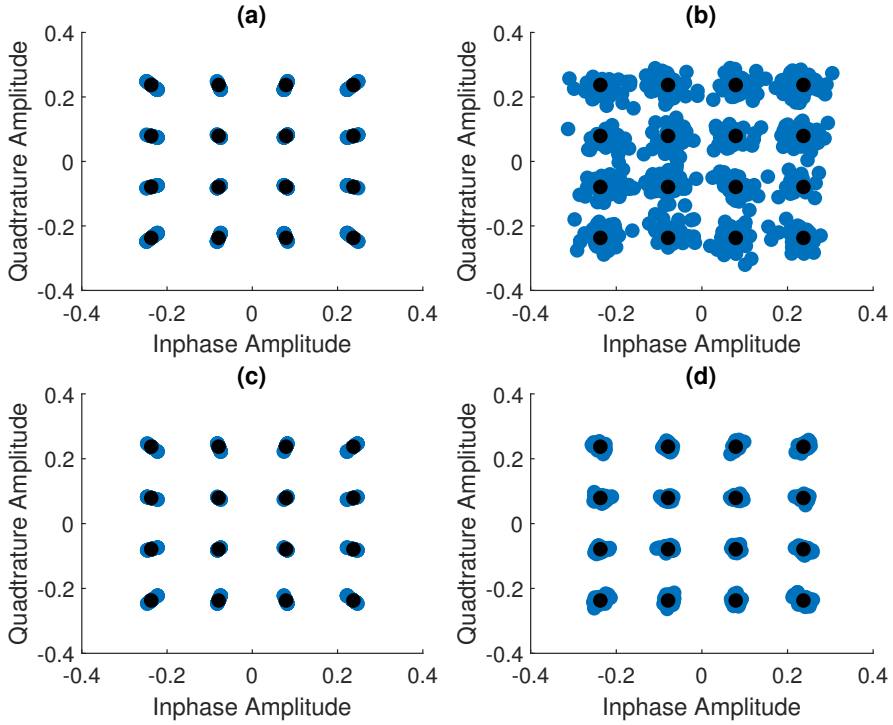

FIGURE 3.11: Received noiseless signal points when transmitting 16-QAM symbols with non-linear amplification over a MIMO frequency selective channel using $N = 64$ subcarriers (a) CE MIMO-OFDM, $M = 50$, $K = 10$, (b) ZF MIMO-OFDM, $M = 50$, $K = 10$, (c) CE MIMO-OFDM, $M = 100$, $K = 10$, (d) ZF MIMO-OFDM, $M = 100$, $K = 10$

order increases.

In order to better showcase the effect of non-linear amplification, in Fig. 3.11 the received signal points without thermal noise of a CE and ZF MIMO-OFDM system are illustrated. It is observed that for the CE system the distortion variance is very small regardless of the number of transmit antennas and as we have seen in the previous figures it does not affect negatively the SER performance. On the other hand, when ZF precoding is employed the distortion variance is very significant, especially when the number of transmit antennas is $M = 50$ which explains why we observed an error floor in the previous figures. As the number of transmit antennas increases to $M = 100$ the distortion variance decreases but so does the efficiency of the amplifier as it was shown in Fig. 3.6.

In the last two figures, the accuracy of the $\hat{\beta}_k$ blind estimation at the UTs and the effect that the different number of sub-carriers and modulation order have on its estimation and the overall performance of the system, will be examined. In Fig. 3.12 the accuracy of $\hat{\beta}_k$ is shown as a function of the SNR when $4-QAM$ and $16-QAM$ modulation is employed. The accuracy is defined as

$$\text{accuracy} = 1 - \frac{\hat{\beta}_k - \beta}{\beta}. \tag{3.46}$$

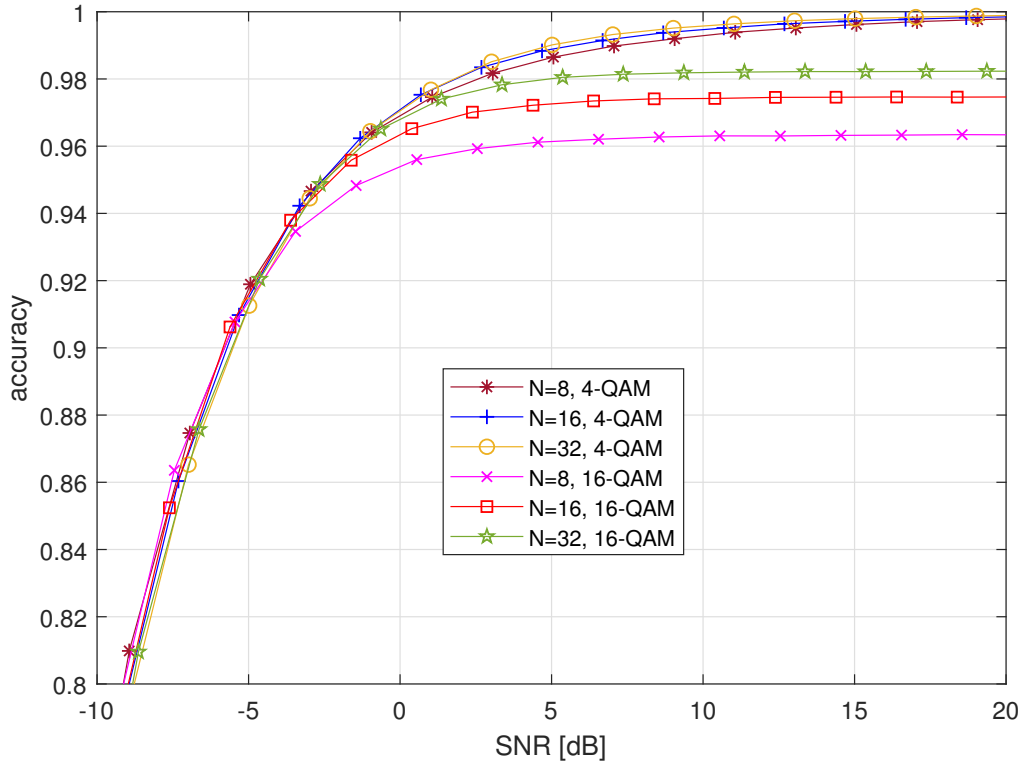

FIGURE 3.12: Accuracy of the estimated $\hat{\beta}_k$ as a function of the SNR for a system with $M = 30$ transmit antennas and $K = 5$ UTs.

We observe that as expected the accuracy of the estimation is improved as the SNR increases. The rate of the increase is dependent on the employed modulation and the length of the OFDM block. For example when 16-QAM is used in an OFDM block of 32 sub-carriers the accuracy of the estimation is 98% for an SNR value of 5dB while the accuracy drops to 96% for the same SNR when the OFDM block has only 8 sub-carriers. Furthermore, we observe that for the higher order modulation the accuracy stops increasing with the SNR after some point, thus creating the need for either using larger OFDM-blocks or inserting pilots to estimate β. In Fig. 3.13, the SER of a system that has perfect knowledge of β and one that estimates it blindly according to (3.12), are compared. We observe that when 4-QAM is used the SER of the systems that have perfect knowledge of β have identical SER performance with those that estimate it no matter the size of the OFDM block. However, for 16-QAM if the size of the OFDM block is relatively small we see that there is a gap between the system with perfect knowledge and the one with the blind estimate of β, which increases as the OFDM block size becomes smaller. This was expected, as we observed from the previous figure that the estimation accuracy took a hit when 16-QAM modulation and small OFDM blocks were used. Therefore, while β is a strong point of the proposed system that makes our algorithm converge faster to a solution and takes into account the array gain, it also introduces some trade-offs that have to be made during the implementation. If large OFDM blocks are used, as in most practical applications, then we can use high order modulations

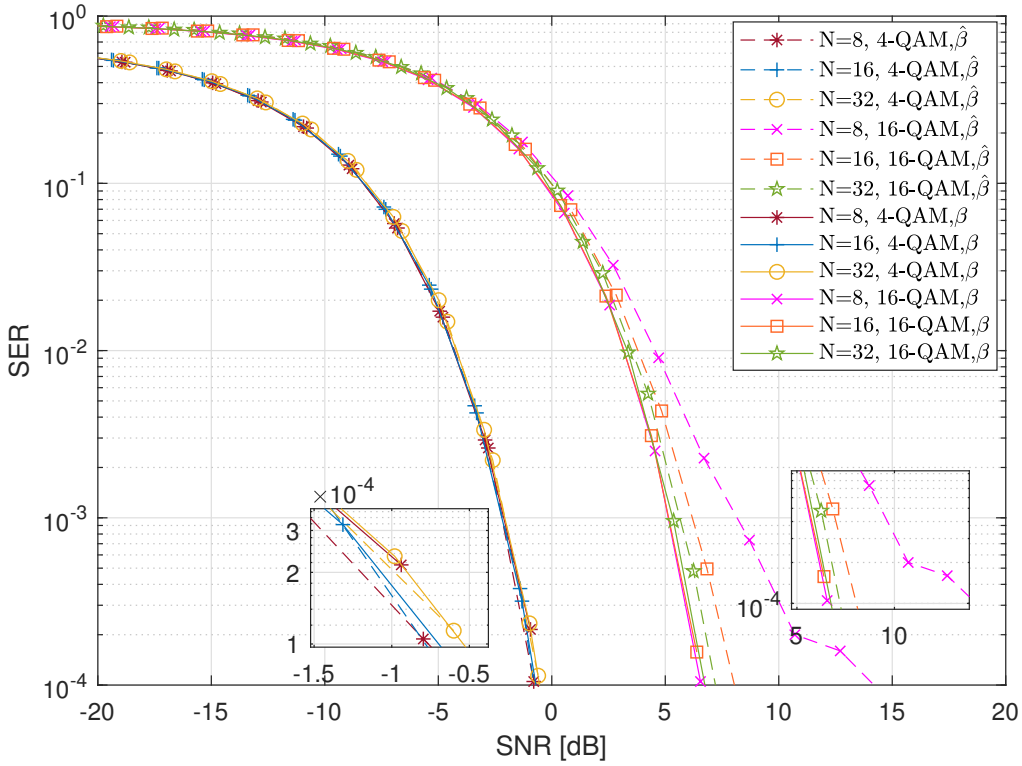

FIGURE 3.13: SER performance comparison of the proposed CE MIMO-OFDM for the cases of perfect knowledge of β and blind estimation of $\hat{\beta}_k$, in a system with $M = 30$ transmit antennas and $K = 5$ UTs.

without degrading the system performance. If on the other hand we have to use smaller OFDM blocks we either have to use lower order modulations to avoid performance degradation due to estimation error or introduce pilot symbols in order to improve the estimation of β.

3.4 Summary

In this chapter, the problem of CE MIMO-OFDM precoding was tackled. A novel formulation of the problem was presented that designed CE precoding in the frequency domain and thus enabled a computationally efficient solution. The precoding problem was initially solved using a CD based algorithm and then it was reformulated and solved using the GN method in order to decrease the computational complexity of the solution. Numerical results, showed that both solutions when compared to prior art CE precoding schemes require less computational costs and manage to reduce even further MUI and achieve good SER performance.

Chapter 4

SLP For CE MIMO-OFDM Systems With Low Resolution DACs

In this chapter, CESLP solutions for MU-MIMO systems with low resolution DACs at the transmitter's side, are presented. The proposed approach is tailored for multi-carrier systems functioning under the well-known OFDM technique.

The chapter is organized as follows. In Section 4.1, the system model and the problem formulation is given. In Section 4.2, the power consumption of the proposed architecture is modelled, In Section 4.3, the derivation of the proposed algorithmic solution for the precoder design is given. Section 4.4 presents some numerical results and Section 5.5 concludes this chapter.

4.1 System Model and Problem Formulation

In this section, the system model and problem formulation will be given. Let us consider a downlink MU-MIMO system with T antennas at the BS that serves $M < T$ single antenna users simultaneously over a frequency selective channel. The system model is shown on Fig. 4.1.

In order to mitigate the effects of the frequency selectivity of the channel, OFDM transmission is employed, where the available bandwidth for transmission W is split among N_{SC} orthogonal subcarriers with $\Delta f = W/N_{SC}$ spacing between them. The purpose of splitting the channel bandwidth is to make sure that the signal over each sub-channel will experience flat fading rather than frequency selective fading by achieving smaller sub-channel bandwidth than the coherence bandwidth of the channel. The multiuser, multipath time domain channel with L resolvable components is modelled as,

$$\mathbf{H}_T(t,m) = [h(t,m,0),\ h(t,m,2),\ \ldots.\ h(t,m,L-1)]\,, \tag{4.1}$$

where $h(t,m,i)$ denotes the ith channel tap between the tth BS antenna and the mth user.

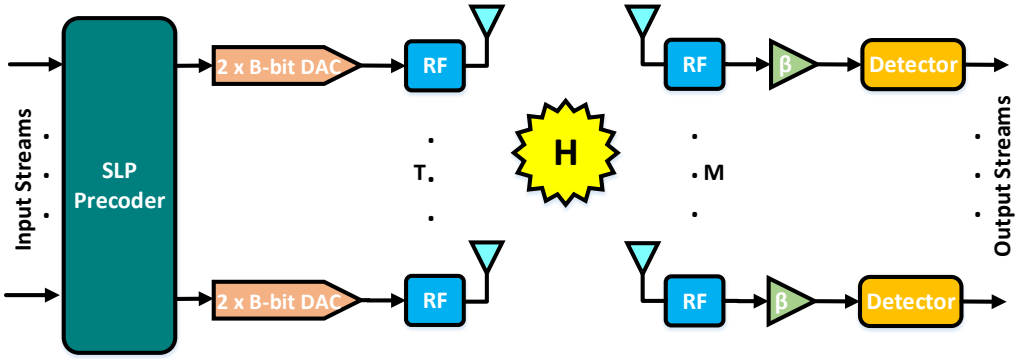

FIGURE 4.1: A MU-MIMO system of T antennas and B-bit DACs at the transmitter's side. A number of M single antenna users are assumed at the receiver's side.

The input-output relationship in the time domain is given by,

$$\mathbf{y}_T(m,n) = \sum_{t=1}^{T}\sum_{l=0}^{L-1} h(t,m,l)\mathbf{x}_T(t,n-l) + z_T(m,n), \tag{4.2}$$

with $m = 1, 2, ..., M$ and $n = 1, 2, ..., N_{SC}$, $\mathbf{x}_T(t, n-l)$ is the signal transmitted by the tth antenna at time index $n-l$ and z_T denotes the additive white complex Gaussian noise. The channel taps $h(t,m,l)$ are assumed to remain constant during the OFDM symbol time and are perfectly known at the BS side.

In OFDM, a Cyclic prefix (CP) of length $L-1$ is prepended that serves as a guard band protecting the received signal from intersymbol interference. At the receivers, the first $L-1$ samples which correspond to the CP are discarded. Then, at each user, the Fast Fourier Transform (FFT) of the received signal is computed before estimating the received information symbols. Therefore, it would be useful to provide the input-output relationship in the frequency domain, given by,

$$y_F(m,n) = \sum_{t=1}^{T} h_F(t,m,n)\mathbf{x}_F(t,n) + z_F(m,n), \tag{4.3}$$

with $n = 1, 2, \ldots, N_{SC}$ and with $h_F(t,m,n)$, $\mathbf{x}_F(t,n)$ and $z_F(m,n)$ denoting the frequency domain channel coefficients, transmitted signals and AWGN samples, respectively.

The BS is assumed to have DACs of resolution of B-bits. In general one DAC per complex dimension is employed that drive the RF hardware of each of the antenna array elements. Due to the finite resolution of the DACS the BS may select input vectors $\mathbf{x}_T(n) = [\mathbf{x}_T(1,n), \ldots, \mathbf{x}_T(T,n)]^T$ that lie in a complex domain $\mathcal{X}^T \subset \mathbb{C}^T$. Since, constant envelope signals are assumed, the entries of set $\mathcal{X}$ are derived by the discretization of the complex unit circle, i.e.,

$$\mathcal{X} = \sqrt{\frac{P}{T}}\left\{1, e^{j\frac{2\pi}{2^{B+1}}}, \cdots, e^{j\frac{2\pi\left(2^{B+1}-1\right)}{2^{B+1}}}\right\}, \tag{4.4}$$

where P is a constraint on the maximum transmission power. Furthermore, in (4.4), it has been used the fact that, DACs of resolution of B-bits are able to support 2^{B+1} discrete states over the complex unit circle.

In SLP, the BS designs the input vectors $\mathbf{x}_T(n) \in \mathcal{X}^T$ in order to transmit a desired symbol vector $\mathbf{s}(n) \in \mathcal{O}^M$ to the M users such that a performance metric is optimized. $\mathcal{O}$ is the set of the employed constellation points.

At the receivers' side, the mth user computes an estimate $\mathbf{s}'(m,n) \in \mathbb{C}$ of the transmitted symbol $\mathbf{s}(m,n) \in \mathcal{O}$ by,

$$\mathbf{s}'(m,n) = \beta_m \mathbf{y}_F(m,n), \tag{4.5}$$

where the scalar $\beta_m \in \mathbb{R}^+$ is the array gain at the mth user terminal. Note that the latter array gain is fixed for the whole block of the N_{SC} subcarriers. Then, each UE performs nearest neighbour decoding, that is the received signal is mapped to the nearest point in $\mathcal{O}$.

At this point, it would be useful to express the input-output relationship in the following matrix form,

$$\tilde{\mathbf{y}}_F = \tilde{\mathbf{H}}_F \tilde{\mathbf{x}}_F + \tilde{\mathbf{z}}_F, \tag{4.6}$$

where $\tilde{\mathbf{y}}_F$, $\tilde{\mathbf{x}}_F$ and $\tilde{\mathbf{z}}_F$ are the frequency domain $MN_{SC} \times 1$ vectors that result by concatenating the received signals, transmit signals and noise samples respectively across all the sub-carries and users. The matrix $\tilde{\mathbf{H}}_F$ is the $MN_{SC} \times MN_{SC}$ block matrix,

$$\tilde{\mathbf{H}}_F = \begin{bmatrix} \tilde{\mathbf{H}}_{F1} & 0 & \dots & 0 \\ 0 & \tilde{\mathbf{H}}_{F2} & \dots & 0 \\ \vdots & \vdots & \ddots & \vdots \\ 0 & 0 & \dots & \tilde{\mathbf{H}}_{FN_{SC}} \end{bmatrix},$$

where $\tilde{\mathbf{H}}_{Fn}$ is a $M \times T$ matrix that denotes the channel frequency response over the nth sub-carrier. Additionally, the frequency domain transmit signal $\tilde{\mathbf{x}}_F$ can be written as,

$$\tilde{\mathbf{x}}_F = \tilde{\mathbf{W}}_{N_{SC}} \tilde{\mathbf{x}}_T, \tag{4.7}$$

where $\tilde{\mathbf{x}}_T$ is time domain transmit signal and $\tilde{\mathbf{W}}_{N_{SC}} = \mathbf{W}_{N_{SC}} \otimes \mathbf{I}_T$ with $\mathbf{W}_{N_{SC}}$ being the $N_{SC} \times N_{SC}$ DFT matrix. Furthermore, let us define $\tilde{\mathbf{s}}' = \beta \mathbf{y}_F$ where it is assumed that $\beta = \beta_1 = \cdots = \beta_M$ for simplicity.

The vector $\tilde{\mathbf{x}}_T$ is designed so that the total Mean Square Error (MSE) between all the N_{SC} transmit symbols of the OFDM block concatenated in a $MN_{SC} \times 1$ vector, $\tilde{\mathbf{s}}$ and their estimates $\tilde{\mathbf{s}}'$ is minimized. The aforementioned MSE is given by,

$$\mathbb{E}_{\tilde{\mathbf{z}}_F}\{\|\tilde{\mathbf{s}} - \tilde{\mathbf{s}}'\|_F^2\} = \|\tilde{\mathbf{s}} - \beta \tilde{\mathbf{H}}_F \tilde{\mathbf{W}}_{N_{SC}} \tilde{\mathbf{x}}_T\|_2^2 + \beta^2 MN_{SC}\sigma_z^2, \tag{4.8}$$

where σ_z^2 is the noise variance.

Given that $\tilde{\mathbf{x}}_T \in \mathcal{X}^{TN_{SC} \times 1}$ and $\beta \in \mathbb{R}^+$, the design of the desired precoder can be expressed as the following constrained optimization problem,

$$(\mathcal{P}_1): \quad \min_{\tilde{\mathbf{x}}_T,\beta} \|\tilde{\mathbf{s}} - \beta\tilde{\mathbf{H}}_F\tilde{\mathbf{W}}_{N_{SC}}\tilde{\mathbf{x}}_T\|_2^2 + \beta^2 M N_{SC}\sigma_z^2$$
$$s.t. \;\; \tilde{\mathbf{x}}_T \in \mathcal{X}^{TN_{SC}\times 1}$$
$$\beta \in \mathbb{R}^+.$$

At this point, it is instructive to point out that because of the introduction of $\tilde{\mathbf{W}}_{N_{SC}}$ inside the optimization problem, the FFT operation is now integrated inside the signal design and the IFFT does not need to be computed before the transmission, as done in classical OFDM systems. Furthermore, the described system model and problem formulation is also applicable to the case of multi-antenna users. In this case, at each symbol time, a symbol is targeted to each one of the antennas of the users. By following the analysis of the present section, it can be seen that the transmit signals of the BS in $\tilde{\mathbf{x}}_T$ can be derived again as the solution to $(\mathcal{P}_1)$.

The optimization problem $(\mathcal{P}_1)$ is NP-hard. A naive exhaustive search approach could require a search over all the possible vectors $\tilde{\mathbf{x}}_T \in \mathcal{X}^{TN_{SC}\times 1}$ which has exponential complexity in the number of transmit antennas, subcarriers and the resolution of the DACs. Thus, the number of possible combinations that should be examined for the optimal one is extremely large, even for systems with very small number of antennas/subcarriers. To that end, such an approach is impossible to be realized for LSAA-based MU-MIMO systems. In Section 4.3, a new method is developed based on a Cyclic Coordinate Descent (CCD) algorithm [128] with the view to provide an efficient solution for $(\mathcal{P}_1)$.

4.2 Power Consumption Model

Let us now derive the model for the transceivers' power consumption based on the employed architecture shown on Fig. 1. The derived power consumption will be used later in Section 4.4 to plot the energy efficiency of the system. The power consumption is constituted by the power consumption for the transmission of a specific signal and the static power consumed by the system's components. Following the analysis in [127], an approximate model for the power consumption at the transmitter's side (BS) is given by,

$$P_{ct}(T, B, f_s) \approx P_{PA} + T[2P_{DAC}(B, f_s) + P_{RF}] + P_{LO}, \tag{4.9}$$

where P_{PA} is the power consumed by the Power Amplifiers (PAs) in order to transmit the intended signals, $P_{DAC}(B, F_s)$ is the power consumed by a B-bit DAC functioning with sampling frequency F_s, P_{RF} is the power consumed by the analog components of the RF chain, i.e. filters and mixers and P_{LO} is the power consumed at the local oscillator.

The power consumed by the PAs can be modeled as,

$$P_{PA} \approx \frac{\mathbb{E}\{\|\tilde{\mathbf{x}}_T\|_2^2\}}{\eta} = \frac{P}{\eta}, \tag{4.10}$$

where η is the efficiency of the PA. Note that the second part in (5.16) is due to the constant envelope property of the transmitted signal (4.4).

LSAA-based MIMO systems must be equipped with power efficient and inexpensive PAs. These criteria are met by class B amplifiers, whose average power efficiency is given by [78],

$$\eta = \frac{\pi \mathbb{E}\{g^2(|\tilde{\mathbf{x}}_T|)\}}{4 r_{o,max} \mathbb{E}\{g(|\tilde{\mathbf{x}}_T|)\}}, \tag{4.11}$$

where $g(\cdot)$ is the AM-AM conversion of the amplifier, $|\tilde{\mathbf{x}}_T|$ is the envelope of the input signal and $r_{o,max}$ is the maximum output amplitude of the amplifier. Here, a simple ideally linearised PA model [78] is considered where the AM-PM conversion is zero and the AM-AM conversion is given by,

$$g(r) = \begin{cases} r_{o,max}\left(\dfrac{r}{r_{max}}\right) & r < r_{max} \\ r_{o,max} & r \geq r_{max} \end{cases}, \tag{4.12}$$

where r_{max} denotes a given input reference amplitude level.

Now, the model of the power consumption of the DAC will be provided. According to the analysis in [127], the previous can be approximated by

$$P_{DAC}(B, f_s) \approx \frac{\alpha}{2}\left[V_{dd} I_0 (2^B - 1) + C_p f_s V_{dd}^2 B\right], \tag{4.13}$$

where V_{dd} is the power supply, I_0 is the unit current source that corresponds to the least significant bit, C_p is the parasitic capacitance of the switches used to select the DACs' supported states and α is a correcting factor that may be used to introduce some second order effects to the model. Furthermore, the sampling frequency f_s, may be approximated as $f_s = 2(2f_b + f_{cor})$, where f_b is the employed bandwidth and f_{cor} is the corner frequency of the $1/f$ noise [137].

In a similar manner, one may derive an approximate power consumption model for the single antenna system of each user. Following once more the results in [127], one may show that the consumed power at each one of the users can be approximately modeled by,

$$P_{cr}(B', f_s) \approx P_{LNA} + 2P_{ADC}(B, f_s) + P_{RF} + P_{LO}, \tag{4.14}$$

where P_{LNA} is the power consumed by the Low Noise Amplifiers (LNAs) and $P_{ADC}(B', F_s)$ is the power consumed by a B'-bit ADC functioning with sampling frequency f_s with power consumption given by [127],

$$P_{ADC}(B', f_s) \approx \frac{3 V_{dd}^2 L_{min} f_s}{2 \times 10^{-0.1525 B' + 4.838}}, \tag{4.15}$$

where L_{min} is the minimum channel length for the employed Complementary Metal Oxide Semiconductor (CMOS) technology. It is now straightforward to see that the total power consumption of a system of T antennas BS and M

Algorithm 5 CESLP for Systems with Finite Resolution DACs

Initialize $\tilde{\mathbf{x}}_T^{(0)} \in \mathcal{X}^{TN_{SC}\times 1}$, $\beta^{(0)} \in \mathbb{R}^+$. Set $\mathbf{G} = \tilde{\mathbf{H}}_F\tilde{\mathbf{W}}_{N_{SC}}$.
$\mathbf{t} = \mathbf{G}\tilde{\mathbf{x}}_T^{(0)}$
while The termination criteria in (4.20) are not met **do**
  for $1 \le l \le TN_{SC}$ **do**
    $\mathbf{t} = \mathbf{t} - \mathbf{G}_l\tilde{\mathbf{x}}_T^{(k)}(l)$
    $\tilde{\mathbf{x}}_T^{(k+1)}(l) \leftarrow \arg\min_{\xi\in\mathcal{X}} \|\tilde{\mathbf{s}} - \beta^{(k)}\mathbf{t} - \beta^{(k)}\mathbf{G}_l\xi\|_2^2$
    $\mathbf{t} = \mathbf{t} + \mathbf{G}_l\tilde{\mathbf{x}}_T^{(k+1)}(l)$
  end for
  $\beta^{(k+1)} \leftarrow \frac{\mathcal{R}\{\tilde{\mathbf{s}}^H\mathbf{G}\tilde{\mathbf{x}}_T^{(k+1)}\}}{\|\mathbf{G}\tilde{\mathbf{x}}_T^{(k+1)}\|_2^2 + MN_{SC}\sigma_z^2}$
  $k \leftarrow k+1$
end whilereturn $\tilde{\mathbf{x}}_T^{(k+1)}$, $\beta^{(k+1)}$

users is given by,

$$P_c(B, B', f_s, T, M) = P_{ct}(T, B, f_s) + MP_{cr}(B', f_s). \tag{4.16}$$

4.3 Solution

In Section 4.1, the design of the CESLP for a system with low resolution DACs has been modeled as a mixed continuous discrete least squares optimization problem $(\mathcal{P}_1)$. In the following, a new method is developed based on a Cyclic Coordinate Descent (CCD) algorithm [128] with the view to provide an efficient solution to $(\mathcal{P}_1)$.

According to the CCD methodology, we may iterate through the directions of a multivariate cost function, one at a time, minimizing the latter with respect to each coordinate direction. Thus, from $(\mathcal{P}_1)$, for the lth entry of vector $\tilde{\mathbf{x}}_T^{(k+1)}$, $\tilde{\mathbf{x}}_T^{(k+1)}(l)$ at the $(k+1)$th iteration of CCD, we have

$$\begin{aligned}\tilde{\mathbf{x}}_T^{(k+1)}(l) = \arg \min_{\xi\in\mathcal{X}^{TN_{SC}\times 1}} f_Q[&\tilde{\mathbf{x}}_T^{(k+1)}(1), \ldots, \\ &\tilde{\mathbf{x}}_T^{(k+1)}(l-1), \xi, \tilde{\mathbf{x}}_T^{(k)}(l+1), \ldots, \\ &\tilde{\mathbf{x}}_T^{(k)}(TN_{SC}), \beta^{(k)}],\end{aligned} \tag{4.17}$$

where

$$\begin{aligned}f_Q[&\tilde{\mathbf{x}}_T^{(k+1)}(1), \ldots, \tilde{\mathbf{x}}_T^{(k+1)}(l-1), \xi, \tilde{\mathbf{x}}_T^{(k)}(l+1), \\ &\ldots, \tilde{\mathbf{x}}_T^{(k)}(TN_{SC}), \beta^{(k)}] = \\ &\|\tilde{\mathbf{s}} - \beta^{(k)}\sum_{m=1}^{l-1}\mathbf{G}_m\mathbf{x}_T^{(k+1)}(m) - \beta^{(k)}\sum_{m=l+1}^{TN_{SC}}\mathbf{G}_m\mathbf{x}_T^{(k)}(m) \\ &- \beta^{(k)}\mathbf{G}_l\xi\|_2^2,\end{aligned}$$

$\beta^{(k)}$ is the update for the value of parameter β at the kth iteration and $\mathbf{G}_m$ and $\mathbf{G}_l$ are the mth and the lth column of matrix $\mathbf{G} = \tilde{\mathbf{H}}_F \tilde{\mathbf{W}}_{N_{SC}}$, respectively. Since the entry $\tilde{\mathbf{x}}_T^{k+1}(l)$ lies in $\mathcal{X}$, CCD may solve (4.17) via an one-dimensional exhaustive search over the set $\mathcal{X}$ and select the value that minimizes the cost function f_Q.

The β coordinate may be updated by solving the optimization problem,

$$\beta^{(k+1)} = \arg \min_{\beta \in \mathbb{R}^+} \|\tilde{\mathbf{s}} - \beta \mathbf{G} \tilde{\mathbf{x}}_T^{(k+1)}\|_2^2 + \beta^2 M N_{SC} \sigma_z^2, \tag{4.18}$$

which admits the closed form solution given by,

$$\beta^{(k+1)} \leftarrow \frac{\mathcal{R}\{\tilde{\mathbf{s}}^H \mathbf{G} \tilde{\mathbf{x}}_T^{(k+1)}\}}{\|\mathbf{G} \tilde{\mathbf{x}}_T^{(k+1)}\|_2^2 + M N_{SC} \sigma_z^2}, \tag{4.19}$$

where $\mathcal{R}\{\cdot\}$ is the real part of a complex number.

The computational complexity of the proposed algorithm is $O(T^2 N_{SC}^2 2^B)$ which is much smaller compared to the one of the exhaustive search approach which is $O(T N_{SC} 2^{BTN_{SC}})$.

The complete procedure is described in Algorithm 5. It is noteworthy to mention that the auxiliary vector variable $\mathbf{t}$ that appears in Algorithm 5 is introduced in order to update efficiently the quantity $\sum_{m=1}^{l-1} \mathbf{G}_m \mathbf{x}_T^{(k+1)}(m) + \sum_{m=l+1}^{TN_{SC}} \mathbf{G}_m \mathbf{x}_T^{(k)}(m)$, among the iterations/cycles of the CCD. The CCD terminates when the following criteria are met

$$\|\tilde{\mathbf{x}}_T^{(k+1)} - \tilde{\mathbf{x}}_T^{(k)}\|_2 \leq \epsilon_x \ \& \ |\beta^{(k+1)} - \beta^{(k)}| \leq \epsilon_b. \tag{4.20}$$

In practice, it has been observed that the algorithm requires a few tenths of iterations to reach convergence. A theoretical study of the convergence of Algorithm 5 is still an open problem. In general, the derivation of theoretical results for CCD-based solutions can be a very challenging task even for cases that the addressed optimization problem is convex [128], [138]. As consequence, theoretical results for the convergence of Algorithm 5 that solves the nonconvex problem ($\mathcal{P}_1$) are a very difficult if not impossible task that cannot be addressed within the context of the present work.

4.4 Numerical Results

In this section, numerical results are presented in order to study the performance of the proposed solutions. Furthermore, their performance is compared to the ones of a) the existing literature solution [125], b) the CESLP precoding for infinite resolution DACs for which an efficient solution can be found in [139] and c) the well-known Zeroforcing (ZF) precoder when quantized such that the output signals are of constant envelope and can support the resolution of the employed DACs, i.e., lie in the set $\mathcal{X}$ in (4.4) [140]. We will refer to the latter approach as the quantized ZF solution. A system of $T = 64$ antennas at the BS is assumed. All of the involved channels are derived via a multipath model of

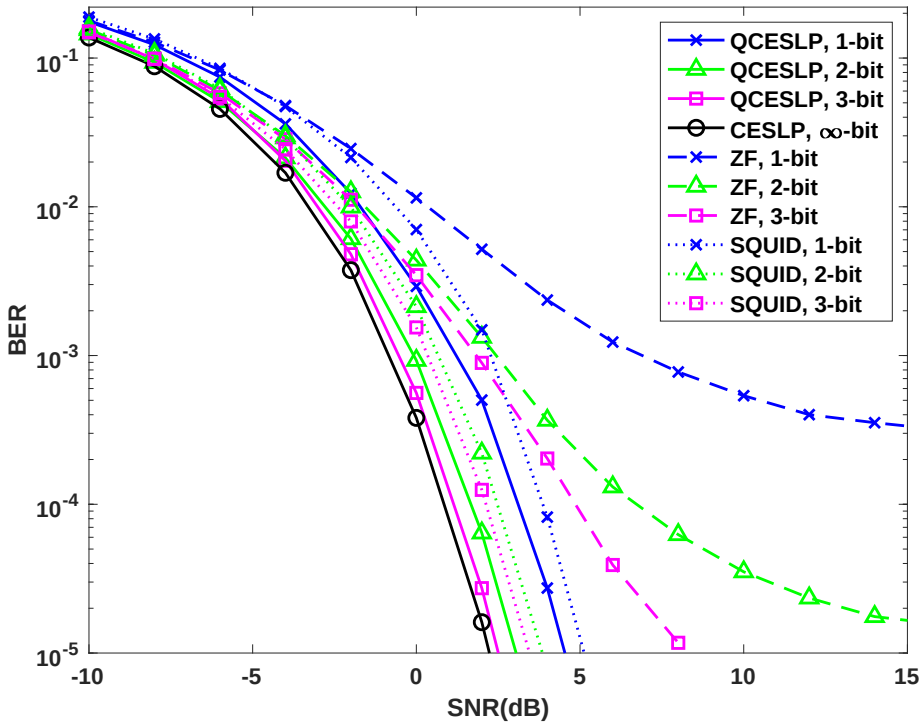

FIGURE 4.2: Impact of the DACs' resolution to the performance of a system employing QPSK on OFDM with $T = 64$ antennas, $M = 8$ users and $N_{sc} = 32$ subcarriers.

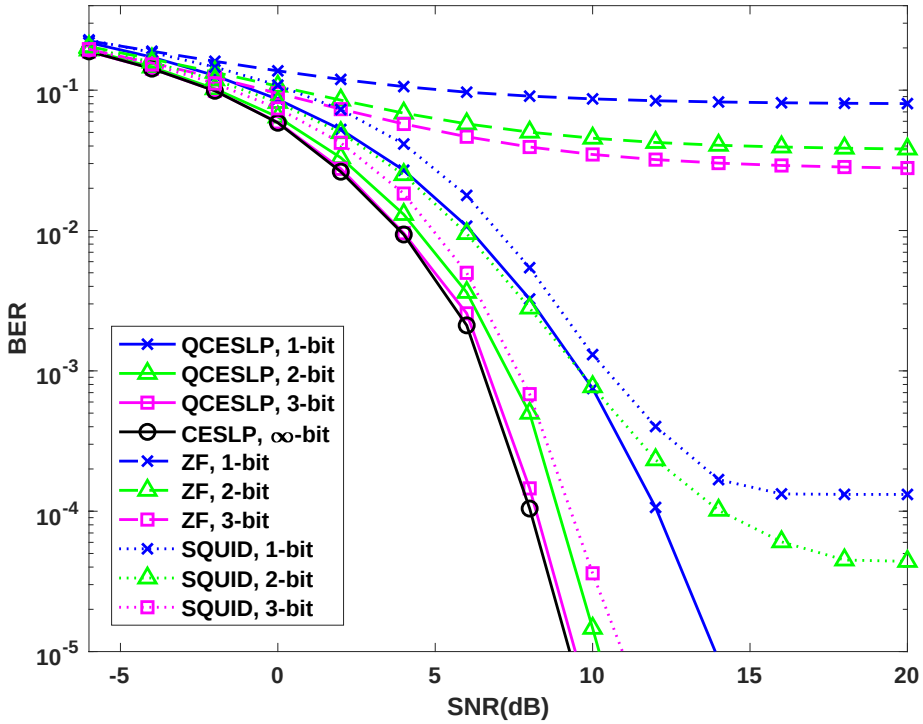

FIGURE 4.3: Impact of the DACs' resolution to the performance of a system employing 16QAM on OFDM with $T = 64$ antennas, $M = 8$ users and $N_{sc} = 32$ subcarriers.

$L = 10$ resolvable taps, that follow an i.i.d Circularly Symmetric Complex Gaussian distribution with zero mean and variance equal to $1/L$, i.e., $\mathcal{CN}(0, 1/L)$. The performance is examined with respect the average uncoded Bit Error Rate (BER) and the energy efficiency achieved by each one of the techniques for different transmit Signal-to-Noise-Ratio (SNR) values. The transmit SNR here is defined as $\mathbb{E}\{\|\mathbf{x}_T(n)\|_2^2\}/\sigma_z^2 = P/\sigma_z^2$. The equality holds due to the constant envelope property of the transmitted signals. The results are averaged over 10^5 channel realizations.

4.4.1 Bit Error Rate

At first the BER performance of a system of $M = 8$ users is examined employing the OFDM technique with $N_{sc} = 32$ subcarriers for DACs of different resolution (1,2 and 3 bits). In Fig. 4.2, the results of the Quadrature Phase Shift Keying (QPSK) modulation are shown whereas in Fig. 4.3, the ones for the 16 Quadrature Amplitude Modulation (16QAM) are depicted, respectively. The proposed solution is designated by the label "QCESLP, X-bit", where "X" is the supported resolution by the DACs. In the same figures the performance of the quantized ZF approach ("ZF, X-bit") and the one of the nonlinear precoder in [125] ("SQUID, X-bit") are also plotted. Furthermore, the performance of a system applying the CESLP technique in [139] for infinite resolution DACs is also depicted ("CESLP").

The performance of the proposed approach is very close to the one of the infinite resolution DACs even for low resolutions such as 2 or 3 bits. Furthermore, the proposed technique is able to achieve significantly improved performance for both the QPSK and 16QAM cases when compared to the approach in [125]. Furthermore, the approach in [125] appears to present a floor error for the cases of 1,2-bit DACs in 16QAM after the SNR = 15dB value. The proposed approach appears to not have similar problems. In addition, the proposed technique presents significantly improved performance as compared to the one of the quantized ZF approach. It is also noteworthy to point out that the quantized ZF approach presents very poor performance when applied to the 16QAM case since the BER curves present a floor error as the SNR value increases. Thus, even though it is a tempting solution due to its simplicity, since it can be derived by the quantization of a closed form solution, it appears to exhibit significant degradation on the performance as the constellation order increases. As a general conclusion, the results in Figs. 4.2-4.3 verify the efficiency of the proposed solution and shows that the performance can be very close to the ideal one (infinite resolution DACs), even if DACs of very low resolution are employed.

Next, the performance of the proposed technique is examined with respect the number of the users that are simultaneously served by the BS. The cases of $M = 2, 4, 8, 16, 24$ users are considered. The resolution of the DACs is fixed to $B = 1$ bit for all of the examined cases. The rest of the parameters are set as in the experimental setup of Figs. 4.2-4.3. The plotted curves are designated by using the label "QCESLP, M = X" where "X" is the number of users. For each of the examined cases, the performance of the approach in [125] is also plotted

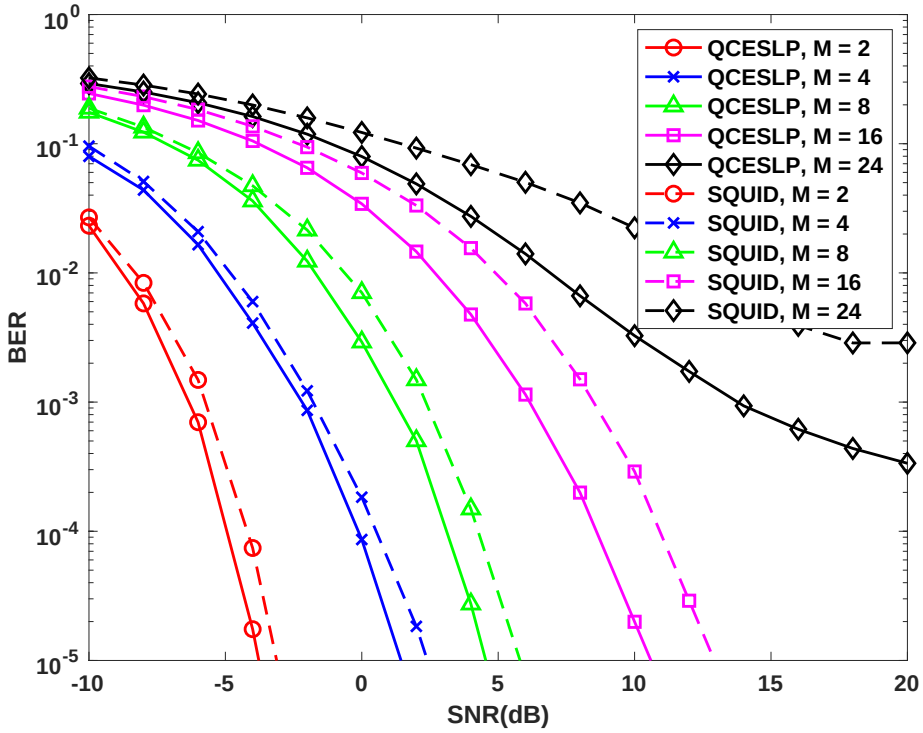

FIGURE 4.4: Impact of the users' number to the performance of a system employing QPSK with $T = 64$ antennas, $B = 1$ bit - DACs and $N_{sc} = 32$ subcarriers.

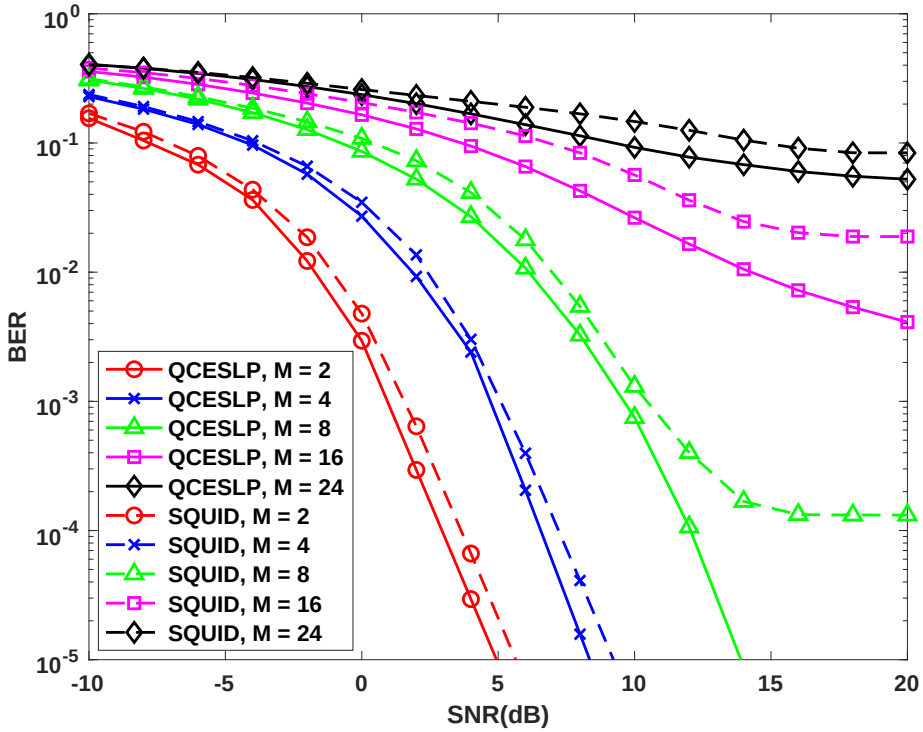

FIGURE 4.5: Impact of users' number to the performance of a system employing 16QAM with $T = 64$ antennas, $B = 1$ bit - DACs and $N_{sc} = 32$ subcarriers.

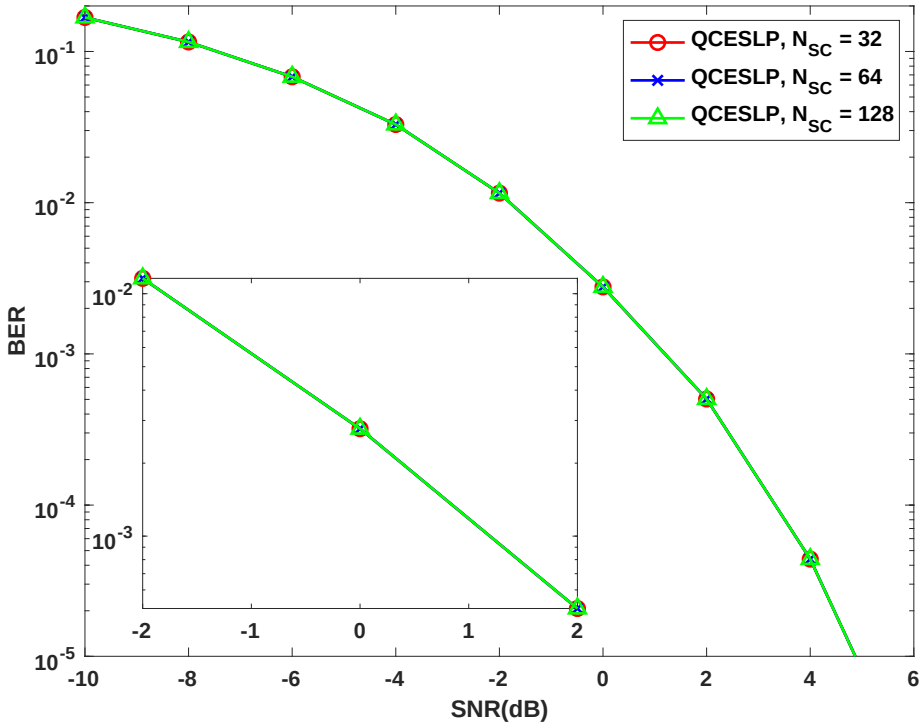

FIGURE 4.6: Impact of the subcarriers' number to the performance of a system employing QPSK with $T = 64$ antennas, $M = 8$ users and $B = 1$ bit - DACs.

(''SQUID, M = X"). In Fig. 4.4, the results of the QPSK modulation are shown while Fig. 4.5 depicts the corresponding ones for 16QAM. As it can be seen on both the Figs. 4.4-4.5, the performance is degraded as the number of the served users M increases. This is the case, since for a given number of transmit antennas, the technique has to design signals to convey information symbols to more users. Thus, as the number of users increases, the optimal value of $\tilde{\mathbf{x}}_T$, $\tilde{\mathbf{x}}_T^\star$ in $(\mathcal{P}_1)$ corresponds, in general, to larger values of the term $\|\tilde{\mathbf{s}} - \beta\tilde{\mathbf{H}}_F\tilde{\mathbf{W}}_{N_{SC}}\tilde{\mathbf{x}}_T\|_2^2$ that lead to the observed performance degradation. Furthermore, we observe that as the number of users increases, the gap on the performance between the proposed approach and the SQUID-based one increases. Especially, for a relative large number of users (with respect to the number of the transmit antennas), it is evident that the proposed approach may offer significant gains over the SQUID-based one.

In the following experiment, the impact of the number of subcarriers on the performance of the proposed technique is examined. To that end, a system of $M = 8$ users is assumed and the resolution of the DACs is fixed to 1 bit. The case of QPSK is shown in Fig. 4.6 and that of 16QAM in Fig. 4.7, respectively. The cases of $N_{SC} = 32, 64, 128$ are examined. The curves are designated by using the label "QCESLP, N_{SC} = X", where "X" is the number of the employed subcarriers. As it is evident by inspection of these figures, the proposed techniques achieve almost identical performance for all the examined cases. Thus, the proposed technique appears to preserve its efficiency even if the number of subcarriers is large, as it is the case with typical real world systems.

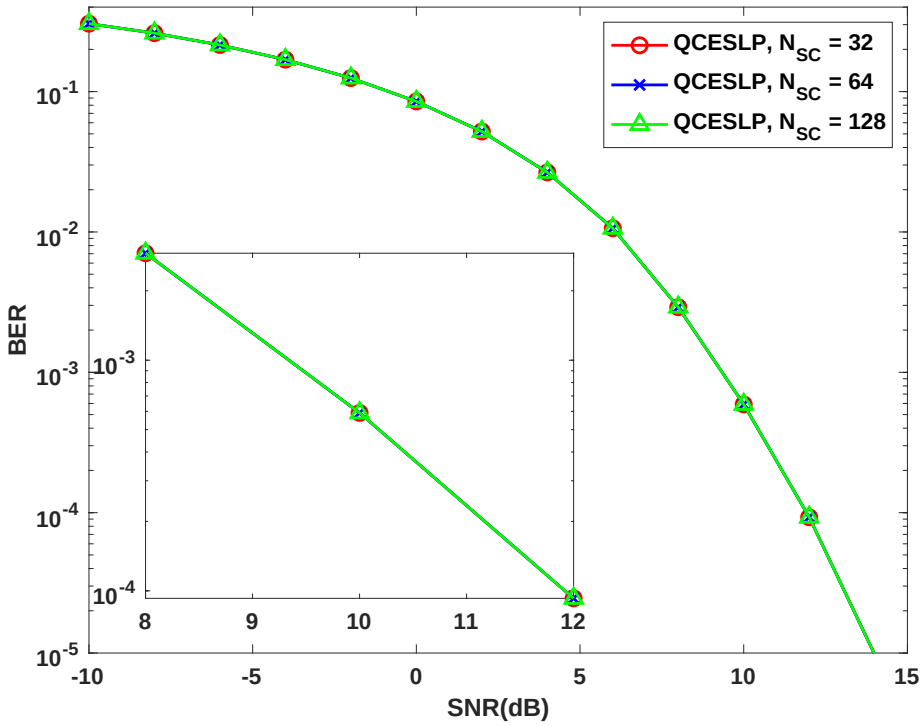

FIGURE 4.7: Impact of the subcarriers' number to the performance of a system employing 16QAM with $T = 64$ antennas, $M = 8$ users and $B = 1$ bit - DACs.

4.4.2 Energy Efficiency

Finally, the section is ended by showing some results regarding the gains on the power consumption that an architecture based on low resolution DACs may offer. A good metric for that is the energy efficiency defined as in [88],

$$EE(P^e_{mn}, k, B, B', f_s, M, N_{sc}) = \frac{N_{SC}}{N_{SC}+L-1}\frac{\sum_{n=1}^{N_{sc}}\sum_{m=1}^{M} R(P^e_{mn}, k)}{P_c(B, B', f_s, T, M)}, \tag{4.21}$$

where the achieved rate per user is approximated by $R(P^e_m, k) = (1 - P^e_{mn})k$, P^e_m is the bit error probability of the mth user at the nth sub-carrier, k is the number of the bits per constellation point and the system's power consumption is calculated as in (4.16). Note that the normalization term $\frac{N_{SC}}{N_{SC}+L-1}$ in (4.21) is due to rate loss from prepending the CP as a guard band.

The simulation set-up on Figs. 4.2-4.3 is repeated and the results showing the energy efficiency achieved from each one of the different approaches for different DAC resolutions ($B = 1, 2, 3$) are depicted in Figs. 4.8-4.9. The cases of QPSK and 16QAM constellations are considered once more. It is assumed that the receiver system at each user is employed with $B' = 14$-bit resolution ADCs which can be considered to introduce negligible quantization error to the received signals. A similar assumption is followed for the infinite resolution CESLP system for which the employment of $B = 14$-bit DACs at the BS is assumed to achieve the observed performance. In order to achieve high PA

TABLE 4.1: Parameters for the Energy Efficiency Calculation

T	64
M	8
N_{sc}	32
k	$2, 4$
η	$\pi/4$
P	1
P_{RF}	32.8mW
P_{LO}	50mW
P_{LNA}	20mW
B	$1, 2, 3, 14$
B'	14
α	1
V_{dd}	3V
I_0	10μA
C_p	1pF
f_b	10KHz
f_{cor}	1MHz
L_{min}	0.5μm

efficiency and to fully exploit the advantages of the CESLP system, we consider that the PAs are operated in the saturation region where the amplitude of the output signal of the PA is given by (4.12) and in this case is equal to $r_{o,max}$. By plugging this in (4.11) and considering that the output signal envelope in the CESLP system is constant, we get the PA efficiency which is equal to $\eta = \pi/4$. The different parameters used for calculating the energy efficiency are enlisted in Table I for the ease of reference.

The energy efficiency of both the quantized ZF and SQUID approaches is also plotted in the same figures. As it is shown, the techniques based on low resolution DACs have significantly improved complexity compared to the CESLP technique, applied on a system with infinite resolution DACs. This can be explained by the inspection of the energy efficiency definition in (4.21). In the numerator, the rate is calculated based on the corresponding bit error probability. The approaches based on low resolution DACs achieve bit error probability quite close to the one for a system with infinite resolution DACs, as shown in Figs. 4.2-4.3. On the other hand, the denominator in (4.21) is the power consumption of each architecture which is significantly smaller for systems with DACs of resolution of few bits. This has to do with the exponential increase on the power consumption, as the resolution of the DACs increases (4.13). From the previous, the ratio in the definition of the energy efficiency is expected to achieve a much greater value for systems of low resolution DACs, as observed in Figs. 4.8- 4.9.

Furthermore, the proposed technique achieves in general better performance in terms of the bit error probability as compared to the quantized ZF and

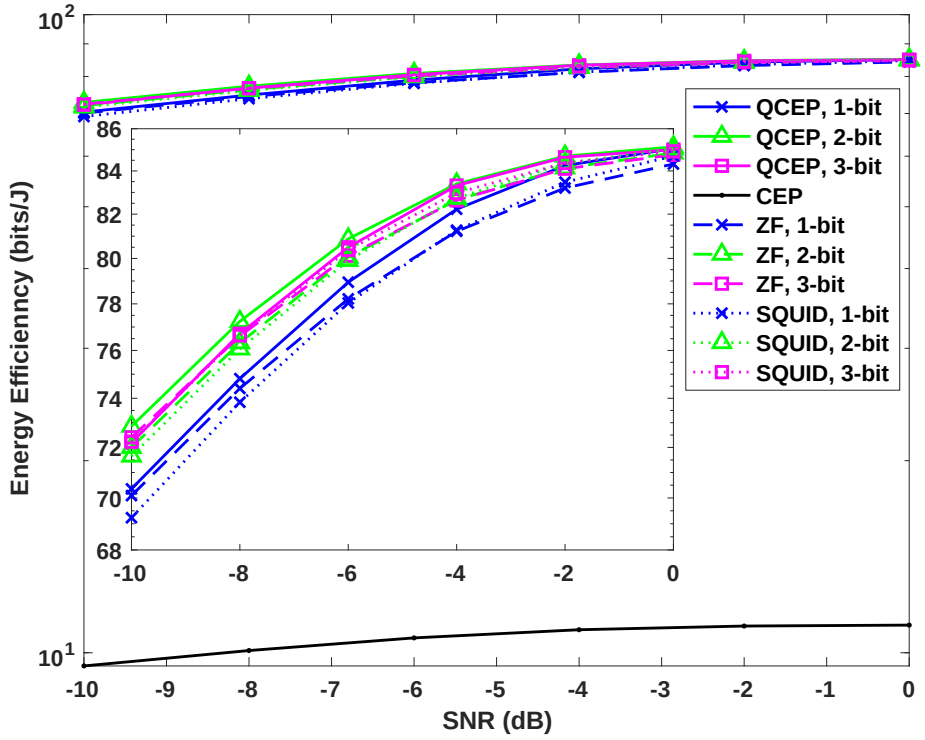

FIGURE 4.8: Energy efficiency of the different techniques under different resolution of the DACs for a system of $T = 64$ antennas, $M = 8$ users and $N_{sc} = 32$ subcarriers that employs QPSK.

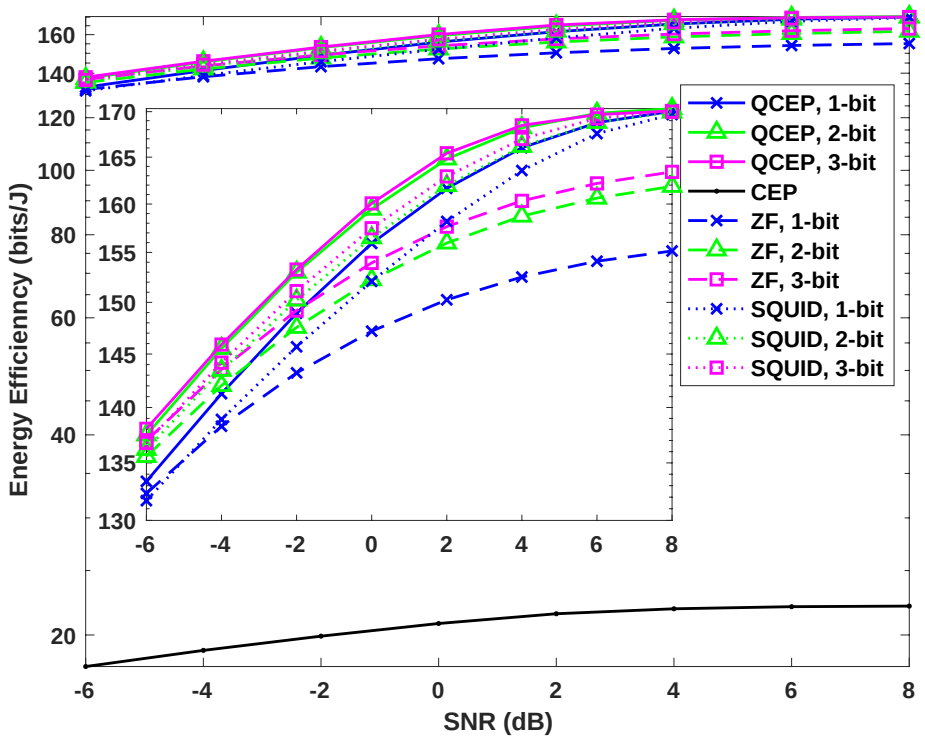

FIGURE 4.9: Energy efficiency of the different techniques under different resolution of the DACs for a system of $T = 64$ antennas, $M = 8$ users and $N_{sc} = 32$ subcarriers that employs 16QAM.

SQUID approaches based again on the results on Figs. 4.2-4.3. Thus, again from the energy efficiency expression in (4.21) and given that the power consumption is the same for each one of these systems (for the same DACs' resolution), the proposed technique is expected to be more energy efficient than the quantized ZF and SQUID approaches. This is in line with the results in Figs. 4.8- 4.9.

Finally, it is instructive to observe that the most energy efficient solution for the QPSK case is the 2-bit DACs case, as shown in Fig. 4.2. This is the case, since the achieved rate for the 2-bit system is already close enough to the one of the system with infinite resolution DACs. Now, going from a 2-bit DACs system to a 3-bit DACs one, can only provide a small improvement in the achieved rate (see also the corresponding bit error probability in Fig. 4.2) while there is an increase in the power consumption which results in the observed slightly worse energy efficiency of the 3-bit DACs system. The situation is reversed for the 16QAM case in Fig. 4.3. Here, the improvement due to the additional bit in the resolution on the DACs is a bit greater compared to the one of the QPSK case (see also the corresponding bit error probability in Fig. 4.3). This improves the energy efficiency of the 3-bit DACs system that now appears to be the most energy efficient solution.

4.5 Summary

In this chapter, an SLP scheme for CE MU-MIMO-OFDM system with low resolution DACs was considered. The SLP design was formulated as a mixed discrete-continuous constrained least squares problem and was solved using an iterative algorithm based on CCD. Additionally, a power consumption model was derived for the studied system model. Numerical results showed that the proposed SLP scheme in combination with the power savings of low resolution DACs results in an improved energy efficiency when compared to systems with infinite resolution DACs.

Chapter 5

SLP For MIMO-OFDM Transceiver Architectures Based on One-Bit DACs and ADCs

In this chapter, an SLP scheme for a point-to-point MIMO-OFDM system which is equipped with both one-bit DACs at the transmitter and one-bit ADCs at the receiver is considered. The chapter is organized as follows.

In Section 5.1, the proposed architectures for a MIMO-OFDM system based on one-bit DACs and ADCs are described. Furthermore, in this section the SLP design problems for the described architectures are formulated as well as the design problem of the analog post-coding matrix. In Section 5.2, the power consumption of the two architectures that were previously described is derived. In Section 5.3, the solutions to the SLP problems as well as the post-coder are presented. Simulation results are presented in Section 5.4, followed by the summary in Section 5.5.

5.1 System Model

5.1.1 Transceiver architecture based on one-bit DACs/ADCs

A MIMO communication system, as shown in Figure 5.1, is considered, where the transmitter is equipped with M antennas and the receiver is equipped with K antennas, so that $K < M$. There are two one-bit DACs per transmit antenna, one for the in-phase and one for the quadrature component, which convert the digital output of the precoder into an analog signal. In a similar manner, the received signal at each antenna of the receiver is quantized by two one-bit ADCs and the digital outputs of the $2K$ ADCs are then combined to provide an estimate of the information symbols that have been sent.

It is assumed that the channel experiences frequency selective fading due to multipath propagation. Consequently, the MIMO time domain channel with L resolvable taps can be modelled as,

$$\mathbf{H}_T(m,k) = \left[h_T(m,k,0), ..., h_T(m,k,L-1)\right], \tag{5.1}$$

where $h_T(m,k,l)$ is the l-th channel tap, between the m-th transmit and k-th receive antenna. The system employs OFDM transmission [134], a well-known

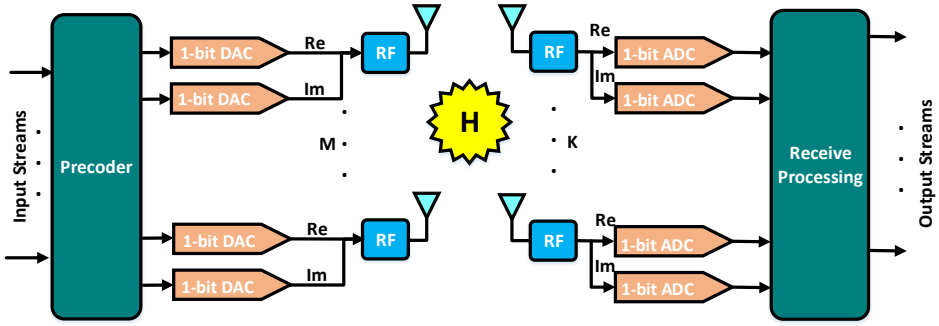

FIGURE 5.1: A MIMO system of T transmit antennas, M receive antennas, 1-bit precision DACs at the transmitter and 1-bit precision ADCs at the receiver.

scheme which is used to mitigate the adverse effects of the channel's frequency selectivity. In OFDM the total available channel bandwidth, BW, is divided into N_{SC} orthogonal subcarriers, with spacing $\Delta f = BW/N_{SC}$ between them, which are modulated independently either with a conventional modulation or in this case with precoded symbols. This results in N_{SC} narrowband channels, with bandwidth smaller than the coherence bandwidth of the channel and therefore, the fading experienced by each one can be considered flat.

The use of one-bit DACs at the transmitter means that the input vectors $\mathbf{x}_T$ have entries that lie in the complex set $\mathcal{X}$ defined as,

$$\mathcal{X} = \{1+j, 1-j, -1+j, -1-j\}, \tag{5.2}$$

where j is the imaginary unit. By denoting $x_T(m,n) \in \mathcal{X}$ the signal transmitted by the m-th antenna at the n-th time index and assuming perfect synchronization, the baseband received time domain signal can be expressed as,

$$y_T(k,n) = \sum_{m=1}^{M} \sum_{l=0}^{L-1} h_T(m,k,l)\, x_T(k, n-l) + z_T(k,n), \tag{5.3}$$

where $k = 1, 2, ..., K$, $n = 1, 2, ..., N_{SC}$ and $z_T(k,n)$ the sample of Additive White Gaussian Noise (AWGN). During the transmission of an OFDM symbol the channel remains constant and perfectly known at the transmitter. It should be also mentioned that a Cyclic Prefix (CP) of length ν is prepended at the transmitter. This means that that last ν samples of $\mathbf{x}_T(n)$ are added at the beginning of the symbol. The CP serves as a guard band that protects the received symbol from delayed copies of the previous one and also enables the modelling of the linear convolution of the signal with the channel as a circular convolution instead.

At the receiver, $\mathbf{y}_T$ is quantized by one-bit ADCs and the output of each ADC is given by,

$$y_{TQ}(k,n) = f_q\{y_T(k,n)\}, \tag{5.4}$$

where $f_q\{w\} = \text{sgn}\{Re\{w\}\} + j\text{sgn}\{Im\{w\}\}$ with $\text{sgn}\{\cdot\}$ denoting the sign function. Consequently, the outputs of the ADCs lie in $\mathcal{X}$. After quantization,

the first ν samples, which correspond to the CP and are corrupted by inter-symbol interference, are discarded and the FFT is computed. The output of the FFT in matrix form is given by,

$$\tilde{\mathbf{y}}_F = \tilde{\mathbf{W}}_{N_{SC},K} f_q\{\tilde{\mathbf{W}}^H_{N_{SC},M}\left(\tilde{\mathbf{H}}_F\tilde{\mathbf{x}}_F + \tilde{\mathbf{z}}_F\right)\} \tag{5.5}$$

where $\tilde{\mathbf{y}}_F$, $\tilde{\mathbf{z}}_F$ are the $KN_{SC}\times 1$ vectors that are produced by concatenating the frequency domain received signals and noise samples respectively across all the subcarriers and receive antennas. Additionally, $\tilde{\mathbf{W}}_{N_{SC},K}$ and $\tilde{\mathbf{W}}^H_{N_{SC},M}$ are reshaped DFT matrices that are used to perform the DFT and IDFT respectively and are defined as

$$\tilde{\mathbf{W}}_{N_SC,N} = \mathbf{W}_{N_{SC}} \otimes \mathbf{I}_N, \tag{5.6}$$

where $\mathbf{W}_{N_{SC}}$ is the classic DFT $N_{SC}\times N_{SC}$ matrix, $\otimes$ is the Kronecker product and $\mathbf{I}_N$ is the $N\times N$ identity matrix. Using (5.6) the frequency domain input vector is given by,

$$\tilde{\mathbf{x}}_F = \tilde{\mathbf{W}}_{N_{SC},M}\tilde{\mathbf{x}}_T. \tag{5.7}$$

Moreover, $\tilde{\mathbf{H}}_F$ is the $KN_{SC}\times MN_{SC}$ block matrix

$$\tilde{\mathbf{H}}_F = \begin{bmatrix} \mathbf{H}_{F1} & 0 & \dots & 0 \\ 0 & \mathbf{H}_{F2} & \dots & 0 \\ \vdots & \vdots & \ddots & \vdots \\ 0 & 0 & \dots & \mathbf{H}_{FN_{SC}} \end{bmatrix},$$

where $\mathbf{H}_{Fn}$ is the $K\times M$ frequency response of the n-th subchannel.

Furthermore, the transmitter applies a combiner $RN_{SC}\times KN_{SC}$ matrix $\mathbf{G}$,

$$\hat{\mathbf{s}} = \mathbf{G}\tilde{\mathbf{y}}_F \tag{5.8}$$

and uses $\hat{\mathbf{s}}$ to take a decision on the symbols that have been sent. The use of the post-coding matrix is critical in this system as it allows to combine the outputs of the $2K$ one-bit ADCs into R data streams, with $R<K$, of higher order modulations.

The transmitter employs an SLP scheme that designs the transmit vector $\mathbf{x}_T(n)\in\mathcal{X}^M$ in a way that minimizes the Euclidean distance between the $RN_{SC}\times 1$ vector $\tilde{\mathbf{s}}$ of information symbols, which must be conveyed to the receiver, and $\hat{\mathbf{s}}$. This objective can be expressed as,

$$\mathcal{F} = ||\tilde{\mathbf{s}} - \hat{\mathbf{s}}||_2^2 = \tag{5.9}$$

$$= ||\tilde{\mathbf{s}} - \beta\mathbf{G}\tilde{\mathbf{W}}_{N_{SC},K} f_q\{\tilde{\mathbf{W}}^H_{N_{SC},M}\left(\tilde{\mathbf{H}}_F\tilde{\mathbf{x}}_F + \tilde{\mathbf{z}}_F\right)\}||_2^2 \approx \tag{5.10}$$

$$\approx ||\tilde{\mathbf{s}} - \beta\mathbf{G}\tilde{\mathbf{W}}_{N_{SC},K} f_q\{\tilde{\mathbf{W}}^H_{N_{SC},M}\left(\tilde{\mathbf{H}}_F\tilde{\mathbf{W}}_{N_{SC},M}\tilde{\mathbf{x}}_T\right)\}||_2^2. \tag{5.11}$$

In the above approximate expression the effect of the AWGN has been ignored in order to simplify the objective, an assumption which is valid as the SNR increases.

The precoder design can be expressed as an optimization problem, by adding to the objective function $\mathcal{F}$ the constraint imposed on the input vector by the

one-bit DACs, $\tilde{\mathbf{x}}_T \in \mathcal{X}^{MN_{SC}\times 1}$ and constrain the scalar β, which is the array gain, to lie in $\mathbb{R}^+$ as,

$$\begin{aligned}(\mathcal{P}_1): \quad & \min_{\mathbf{G},\tilde{\mathbf{x}}_T,\beta} \mathcal{F} \\ & s.t. \;\; \tilde{\mathbf{x}}_T \in \mathcal{X}^{MN_{SC}\times 1} \\ & \qquad \beta \in \mathbb{R}^+.\end{aligned}$$

The above formulation is quite complex as a result of the discrete constraint and the nonlinear quantizer. In order to eliminate the quantizer from the cost function of the above problem the following splitting into two separate optimization problems is proposed.

First, the vector of the ADCs' outputs, $\tilde{\mathbf{r}}_T \in \mathcal{X}^{KN_{SC}\times 1}$ is designed in a way that minimizes the distance between it and the vector of information symbols. This can be formulated as an optimization problem as,

$$\begin{aligned}(\mathcal{P}_2): \quad & \min_{\tilde{\mathbf{r}}_T,\beta_1} \|\tilde{\mathbf{s}} - \beta_1 \mathbf{G}\tilde{\mathbf{W}}_{N_{SC},K}\tilde{\mathbf{r}}_T\|_2^2 \\ & s.t. \;\; \tilde{\mathbf{r}}_T \in \mathcal{X}^{KN_{SC}\times 1} \\ & \qquad \beta_1 \in \mathbb{R}^+.\end{aligned}$$

In $(\mathcal{P}_2)$ matrix $\mathbf{G}$ is also unknown. However, a joint optimization is difficult and impractical and this is why a decoupled approach is followed for the design of the combiner matrix. Moreover, this is supported by the different rate that $\tilde{\mathbf{x}}_T$ and $\mathbf{G}$ need to be updated. The precoding vector $\tilde{\mathbf{x}}_T$ needs to updated on a symbol rate while $\mathbf{G}$ only when the CSI changes. In Sec 5.3 an approach based on SVD is proposed for the design of $\mathbf{G}$.

It should be noted that while the value of β_1 is derived by solving $(\mathcal{P}_2)$ at the transmitter, it is applied at the receiver side to scale the signal appropriately. However, there is no need to transmit the value of β_1, which would introduce significant communication overhead as it is updated on a symbol rate, but rather it can be blindly estimated at the receiver using the equation

$$\hat{\beta}_1 = \sqrt{\frac{||\mathcal{Q}||_2^2/M_Q}{||\tilde{\mathbf{y}}_F||_2^2/(RN_{SC})}}, \tag{5.12}$$

where $\mathcal{Q}$ is the employed symbol constellation and M_Q the modulation order.

Once $(\mathcal{P}_2)$ is solved, the vector of the desirable ADC outputs $\tilde{\mathbf{r}}_T$ is used to formulate a second optimization problem, with the objective to select the input vector $\tilde{\mathbf{x}}_T \in \mathcal{X}^{MN_{SC}}$ that minimizes the distance in the frequency domain between the noiseless received signal $\tilde{\mathbf{H}}_F\tilde{\mathbf{W}}_{N_{SC},M}\tilde{\mathbf{x}}_T$ and the vector of optimal ADC outputs $\tilde{\mathbf{r}}_F = \tilde{\mathbf{W}}_{N_{SC},K}\tilde{\mathbf{r}}_T$.

$$\begin{aligned}(\mathcal{P}_3): \quad & \min_{\tilde{\mathbf{x}}_T,\beta} \|\tilde{\mathbf{r}}_F - \beta\tilde{\mathbf{H}}_F\tilde{\mathbf{W}}_{N_{SC},M}\tilde{\mathbf{x}}_T\|_2^2 \\ & s.t. \;\; \tilde{\mathbf{x}}_T \in \mathcal{X}^{MN_{SC}\times 1} \\ & \qquad \beta \in \mathbb{R}^+.\end{aligned}$$

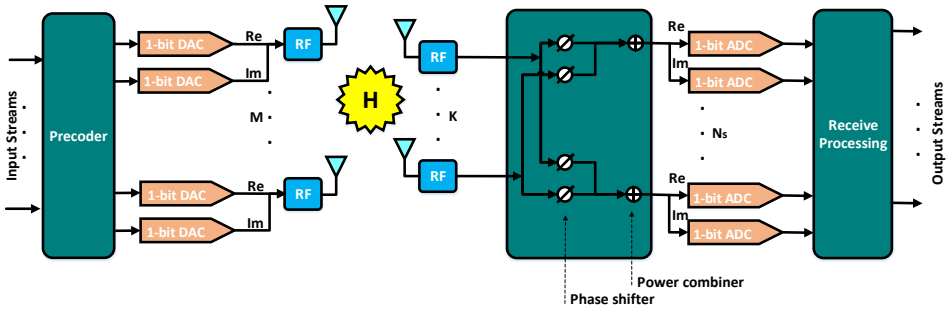

FIGURE 5.2: A MIMO system of T transmit antennas, M receive antennas, 1-bit precision DACs at the transmitter and 1-bit precision ADCs at the receiver, which is equipped with an network of phase shifters.

It should be highlighted here that the introduction of $\tilde{\mathbf{W}}_{N_{SC},M}$ in the problem $(\mathcal{P}_3)$ means that the IFFT is integrated in the design of the transmit signal and there is no need for a separate IFFT computation block at the transmitter as in conventional OFDM systems.

One can observe that the optimization problems $(\mathcal{P}_2)$ and $(\mathcal{P}_3)$ are very similar and an algorithmic solution that is developed for one can be easily applied to the other. The problems are NP-hard and one solution could be an exhaustive search over all the possible vectors $\tilde{\mathbf{x}}_T \in \mathcal{X}^{MN_{SC}}$. The complexity of this solution increases exponentially with the number of antennas and subcarriers and therefore, the complexity would be enormous even for a system with few antennas and a short OFDM block. Instead, in section 5.3 an efficient solution for both problems based on a Cyclic Coordinate Descent (CCD) framework [128] is proposed.

5.1.2 Transceiver architecture based on one-bit DACs/ADCs and a network of analog phase shifters

In the previously discussed system, the large number of antennas mitigates the effects of coarse quantization both at the transmitter and at the receiver. However, this leads to an inherent disadvantage, an increase in the number of receive antennas K will increase function (5.11) as it will decrease the number of available degrees of freedom from the side of the transmitter. This will deteriorate the system performance rather than improve it as it would happen in a classical MIMO system. This motivates us to research an alternative power efficient architecture where the increase of receive antennas will lead to an improved SNR but without negatively affecting available degrees of freedom of the system.

To this end, the system architecture shown in Figure 5.2 is proposed. This is a similar system architecture to the one described above but a network of analog phase shifters has been added before the one-bit ADCs. Furthermore the number of ADCs is now reduced to $2N_s$ from $2K$ and this means that the network of KN_s phase shifters maps the received signal of the K antennas to the $2N_s$ ADCs.

The network of phase shifters can be mathematically modelled as a $N_s \times K$ matrix $\mathbf{Q}$ with unit-modulus entries, $|Q_{ij}| = 1, \forall i, j$ that is applied on the received signal in the RF domain and therefore, the output of the ADCs is now given by

$$\tilde{\mathbf{y}}_{TQ} = f_q\{\mathbf{Q}\tilde{\mathbf{y}}_T\}. \tag{5.13}$$

The precoder design is split into two problems that must be solved successively as before. The first problem is identical to $(\mathcal{P}_2)$ with the only difference being the dimension of $\tilde{\mathbf{r}}_T$ changing to $N_s N_{SC} \times 1$ from $K N_{SC} \times 1$. The second problem is altered by the addition of $\tilde{\mathbf{Q}} = \mathbf{I}_{N_{SC}} \otimes \mathbf{Q}$ at the cost function and becomes

$$\begin{aligned} (\mathcal{P}_4): \quad & \min_{\tilde{\mathbf{x}}_T, \beta} \|\tilde{\mathbf{r}}_F - \beta \tilde{\mathbf{Q}} \tilde{\mathbf{H}}_F \tilde{\mathbf{W}}_{N_{SC},M} \tilde{\mathbf{x}}_T\|_2^2 \\ & s.t. \;\; \tilde{\mathbf{x}}_T \in \mathcal{X}^{MN_{SC} \times 1} \\ & \beta \in \mathbb{R}^+. \end{aligned}$$

Finally, while addressing $(\mathcal{P}_4)$ matrix $\mathbf{Q}$ was not considered an optimization variable. This is because the joint problem is difficult to address and is also impractical, as $\mathbf{Q}$ is updated when the CSI changes rather than on a symbol rate. Thus, we opt to decouple the problem of designing $\mathbf{Q}$ from the precoding design. The purpose of introducing $\mathbf{Q}$ is to increase the SNR at the receiver, without increasing significantly the hardware complexity or power consumption. This objective can be achieved if $\mathbf{Q}$ is designed to maximize the Frobenius norm of the product $\tilde{\mathbf{Q}}\tilde{\mathbf{H}}_F$. Additionally, it is crucial for the system's performance to have available as many degrees of freedom as possible and this means that we want to design $\mathbf{Q}$ to also maximize the rank of the product $\tilde{\mathbf{Q}}\tilde{\mathbf{H}}_F$. These two objectives can be achieved at the same time by maximizing the nuclear norm of the product, $||\tilde{\mathbf{Q}}\tilde{\mathbf{H}}_F||_*$. This is because the nuclear norm is related with the rank and the Frobenius norm of a matrix via the following inequality,

$$||\tilde{\mathbf{Q}}\tilde{\mathbf{H}}_F||_* \leq rank(\tilde{\mathbf{Q}}\tilde{\mathbf{H}}_F)||\tilde{\mathbf{Q}}\tilde{\mathbf{H}}_F||_F^2. \tag{5.14}$$

The expression above is derived by applying the Cauchy–Schwarz inequality to the nuclear norm and by using the definitions of the nuclear norm, $||A||_* = \sum_{i=1}^{rank(A)} \sigma_i$, and Frobenius norm $||A||_F = \sqrt{\sum_{i=1}^{rank(A)} \sigma_i^2}$, with σ_i denoting the i-th singular value of the matrix. As a result of the above, the design of $\mathbf{Q}$ can be expressed as an optimization problem,

$$\begin{aligned} (\mathcal{P}_5): \quad & \max_{\mathbf{Q}} ||\tilde{\mathbf{Q}}\tilde{\mathbf{H}}_F||_*^2 \\ & s.t. \;\; \tilde{\mathbf{Q}} = \mathbf{I}_{N_{SC}} \otimes \mathbf{Q} \\ & ||Q_{i,j}|| = 1, \forall i, j \end{aligned}$$

It should be noted that $\mathbf{Q}$ is dependent only on the channel and therefore, is updated only when the channel matrix changes. While the objective function of problem $(\mathcal{P}_5)$ is convex the unit-modulus constraint for the entries of the matrix is not and therefore it is NP hard. In section 5.3 the problem is reformulated and and a new algorithm based on the ADMM framework is proposed for its

solution. It is also worth mentioning that since the design of the combiner $\mathbf{Q}$ is not dependent on the specific one-bit architecture that is presented here it can also be used in other communications systems with multi antenna receivers.

5.2 Power Consumption Model

Since the motivation for researching the proposed systems is the increase of the power efficiency, it is essential to provide a model for the power consumption of such systems. Generally the power consumption of a communication system is given by the addition of the power of the transmitted signal and the static power, consumed by the components of the transceiver. Based on the appropriate modelling and approximations,[127], the power consumption of the transmitter can be shown to be given by

$$P_{ct}(T, B, f_s) \approx P_{PA} + T[2P_{DAC}(B, f_s) + P_{RF}] + P_{LO}, \tag{5.15}$$

where P_{PA}, $P_{DAC}(B, F_s)$, P_{RF} and P_{LO} denote the power consumption of the Power Amplifiers (PAs), DACs, RF components (e.g filers, mixers) and Local Oscillator, receptively.

The power efficiency η of the employed PAs contributes significantly to the overall power consumption of the system and in this work, it is assumed that the transmitter is equipped with the widely used class B amplifiers, whose power consumption is given by,

$$P_{PA} \approx \frac{\mathbb{E}\{\|\tilde{\mathbf{x}}_T\|_2^2\}}{\eta}. \tag{5.16}$$

The power efficiency of class B amplifiers according to [78] is given by,

$$\eta = \frac{\pi \mathbb{E}\{g^2(|\tilde{\mathbf{x}}_T|)\}}{4A_{o,max}\mathbb{E}\{g(|\tilde{\mathbf{x}}_T|)\}}, \tag{5.17}$$

where $g(\cdot)$ denotes the AM-AM conversion and $A_{o,max}$ is the maximum amplitude of the output signal given by $A_{o,max} = \upsilon A_{max}$ where υ is the gain of the amplifier and A_{max} is the input reference amplitude. It is assumed that the system uses TWT amplifiers whose AM-AM conversion is given by [78]

$$g(A) = A_{o,\max}\frac{A/A_{\max}}{1 + \frac{1}{4}(A/A_{\max})^2}, \tag{5.18}$$

and its AM-PM conversion by [78]

$$\Phi(A) = \frac{\pi}{12}\frac{(A/A_{\max})^2}{1 + \frac{1}{4}(A/A_{\max})^2} \quad \text{(rad)}, \tag{5.19}$$

where A is the envelope of the input signal given by $A = |\tilde{\mathbf{x}}_T|$.

Now, the power consumption model for the DAC will be provided, which following the analysis in [127] is given by

$$P_{DAC}(B, f_s) \approx \frac{\alpha}{2}\left[V_{dd}I_0(2^B - 1) + C_p f_s V_{dd}^2 B\right], \tag{5.20}$$

where V_{dd} denotes the power supply voltage, I_0 denotes the value of the current source which corresponds to the least significant bit, C_p denotes the parasitic capacitance of the switches that select one of the possible states of the DAC and α is a factor which is used to models some second order effects. Additionally, the sampling frequency is given by $f_s = 2(2f_b + f_{cor})$, where f_b denotes the employed bandwidth and f_{cor} the corner frequency of the $1/f$ noise [137]. The power consumption model for the multi-antenna receiver can be derived in a similar way. Using the results of [127], the consumed power of the K antenna receiver in Fig. 5.1 is approximated as,

$$P_{cr,1}(B', f_s) \approx K\left(P_{LNA} + 2P_{ADC}(B, f_s) + P_{RF}\right) + P_{LO}, \tag{5.21}$$

while the the consumed power of the receiver in Fig. 5.2 with the network of phase shifters is approximated as,

$$\begin{aligned} P_{cr,2}(B', f_s) \approx & N_s(P_{LNA} + 2P_{ADC}(B, f_s) + P_{RF} \\ & + KP_{ps}) + P_{LO}, \end{aligned} \tag{5.22}$$

where P_{LNA}, P_{ps} denotes the Low Noise Amplifiers' (LNAs) and phase shifters' power consumption, respectively and $P_{ADC}(B', F_s)$ is the power consumption of a B'-bit ADC with f_s sampling frequency, given by [127],

$$P_{ADC}(B', f_s) \approx \frac{3V_{dd}^2 L_{min} f_s}{2 \times 10^{-0.1525B'+4.838}}, \tag{5.23}$$

where L_{min} is the minimum channel length for the employed Complementary Metal Oxide Semiconductor (CMOS) technology.

The total power consumption of the system is simple the addition of the power consumed by the transmitter and the receiver and is given by,

$$P_c(B, B', f_s, T, M) = P_{ct}(T, B, f_s) + P_{cr}(B', f_s). \tag{5.24}$$

5.3 Solution

5.3.1 Precoding solution for system based on one-bit DACs/ADCs

In this section the solution to the precoding problems with one-bit DACs and ADCs, as they were formulated in Section 5.1, is presented. By observing problems $(\mathcal{P}_2)$ as well as $(\mathcal{P}_3) - (\mathcal{P}_4)$, that correspond to the two proposed one-bit DACs/ADCs architectures, it is noted that they are very similar and the same algorithmic solution can be applied to all of them. The solution that is derived here for these problems is based on Cyclic Coordinate Descent (CCD) framework [128]. In addition to deriving the optimal precoding vector, the algorithmic solution for designing the analog post-coder matrix $\mathbf{Q}$ by applying the Alternating Direction Method of Multipliers (ADMM) [141] is also provided in this section.

Algorithm 6

Initialize $\tilde{\mathbf{r}}_T^{(0)} \in \mathcal{X}^{KN_{SC}\times 1}$, $\beta_1^{(0)} \in \mathbb{R}^+$. Set $\mathbf{A} = \mathbf{G}\tilde{\mathbf{W}}_{N_{SC}}$.
$\mathbf{t} = \mathbf{A}\tilde{\mathbf{r}}_T^{(0)}$
while The termination criteria in (5.29) are not met **do**
  for $1 \leq l \leq length(\tilde{\mathbf{r}}_T)$ **do**
    $\mathbf{t} = \mathbf{t} - \mathbf{A}_l\tilde{\mathbf{r}}_T^{(i)}(l)$
    $\tilde{\mathbf{r}}_T^{(i+1)}(l) \leftarrow \arg\min_{\psi\in\mathcal{X}} \|\tilde{\mathbf{s}} - \beta_1^{(i)}\mathbf{t} - \beta_1^{(i)}\mathbf{A}_l\psi\|_2^2$
    $\mathbf{t} = \mathbf{t} + \mathbf{A}_l\tilde{\mathbf{r}}_T^{(i+1)}(l)$
  end for
  $\beta_1^{(i+1)} \leftarrow \frac{\mathcal{R}\{\tilde{\mathbf{s}}^H\mathbf{A}\tilde{\mathbf{r}}_T^{(i+1)}\}}{\|\mathbf{A}\tilde{\mathbf{r}}_T^{(i+1)}\|_2^2}$
  $i \leftarrow i + 1$
end whilereturn $\tilde{\mathbf{r}}_T^{(i+1)}$, $\beta_1^{(i+1)}$

In the case where there is no analog processing of the signal at the receiver, which corresponds to the system shown in Fig. 5.1, the design of the precoded symbols include two steps. At the first step the informations symbols drawn from a constellation are given as an input to $(\mathcal{P}_2)$ which is solved and at the second step the output is fed as an input to $(\mathcal{P}_3)$. The solution of $(\mathcal{P}_3)$ is the vector of the precoded OFDM symbol in the time domain and is transmitted by the M antennas of the transmitter. As it was mentioned, both problems are solved using the CCD method, which enables the minimization of a multivariate cost function by iterating through the different coordinate directions and minimizing the latter over one direction at a time. Therefore, by applying the CCD method to $(\mathcal{P}_2)$ the k-th component of $\tilde{r}_T^{(i+1)}(k)$ at the $i+1$-th iteration of the algorithm is given by

$$\begin{aligned}\tilde{r}_T^{(i+1)}(k) = arg\min_{\psi\in\mathcal{X}} f(\tilde{r}_T^{(i+1)}(1), ..., \tilde{r}_T^{(i+1)}(k-1),\\ \psi, \tilde{r}_T^{(i)}(k+1), ..., \tilde{r}_T^{(i)}(KN_{SC}), \beta_1^{(i)})\end{aligned} \tag{5.25}$$

where

$$\begin{aligned}&f(\tilde{r}_T^{(i+1)}(1), ..., \tilde{r}_T^{(i+1)}(k-1), \psi, \tilde{r}_T^{(i)}(k+1), ...,\\ &\tilde{r}_T^{(i)}(KN_{SC}), \beta_1^{(i)}) = ||\tilde{\mathbf{s}} - \beta_1^{(i)}\sum_{m=1}^{(i-1)}\mathbf{A}_m\tilde{r}_T^{(i+1)}(m)\\ &- \beta_1^{(i)}\sum_{m=k+1}^{KN_{SC}}\mathbf{A}_m\tilde{r}_T^{(i)}(m) - \beta_1^{(i)}A_k\psi||_2^2,\end{aligned} \tag{5.26}$$

$\beta_1^{(i)}$ denotes the value of the variable after its i-th iteration, $\mathbf{A} = \mathbf{G}\tilde{\mathbf{W}}_{N_{SC},K}$ and the indices m and k denote the m-th and k-th respectively columns of matrix $\mathbf{A}$. Solving (5.25) requires a simple one dimensional exhaustive search to find which out of the four elements of $\mathcal{X}$ minimizes f and once it is found, $\tilde{r}_T^{(i+1)}(k)$ is updated accordingly. To update the value of the variable β_1, the following

optimization problem is solved

$$\beta_1^{(i+1)} = arg \min_{\beta \in \mathbb{R}^+} ||\tilde{\mathbf{s}} - \beta \mathbf{A}\tilde{\mathbf{r}}_T^{(i+1)}||_2^2 \tag{5.27}$$

and yields the closed form solution

$$\beta_1^{(i+1)} \leftarrow \frac{Re\{\tilde{\mathbf{s}}^H \mathbf{A}\tilde{\mathbf{r}}_T^{(i+1)}\}}{||\mathbf{A}\tilde{\mathbf{r}}_T^{(i+1)}||_2^2} \tag{5.28}$$

where the operator $Re\{\cdot\}$ denotes the real part of a complex part.

The full description of the iterative solution can be seen in Algorithm 6. It is worth noting that the variable $\mathbf{t}$ is introduced to perform efficiently the update of one coordinate at a time of CCD. The algorithm is terminated when the following criteria are met

$$||\tilde{\mathbf{r}}_T^{(i+1)} - \tilde{\mathbf{r}}_T^{(i)}||_2 \leq \epsilon_1 \ \& \ ||\beta_1^{(i+1)}\beta_1^{(i)}|| \leq \epsilon_2 \tag{5.29}$$

The same procedure is followed to derive the solution for problems $(\mathcal{P}_3)$ and $(\mathcal{P}_4)$ after performing the appropriate replacements in equations (5.25)-(5.28). The input vector $\tilde{\mathbf{s}}$ is replaced by $\tilde{\mathbf{r}}_F$, β_1 is replaced by β, $\tilde{\mathbf{r}}_T$ is replaced by $\tilde{\mathbf{x}}_T$ and finally $\mathbf{A}$ is replaced by $\mathbf{A}_1 = \tilde{\mathbf{H}}_F\tilde{\mathbf{W}}_{N_{SC},M}$ for $(\mathcal{P}_3)$ and $\mathbf{A}_2 = \tilde{\mathbf{Q}}\tilde{\mathbf{H}}_F\tilde{\mathbf{W}}_{N_{SC},M}$ for $(\mathcal{P}_4)$, respectively.

So far there has not been a discussion regarding the derivation of the digital post-coding matrix $\mathbf{G}$. For the first proposed architecture, $\mathbf{G}$ is formed by placing in its columns the first RN_{SC} left-singular vectors of $\tilde{\mathbf{H}}_F$ which are derived by computing its singular value decomposition (SVD). For the second architecture, where the receiver also performs analog processing with its network of phase shifters, we use again the first RN_{SC} left-singular vectors but this time of the matrix $\tilde{\mathbf{Q}}\tilde{\mathbf{H}}_F$.

5.3.2 Precoding solution for system based on one-bit DACs/ADCs and a network of analog phase shifters

It is now time to present the solution for the phase shifting matrix $\mathbf{Q}$ that is applied at the receiver in the second proposed system architecture. It is worth noting that $\mathbf{Q}$ depends only on the channel and not on the symbols and therefore there is no need to calculate it on a symbol rate, but only when the channel changes. The problem $(\mathcal{P}_5)$ must be first reformulated appropriately in order to be solved using ADMM [141]. To do this we need to utilize an alternative definition of the nuclear norm [142]

$$\|\tilde{\mathbf{Q}}\|_* = \max_{\substack{\mathbf{D}_i \in \mathbb{C}^{M \times N_s}, \\ \mathbf{D}_i^H \mathbf{D}_i = \mathbf{I}_{N_s}}} \sum_{i=1}^{N_{SC}} Re\{Tr(\mathbf{D}_i^H \mathbf{H}_{Fi}^T \mathbf{F}^T)\}, \tag{5.30}$$

as well as the indicator function of the set $\mathcal{U}$ which is defined as

$$\mathbb{I}_{\mathcal{U}}\{\mathbf{Q}\} = \begin{cases} 0, & \mathbf{Q} \in \mathcal{U} \\ \infty, & \mathbf{Q} \notin \mathcal{U} \end{cases} \tag{5.31}$$

where $\mathcal{U}$ is the set of $N_s \times K$ matrices of unit-modulus entries.

Algorithm 7

Initialize $\mathbf{D}_i^{(0)}, \mathbf{F}^{(0)}, \mathbf{Q}^{(0)}$ with random values and $\mathbf{\Lambda}^{(0)}$ with zeros.
while The termination criteria in (5.37) are not met **do**
  $n \leftarrow n + 1$
  for $1 \leq i \leq N_{SC}$ **do**
    $\mathbf{D}_i^{(n)} \leftarrow \mathbf{U}_i \mathbf{V}_i^H$
  end for
  $F^{(n)} \leftarrow \mathbf{\Lambda}^{(n-1)}/\alpha + \mathbf{Q}^{T(n-1)} + \sum_{i=1}^{N_{SC}} (\mathbf{D}_i^{H\,(n)} \mathbf{H}_{Fi}^T)^H$
  $\mathbf{Q}^{(n)} \leftarrow \Pi_{\mathcal{U}}\{\mathbf{F}^{(n)} - \mathbf{\Lambda}^{(n)}/\alpha\}$
  $\mathbf{\Lambda}^{(n)} \leftarrow \mathbf{\Lambda}^{(n-1)} + \alpha(\mathbf{Q}^{(n)} - \mathbf{F}^{(n)})$
end whilereturn Q

The problem can now be cast in a separable form as

$$\begin{aligned} (\mathcal{P}_6): \quad & \min_{\mathbf{D}_i, \mathbf{Q}} - \sum_{i=1}^{N_{SC}} Re\{Tr(\mathbf{D}_i^H \mathbf{H}_{Fi}^T \mathbf{F}^T)\} + \mathbb{I}_{\mathcal{U}}(\mathbf{Q}) \\ & s.t. \;\; \mathbf{F} = \mathbf{Q} \\ & \quad \mathbf{D}_i^H \mathbf{D}_i = \mathbf{I}_{N_s} \quad \forall i. \end{aligned}$$

Its augmented Lagrangian function is given by

$$\begin{aligned} \mathcal{L}(\mathbf{D}_i, \mathbf{F}, \mathbf{Q}, \mathbf{\Lambda}) = & - \sum_{i=1}^{N_{SC}} Re\{Tr(\mathbf{D}_i^H \mathbf{H}_{Fi}^T \mathbf{F}^T)\} + \\ & + \mathbb{I}_{\mathcal{U}}(\mathbf{Q}) + \frac{\alpha}{2} ||\mathbf{Q} + \frac{\mathbf{\Lambda}}{\alpha} - \mathbf{F}||_F^2, \end{aligned} \tag{5.32}$$

where $\mathbf{\Lambda} \in \mathbb{C}^{K \times N_s}$ is a matrix of Lagrange Multipliers and α is a scalar penalty parameter.

According to the ADMM [141] methodology the augmented Lagrangian function (5.32) is minimized alternatingly with respect to the matrices $\mathbf{D}, \mathbf{F}$ and $\mathbf{Q}$, followed by a steepest ascent step for the update of variable $\mathbf{\Lambda}$

$$
\begin{aligned}
(\mathcal{P}_{6a}) : \mathbf{D}_i^{(n+1)} &= arg \min_{\mathbf{D}_i^H \mathbf{D}_i = \mathbf{I}_{N_s}} \mathcal{L}(\mathbf{D}_i, \mathbf{F}^{(n)}, \mathbf{Q}^{(n)}, \mathbf{\Lambda}^{(n)}) \\
(\mathcal{P}_{6b}) : \mathbf{F}^{(n+1)} &= arg \min_{\mathbf{F}} \mathcal{L}(\mathbf{D}_i^{(n+1)}, \mathbf{F}, \mathbf{Q}^{(n)}, \mathbf{\Lambda}^{(n)}) \\
(\mathcal{P}_{6c}) : \mathbf{Q}^{(n+1)} &= arg \min_{\mathbf{Q}} \mathcal{L}(\mathbf{D}_i^{(n+1)}, \mathbf{F}^{(n+1)}, \mathbf{Q}, \mathbf{\Lambda}^{(n)}) \\
\mathbf{\Lambda}^{(n+1)} &= \mathbf{\Lambda}^{(n)} + \alpha(\mathbf{Q}^{(n+1)} - \mathbf{F}^{(n+1)})
\end{aligned}
$$

where n is the iteration index. Sub-problem $(\mathcal{P}_{6a})$ admits a closed form solution, [142],

$$\mathbf{D}_i^{(n)} = \mathbf{U}_i \mathbf{V}_i^H, \tag{5.33}$$

where $\mathbf{U}_i$ and $\mathbf{V}_i$ are the unitary matrices that are composed by the left-singular and right-singular vectors of $\mathbf{H}_{Fi}^T \mathbf{F}^T$, respectively. The following optimization problem $(\mathcal{P}_{6b})$ also admits a closed form solution to which we arrive by equating the gradient of (5.32) with zero and is given by

$$\mathbf{F}^{(n)} = \frac{\mathbf{\Lambda}}{\alpha} + \mathbf{Q}^T + \sum_{i=1}^{N_{SC}} (\mathbf{D}_i^H \mathbf{H}_{Fi}^T)^H. \tag{5.34}$$

Finally, the sub-problem $\mathcal{P}_{6c}$ can be written as

$$\min_{\mathbf{Q}} \mathbb{I}_{\mathcal{U}}(\mathbf{Q}) + \frac{\alpha}{2} ||\mathbf{Q} + \frac{\mathbf{\Lambda}}{\alpha} - \mathbf{F}||_F^2.$$

The latter problem is essentially the projection of $\mathbf{F} - \mathbf{\Lambda}/\alpha$ on the set $\mathcal{U}$ and its solution is given by,

$$\mathbf{Q}^{(n)} = \Pi_{\mathcal{U}}\{\mathbf{F} - \mathbf{\Lambda}/\alpha\} \tag{5.35}$$

where $\Pi_{\mathcal{U}}$ denotes the projection function onto the set $\mathcal{U}$ which is defined for an arbitrary matrix $\mathbf{M}$ as

$$\Pi_{\mathcal{U}}\{M(i,j)\} = \begin{cases} 0, & M(i,j) = 0 \\ \frac{M(i,j)}{|M(i,j)|}, & M(i,j) \neq 0. \end{cases} \tag{5.36}$$

The algorithm, as was described above, for deriving the phase shifting matrix $\mathbf{Q}$ can be seen in Algorithm 7. The algorithm is terminated when the following criteria are met

$$||\mathbf{Q}^{(n)} - \mathbf{F}^{(n)}||_F^2 \leq \epsilon_3 \;\&\; \alpha ||\mathbf{Q}_n - \mathbf{Q}_{n-1}||_F^2 \leq \epsilon_4. \tag{5.37}$$

Finally, the section will end with the discussion regarding the computational complexity of the proposed algorithms. First, Algorithm 6 has a complexity per iteration of $O(K^2 N_{SC}^2)$ for solving problem $(\mathcal{P}_2)$ and $O(M^2 N_{SC}^2)$ when solving $(\mathcal{P}_3)$ and $(\mathcal{P}_4)$. This leads to a significant reduction in complexity when compared with the computational complexity that an exhaustive search would require for the same problems and would be $O(K N_{SC} 2^{K N_{SC}})$ for $(\mathcal{P}_2)$ and

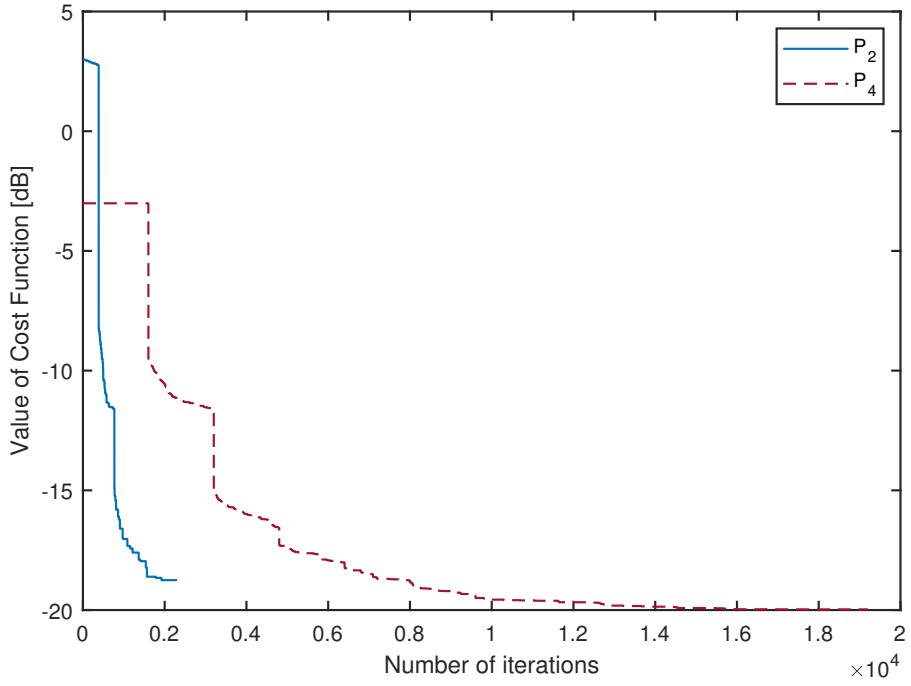

FIGURE 5.3: The average value of the cost functions of the optimization problems $(\mathcal{P}_2)$ and $(\mathcal{P}_4)$ as a function of the number of iterations in a system that employs 16-QAM, $M = 50$ transmit antennas, $K = 50$ receive antennas, $N_s = 12$ ADCs and $N_{SC} = 32$ sub-carriers.

$O(MN_{SC}2^{MN_{SC}})$ for $(\mathcal{P}_3)$ and $(\mathcal{P}_4)$, respectively. Furthermore, the complexity per iteration of Algorithm 7 for computing the phase shifting matrix $\mathbf{Q}$ is dominated by the SVD operation and is $O(MN_sN_{sc})$.

5.4 Numerical Results

In this section, the performance of the proposed solutions is evaluated through extensive numerical simulations. Additionally, the monotonic convergence of the proposed algorithms is confirmed through the numerical results. Furthermore, the performance of the proposed systems is compared to the one of a system using SVD precoding which is known to achieve MIMO channel capacity [143].

For the numerical results a system with $M = 50$ transmit antennas, a channel with $L = 8$ resolvable taps and a cyclic prefix with a length of $CP = 12$ symbols were assumed. The SNR is defined as the average transmit power over the noise variance, $E\{||\tilde{\mathbf{x}}_T||_2^2\}/\sigma_z = P/\sigma_z$, where P is the total transmit power and σ_z the noise variance. The equality above holds because $\tilde{\mathbf{x}}_T \in \mathcal{X}^{MN_{SC}\times 1}$.

Deriving theoretical results for the convergence of the proposed algorithmic solutions is a very challenging task due to the non-convexity of the addressed problems. Thus, any such study could require an independent research work and thus, it is beyond the scopes of this thesis. Though, it is possible to evaluate the convergence of the algorithms via numerical simulations.

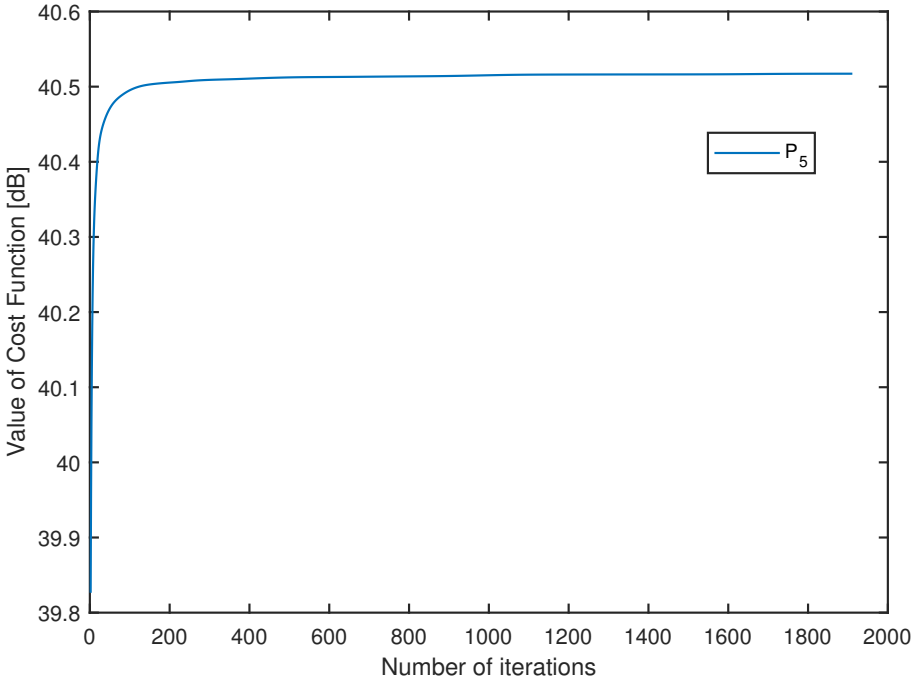

FIGURE 5.4: The average value of the cost function of the optimization problem ($\mathcal{P}_5$) as a function of the number of iterations in a system that employs 16-QAM, $M = 50$ transmit antennas, $K = 50$ receive antennas, $N_s = 12$ ADCs and $N_{SC} = 32$ subcarriers.

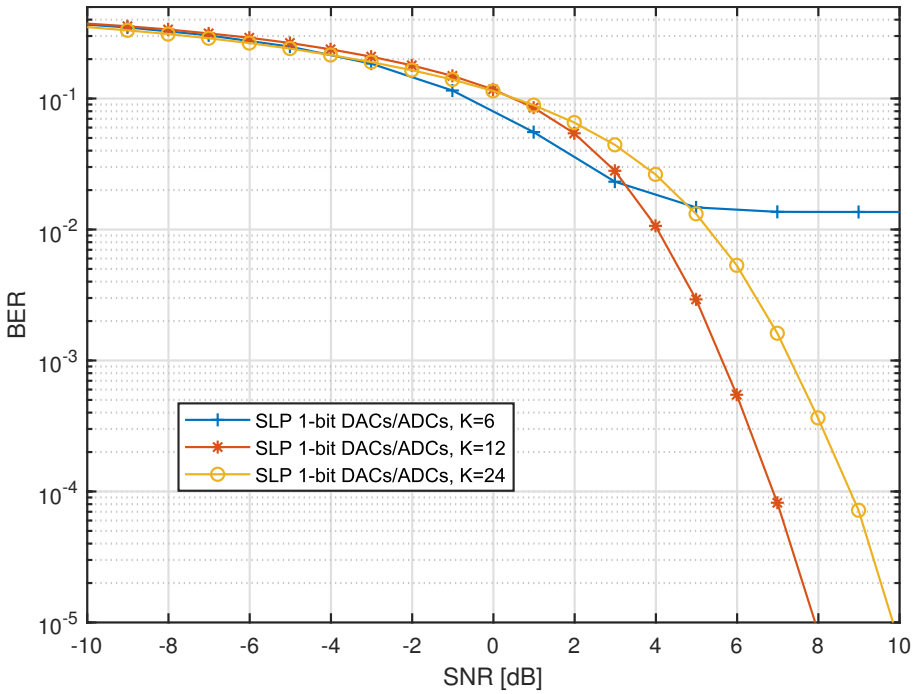

FIGURE 5.5: Impact of the number of receive antennas to the performance of a system employing 16-QAM OFDM with $M = 50$ antennas, $R = 2$ data streams and $N_{SC} = 32$ subcarriers

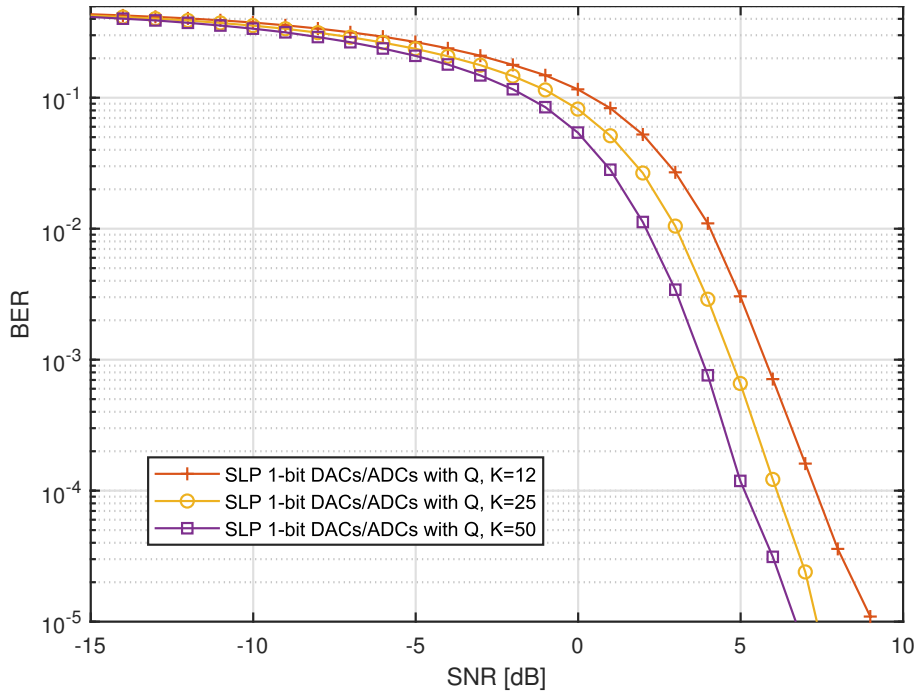

FIGURE 5.6: Impact of the number of receive antennas to the performance of a system equipped with a phase shifting network at the receiver employing 16-QAM OFDM with $M = 50$ antennas, $N_s = 12$ ADCs, $R = 2$ data streams and $N_{SC} = 32$ subcarriers.

First, in Fig. 5.3, it is shown how the cost functions of the optimization problems $(\mathcal{P}_2)$ and $(\mathcal{P}_4)$ are reduced at each iteration. It should be noted that in this figure, an iteration is considered the update of each component of $\tilde{\mathbf{r}}_T$ and $\tilde{\mathbf{x}}_T$. It is observed that in both cases there is monotonic convergence to the minima, which can be intuitively explained by how CCD works. CCD minimizes the cost function over one coordinate at a time and therefore, this guarantees that at each coordinate update the cost function will have less or equal value than before. Additionally, it is observed that while problems $(\mathcal{P}_2)$ and $(\mathcal{P}_4)$ are solved by the same algorithm it takes significant more iterations to converge for the problem $(\mathcal{P}_4)$. This is because of the different size of the optimization variables $\tilde{\mathbf{r}}_T$ and $\tilde{\mathbf{x}}_T$ the first being a $KN_{SC} \times 1$ vector while the second a $MN_{SC} \times 1$ one.

Next, in Fig. 5.4, we can see how the value of the cost function of the maximization problem $(\mathcal{P}_5)$ increases with the number of iterations. Again, it is observed that the convergence is monotonic. For ADMM, convergence results have been derived for convex problems that involve two blocks of variables [144]. However, here the problem that is tackled is strongly non-convex with three blocks of variables and convergence results is also a very difficult task that it is not possible to be addressed in the context of the present work.

In Fig. 5.5, the BER performance of the proposed precoding scheme with one-bit DACs and ADCs is examined for systems with different number of receive antennas. In a MIMO system with high resolution ADCs it would be expected that the increase of receive antennas would increase the received SNR

and therefore the system performance. However, as one can observe in this figure this is not always the case with one- bit ADCs. For a small number of receive antennas, $K = 6$, an error floor appears to the BER curve. This is because there are not enough degrees of freedom to achieve a minimum for $\mathcal{P}_2$ that can guarantee error free communication at high SNRs. As the number of receive antennas increases to $K = 12$, the error floor goes away and the BER performance improves significantly. However, when the number of receive antennas increases again to $K = 24$ the BER performance deteriorates. While a high number of receive antennas provides degrees of freedom to problem $\mathcal{P}_2$, it takes them away from $\mathcal{P}_3$ where the transmitter which is equipped with $M = 50$ antennas and one-bit DACs struggles to find a good minimum for $\mathcal{P}_3$ and this leads to an increased transmit power and to the observed performance degradation.

The results in Fig. 5.5 underline the need for the second proposed system architecture that is shown in Fig. 5.2 where a phase shifting network maps the signal of the K receive antennas to N_s one-bit ADCs. In Fig. 5.6 the impact of the different number of receive antennas is shown for a system which employs $N_s = 12$ one-bit ADCs and a network of KN_s phase shifters. It is observed that as the number of receive antennas almost doubles from 12 to 25 and from 25 to 50 we gain 1 dB and 2 dB in performance respectively. Therefore, we can overcome one of the disadvantages of one-bit ADCs by adding phase shifters at the receiver and using the proposed analog post-coder $\mathbf{Q}$. It is also worth mentioning that the power consumption of phase shifters is significantly smaller than that of the ADCs.

Next, in Fig. 5.7, the effect of the different number of sub-carriers is evaluated for the two proposed system architectures. The employed modulation is 16-QAM and three different scenarios are simulated for $N_{SC} = 16, 32, 64$ sub-carriers. It is observed that for both systems, the performance is almost identical for the different number of sub-carriers. In general real, world systems use OFDM blocks with large number of sub-carriers and therefore, the proposed schemes seem an appropriate solution as the system performance is preserved.

In the following numerical simulation in Fig.5.8 the BER performance of the proposed schemes is compared to that of SVD precoding [143] when 4-QAM and 16-QAM modulation is employed. Additionally, the BER performance of a system which employs one-bit quantized SVD precoding is evaluated where the transmitted and received signals are coarsely quantized by one-bit DACs and ADCs respectively. First, when 4-QAM is employed the gap between SVD precoding that uses full resolution DACs and ADCs and the two proposed one-bit SLP schemes is about 10 dB while when 16-QAM is employed the respective gap reduces to about 3 dB. This shows that the proposed schemes are more appropriate for higher order modulations and in both cases the power consumption savings of one-bit DACs and ADCs over the full resolution DACs and ADCs is so significant that more than makes up for this performance gap. Furthermore, we observe that the performance gap between the two proposed one-bit SLP schemes remains constant at 2 dB for different modulation orders. Finally, the BER curves of quantized SVD show an error floor even when 4-QAM is employed. This highlights the need for appropriate precoding schemes as the ones

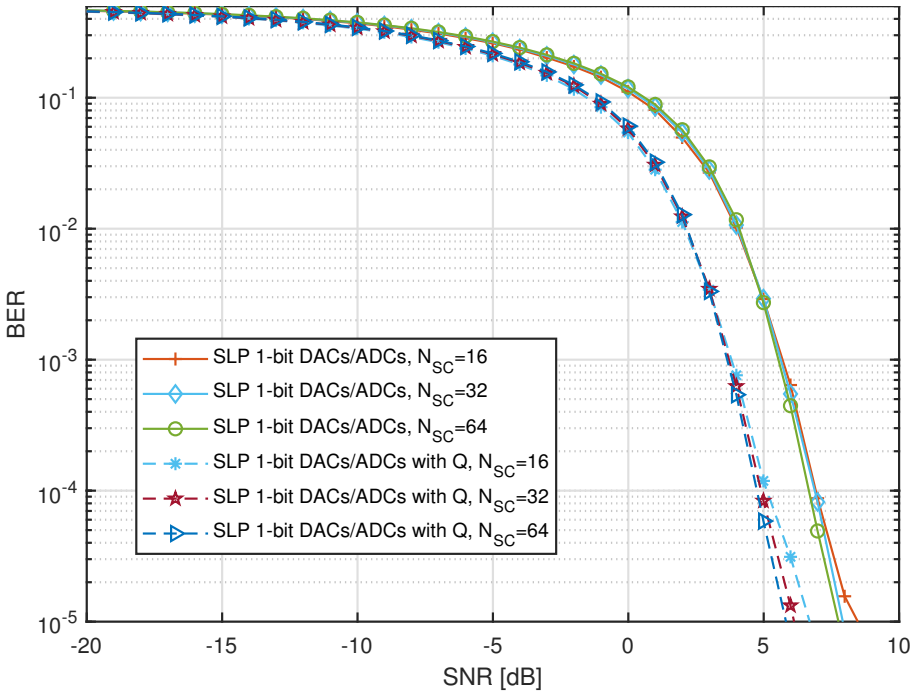

FIGURE 5.7: Impact of the number of OFDM subcarriers to the performance of two systems employing 16-QAM and $M = 50$ antennas and $R = 2$ data streams. The system that is equipped with the network of phase shifters employs $K = 50$ antennas and $N_s = 12$ ADCs while the other one employs $K = 12$ antennas.

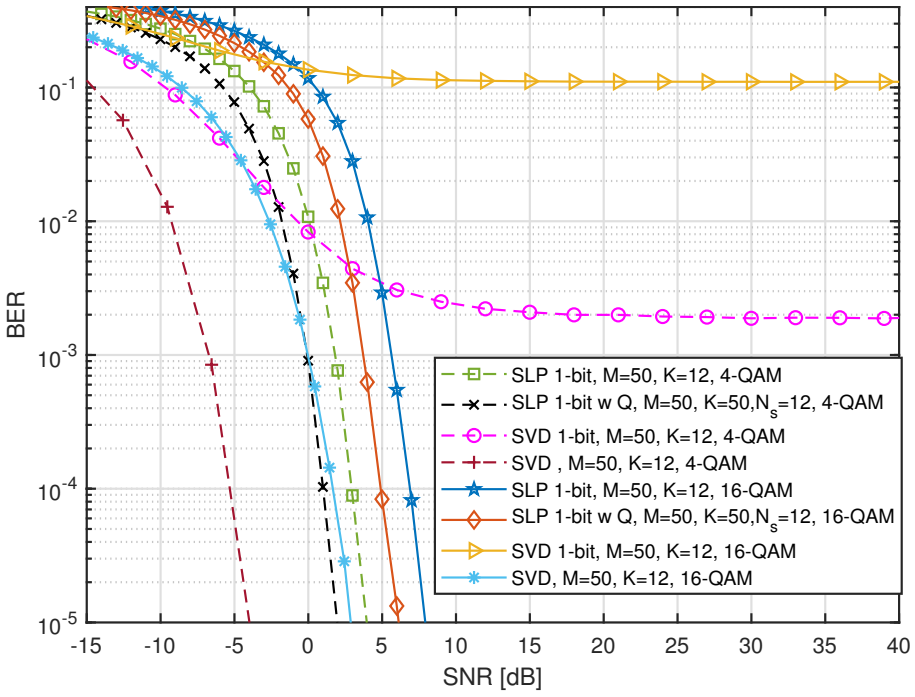

FIGURE 5.8: Comparison of the BER performance of the proposed SLP schemes with SVD precoding for an OFDM system with $N_{SC} = 32$ sub-carriers and $R = 2$ data streams.

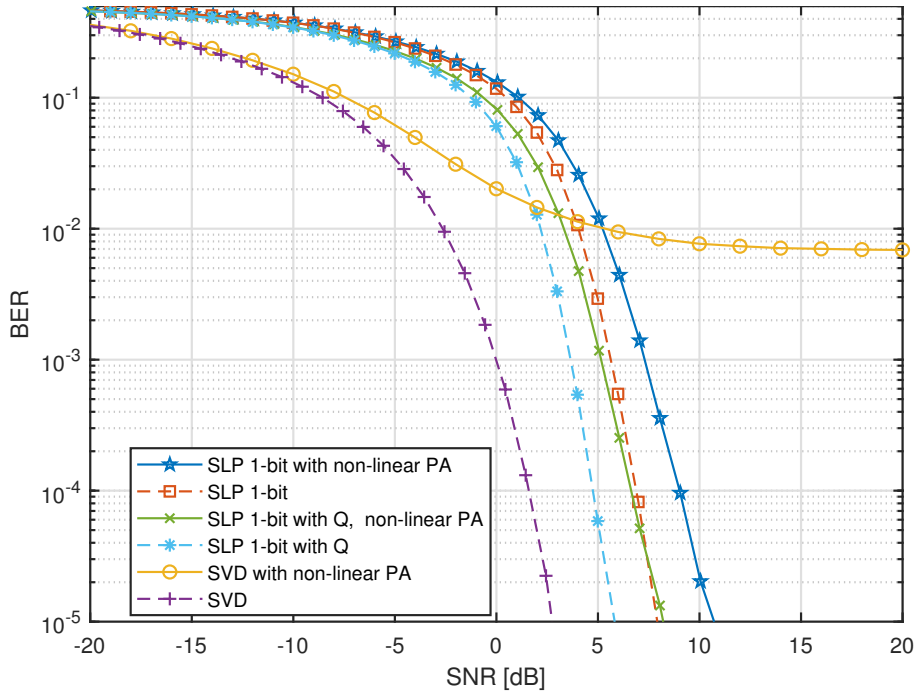

FIGURE 5.9: Comparison of the BER performance of the proposed SLP schemes with SVD precoding for an OFDM system with $N_{SC} = 32$ sub-carriers and $R = 2$ data streams when the transmitter employs PAs wich are modelled according to (5.18)-(5.19).

proposed here in large MIMO systems that use one-bit DACs and ADCs.

In Fig. 5.9, the effects of a PA, that is modelled according to (5.18)-(5.19), on the BER performance are evaluated. The gain of the amplifier is set to $\upsilon = 4$ and the input reference amplitude to $A_{max} = 1$. The solid lines are used to plot the BER curves of systems that use the non-linear PAs while the dashed lines correspond to systems that do not take into account the effects of the PAs and have been added for reference. By inspection, it is observed that the introduction of the PAs leads to a constant 2 dB performance degradation of the two one-bit SLP proposed schemes. The BER performance of SVD precoding takes a big hit when the effects of non-linear PAs are considered. This is because the amplitude of the transmitted signal is not constant as in the case of one-bit SLP and this leads to significant amplitude and phase distortion. On the other hand, the advantage of the one-bit SLP schemes is that the amplitude of the transmitted symbols is constant across the time and across the antennas which leads to a uniform distortion of amplitude and phase.

This can be better observed in Fig. 5.10 where the effect of non-linear amplification is shown for one-bit SLP and SVD precoding and then how this affects the received constellation. In scatter-plots (a) and (c) we can see with black the input signals to the PA and with blue the output signals from the PA, while in scatter-plots (b) and (d) the black points correspond to the original constellation points and the blue points are the received symbols for SLP based on one-bit DACs/ADCs and SVD precoding, respectively. The proposed SLP scheme produces signals with constant amplitude across all time instances and

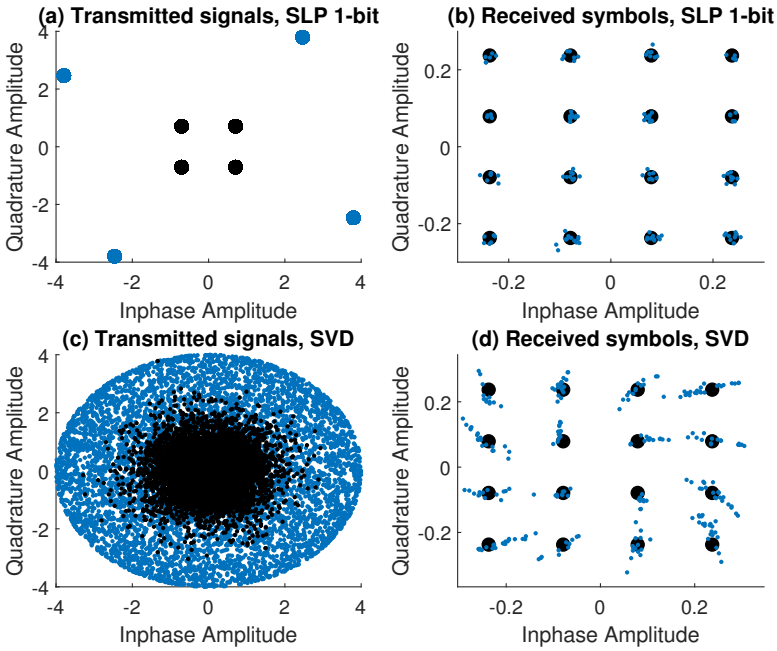

FIGURE 5.10: Scatter-plots of the transmitted and received symbols of the proposed SLP scheme and SVD precoding for an OFDM system with $N_{SC} = 32$ sub-carriers and $R = 2$ data streams when the transmitter employs PAs which are modelled according to (5.18)-(5.19) .

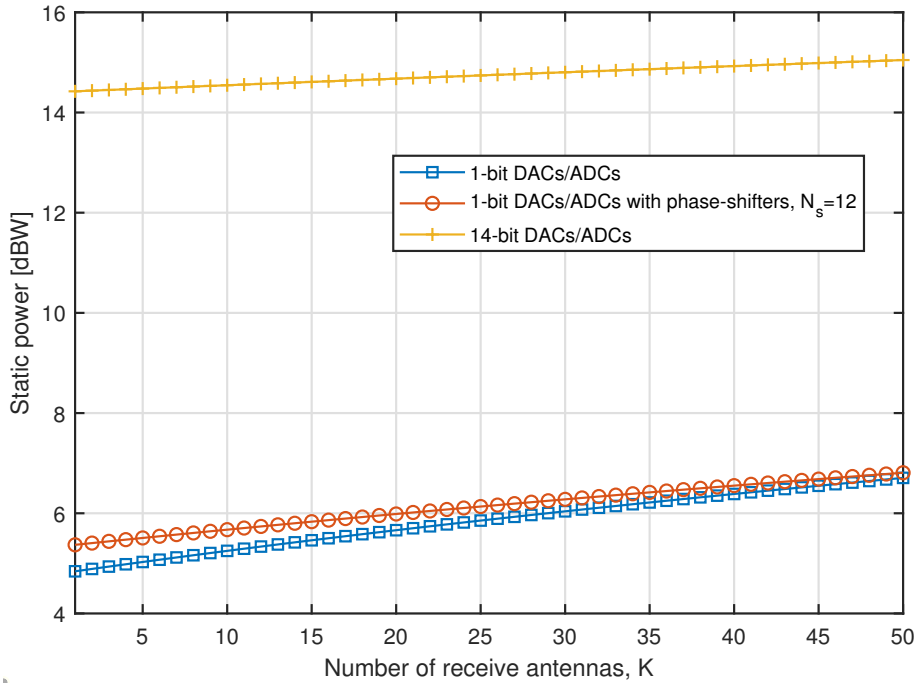

FIGURE 5.11: Static power consumption of the proposed system architectures based on 1-bit DACs/ADCs with $M = 50$ transmit antennas.

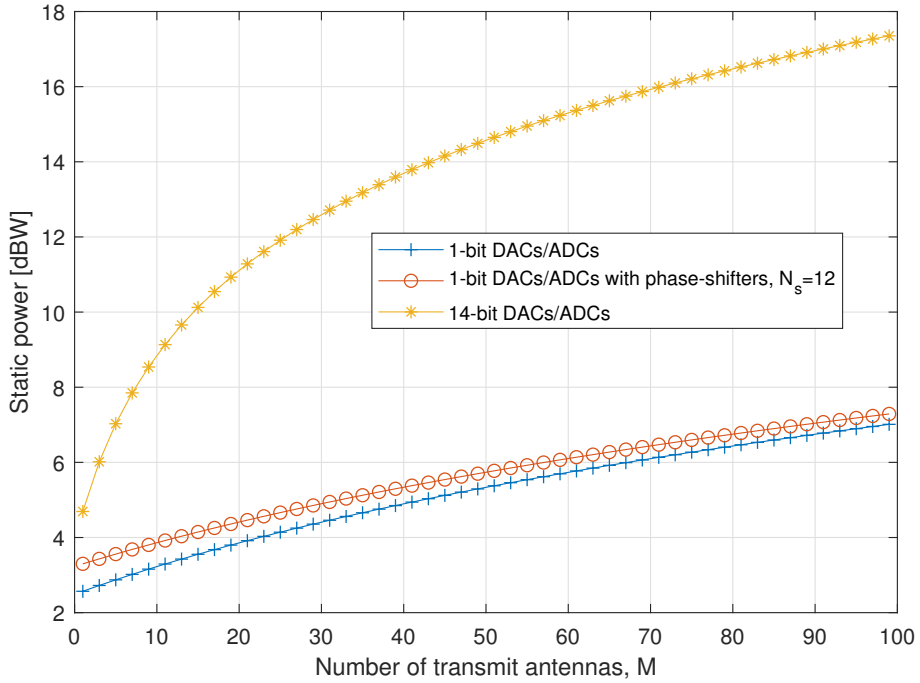

FIGURE 5.12: Static power consumption of the proposed system architectures based on 1-bit DACs/ADCs with $K = 12$ receive antennas.

therefore the non-linear amplification inserts constant amplitude and phase distortion. On the other hand, the SVD based system produces transmit signals with varying amplitude and the non-linear amplification inserts varying phase and amplitude distortions dependent on the amplitude of the input signal to the PA. This explains why the received symbols of the SVD based system are significantly more scattered than the symbols of the proposed one-bit SLP scheme.

Finally, the numerical results are concluded with Figures 5.11 and 5.12 where the static power consumption of the two proposed system architectures is compared with a MIMO system based on 14-bit DACs and ADCs. The power consumption of these systems is calculated by plugging in the parameters of table 5.1 into the equations (5.15)-(5.24). First, in Fig. 5.11 the power consumption of the systems in Figures 5.1 and 5.2 is plotted for a fixed number of transmit antennas in order to observe the effect of the different number of receive antennas to the power consumption. The system with the network of phase shifters consumes about 1 dBW more than the system without it but as the number of receive antennas increases for both systems the gaps becomes even smaller. This is because the number of ADCs remains constant, $N_s = 12$, for the system with the phase shifters. On the other hand the same MIMO system based on 14-bit DACs and ADCs has an increased power consumption of more than 9 dBW when compared to the two proposed systems based on one-bit DACs and ADCs. In Fig. 5.12 the number of receive antennas remains fixed to $K = 12$ and the power consumption is plotted for a different number of transmit antennas. Again we see that the gap between the two proposed systems is less than 0.5 dBW and is due to the increased power consumption of

TABLE 5.1: Parameters for the Static Power Calculation

η	$\pi/4$
P	1
P_{RF}	32.8mW
P_{LO}	50mW
P_{LNA}	20mW
B	$1, 14$
B'	$1, 14$
α	1
V_{dd}	3V
I_0	10μA
C_p	1pF
f_b	10KHz
f_{cor}	1MHz
L_{min}	0.5μm
P_{ps}	2.3mW

the network of phase shifters. On the other hand the gap between the propose systems and the conventional system based on 14-bit DACs and ADCs is about 1 dBW for 1 transmit antenna but widens up to 12 dBW when the number of transmit antennas increases to 100. These results show that the proposed system architectures are very suitable for large-scale MIMO systems as they manage to reduce significantly the static power consumption.

5.5 Summary

In this chapter, an SLP scheme for MIMO-OFDM systems with one-bit DACs and ADCs was considered for the first time in the literature. Two novel transceiver architectures based on one-bit DACs and ADCs were presented and the precoding design for both systems was formulated. The derived design problem was decoupled into two NP-hard optimization problems and algorithmic solutions were developed for both that were based on the CCD algorithmic framework. Additionally, an analog post coding matrix was introduced for the second architecture and its design was formulated as a nuclear norm maximization and was solved by applying the ADMM. The numerical results showed that the proposed architectures lead to a significant decrease in power consumption without sacrificing BER performance when compared to traditional systems that are based on infinite resolution DACs and ADCs.

Chapter 6

Conclusions and Future Works

6.1 Conclusions

In Chapter 2, power efficient transmitters for systems that are equipped with large antenna arrays were considered and novel algorithms for SLP design were developed for the proposed architectures. First, the SLP design problems were formulated by considering the constraints that the proposed architectures imposed and the power consumption of the considered systems was examined. The proposed solutions, based on coordinate descent, were then derived and their computational complexity was also calculated. Extensive simulations were used to show the performance of various configurations of the proposed schemes. Furthermore, a comparison of the proposed solutions with several existing literature solutions such as fully digital DM SLP and AS SLP techniques, hybrid solutions and fully digital ZF was conducted. The AS-SLP, where the transmitter is equipped with a much larger number of transmit antennas than RF chains and the algorithm chooses which antennas will be activated, proved to be very efficient when the number of UTs was equal or even more than the number of active transmit antennas by exploiting the spatial redundancy of the large number of available antennas. On the other hand the proposed RF domain SLP systems, where RF chains are eliminated and replaced by a VGA and analog phase shifters, outperformed other schemes when the number of transmit antennas was much larger than the number of UTs due to the low power consumption of the analog phase shifters. Finally, the addition of a second phase shifter parallel connected to the first provides an interesting trade off, as it results to a small increase in power consumption but also provides and efficient SLP solution since the set of constraints of the optimization problem is now convex.

In Chapter 3, the per antenna CE precoding in a MIMO-OFDM system was addressed. A new system model was introduced that enables the design the time domain CE precoder in the frequency domain in order to avoid using the computationally complex convolution. This was achieved, by reshaping the channel matrix and the DFT matrix and and formulating the precoder design into a least-squares problem with a constant-modulus constraint. Additionally, the factor β was introduced, which changes per OFDM block and is estimated blindly at the UTs where it is used to rescale the received signal. First, the problem was solved by using a CD based algorithm. However, the per iteration complexity of the solution increased rapidly with the number of transmit antennas. For this reason, a more efficient solution was developed that is based on the

GN method. To solve it using GN, the problem was first reformulated into an unconstrained non-linear least-squares problem. The solution proved to be very efficient and achieved improvements both in runtime and minimizing the MUI, when compared to similar solutions in the literature and our proposed CD based algorithm. The SER performance of the two proposed solutions was shown to be identical and outperformed ZF precoding which was used as a benchmark. Furthermore, because of the power consumption gains that were derived from the implementation of the transmitter architecture for CE precoding with efficient non-linear power amplifiers and analog phase shifters rather than DACs, the proposed CE MIMO-OFDM precoding scheme and transmitter architecture was shown to be an excellent candidate for large scale antenna systems.

In Chapter 4, a SLP solution was presented for constant envelope systems with low resolution DACs. The case of a MU-MIMO system employing the OFDM technique over frequency selective channels was considered. The precoding design was formulated as a mixed discrete-continuous constrained least squares problem which is NP hard. An effective algorithmic solution was developed for the solution of the previous problem based on CCD. An approximate power consumption model for the system was calculated in order to quantify the power gains for systems with lower resolution DACs. Simulation results show that the performance in terms of the bit error rate is very close to the one of a system with infinite resolution DACs even if DACs of resolution of few bits are employed. Moreover, due to the significantly reduced power consumption, as compared to the one of systems with infinite resolution DACs, systems based on low resolution DACs are shown to be much more energy efficient than the latter. Furthermore, the proposed approach outperforms the state-of-the-art solutions in terms of the achieved bit error rate and energy efficiency. Thus, with the proposed approach, the CESLP precoder may be efficiently designed for systems based on low resolution DACs without presenting significant losses on the performance and by using transmitters that consume much less power.

Finally, in Chapter 5, two MIMO-OFDM systems with one-bit DACs and ADCs were presented and an appropriate SLP solution was proposed. The precoding design was formulated as a non-linear least squares problem and it order to be tackled efficiently it was split into two NP hard mixed discrete continuous constrained problems. The problems were solved efficiently with an iterative algorithm which is based on the CCD framework. Additionally, the second proposed system architecture required the design of the analog post-coding matrix which was formulated as a nuclear norm maximization problem with a unit-modulus constraint and a an efficient ADMM-based solution was proposed. Furthermore, an approximate power consumption model was derived for the two proposed transceivers. The numerical results showed the necessity of appropriate precoding schemes for one-bit DACs and ADCs transceivers, as the optimal SVD-based precoding for full resolution DACs and ADCs could not guarantee error free communication when quantized to the desired one-bit precision. In addition, the results showed that the proposed one-bit SLP schemes were significantly less affected by the non-linearities of the PAs as the transmitted signals have constant envelope across the time and the transmit antennas.

Thus, the proposed approaches for large MIMO-OFDM systems look very appealing as they lead to significant reduction of power consumption without loosing too much in performance when compared to conventional systems.

6.2 Future Works

The results presented in this thesis have demonstrated the advantages of using the proposed hardware and power efficient systems in combination with the proposed SLP schemes. However, there are topics that have not been addressed within the scope of this thesis. This section discusses some of the topics that are considered of increased significance for future works.

- **Derivation of theoretical results for convergence:** The proposed algorithmic solutions were proven to be very efficient and their convergence was evaluated via numerical simulations. However, deriving theoretical results for the convergence of the proposed algorithmic solutions is a very challenging task due to the non-convexity of the addressed problems and was considered beyond the scopes of the present thesis. Therefore, it would be a significant contribution if theoretical convergence results were derived in a future work.

- **Implementation of proof-of-concept testbeds:** In this thesis, the benefits of hardware and power efficient architectures and the respective SLP schemes were studied. The theoretical results and the numerical simulations showed that the proposed techniques have significant advantages over traditional MIMO systems. However, a proof-of-concept implementation of these systems and the verification of the theoretical results would advocate even further the use of these architectures for next generation wireless communications systems. Testbed implementations could be used to verify that the proposed schemes have lower PAPR and superior error rate performance, when power efficient nonlinear PAs are used, compared to competing precoding techniques.

- **CI SLP for hardware and power efficient transceiver architectures:** In the scope of this thesis the objective of MUI minimization was adopted, because of its simplicity. However, in SLP literature CI objectives have been used to improve the error rate performance of MIMO systems. Therefore, it would be a challenging but significant next step to introduce CI in the proposed transceiver architectures that could result in improved system performance at the cost of computational efficiency.

- **Joint design of SLP with Forward Error Correction (FEC) coding:** The SLP schemes that were presented in this thesis were designed for uncoded transmission. This means that applying an error correction separately from the precoding will not necessarily provide optimal results in the system performance. Therefore, significant performance improvements may be achieved if the error correction code is inserted into the precoding design in a way that the probability of correct decoding is maximized at the receivers' side.

- **Design of continuous-time CE transmit signals:** In the scope of this thesis, only the discrete-time complex baseband model is considered. This means that the proposed precoding methods do not necessarily lead to continuous-time signals with the exact same characteristics. As an example, CE precoding is expected to result in continuous-time transmit signals with a significantly reduced PAPR, when compared to conventional precoding schemes, but not necessarily of perfect CE. To achieve a truly CE transmit signal, constant envelope constraints should be inserted in the design of the continuous-time waveforms. A possible way to achieve this is to enforce this constraints on the oversampled signal. Therefore, the generation of CE continuous-time signals is still an open topic of significant importance.

Bibliography

[1] Lizhong Zheng and D. N. C. Tse, "Diversity and multiplexing: A fundamental tradeoff in multiple-antenna channels", *IEEE Transactions on Information Theory*, vol. 49, no. 5, pp. 1073–1096, 2003.

[2] M. Costa, "Writing on dirty paper (corresp.)", *IEEE Transactions on Information Theory*, vol. 29, no. 3, pp. 439–441, 1983.

[3] M. Joham, W. Utschick, and J. A. Nossek, "Linear transmit processing in mimo communications systems", *IEEE Transactions on signal Processing*, vol. 53, no. 8, pp. 2700–2712, 2005.

[4] T. Haustein, C. Von Helmolt, E Jorswieck, V. Jungnickel, and V. Pohl, "Performance of mimo systems with channel inversion", in *Vehicular Technology Conference. IEEE 55th Vehicular Technology Conference. VTC Spring 2002 (Cat. No. 02CH37367)*, IEEE, vol. 1, 2002, pp. 35–39.

[5] C. B. Peel, B. M. Hochwald, and A. L. Swindlehurst, "A vector-perturbation technique for near-capacity multiantenna multiuser communication-part i: Channel inversion and regularization", *IEEE Transactions on Communications*, vol. 53, no. 1, pp. 195–202, 2005.

[6] L. Sun and M. Lei, "Quantized csi-based tomlinson-harashima precoding in multiuser mimo systems", *IEEE transactions on wireless communications*, vol. 12, no. 3, pp. 1118–1126, 2013.

[7] C. Masouros, M. Sellathurai, and T. Ratnarajah, "Interference optimization for transmit power reduction in tomlinson-harashima precoded mimo downlinks", *IEEE Transactions on Signal Processing*, vol. 60, no. 5, pp. 2470–2481, 2012.

[8] A. Garcia-Rodriguez and C. Masouros, "Power-efficient tomlinson-harashima precoding for the downlink of multi-user miso systems", *IEEE transactions on communications*, vol. 62, no. 6, pp. 1884–1896, 2014.

[9] B. M. Hochwald, C. B. Peel, and A. L. Swindlehurst, "A vector-perturbation technique for near-capacity multiantenna multiuser communication-part ii: Perturbation", *IEEE Transactions on Communications*, vol. 53, no. 3, pp. 537–544, 2005.

[10] A. Li and C. Masouros, "A constellation scaling approach to vector perturbation for adaptive modulation in mu-mimo", *IEEE Wireless Communications Letters*, vol. 4, no. 3, pp. 289–292, 2015.

[11] ——, "A two-stage vector perturbation scheme for adaptive modulation in downlink mu-mimo", *IEEE Transactions on Vehicular Technology*, vol. 65, no. 9, pp. 7785–7791, 2015.

[12] R. de Miguel and R. R. Muller, "On convex vector precoding for multiuser mimo broadcast channels", *IEEE Transactions on Signal Processing*, vol. 57, no. 11, pp. 4497–4508, 2009.

[13] M. Alodeh, D. Spano, A. Kalantari, C. G. Tsinos, D. Christopoulos, S. Chatzinotas, and B. Ottersten, "Symbol-level and multicast precoding for multiuser multiantenna downlink: A state-of-the-art, classification, and challenges", *IEEE Communications Surveys & Tutorials*, vol. 20, no. 3, pp. 1733–1757, 2018.

[14] A. Li, D. Spano, J. Krivochiza, S. Domouchtsidis, C. G. Tsinos, C. Masouros, S. Chatzinotas, Y. Li, B. Vucetic, and B. Ottersten, "A tutorial on interference exploitation via symbol-level precoding: Overview, state-of-the-art and future directions", *IEEE Communications Surveys Tutorials*, vol. 22, no. 2, pp. 796–839, 2020.

[15] M. Bengtsson and B. Ottersten, "Optimal and suboptimal transmit beamforming", 2001.

[16] M. Schubert and H. Boche, "Solution of the multiuser downlink beamforming problem with individual sinr constraints", *IEEE Transactions on Vehicular Technology*, vol. 53, no. 1, pp. 18–28, 2004.

[17] C. Masouros, T. Ratnarajah, M. Sellathurai, C. B. Papadias, and A. K. Shukla, "Known interference in the cellular downlink: A performance limiting factor or a source of green signal power?", *IEEE Communications Magazine*, vol. 51, no. 10, pp. 162–171, 2013.

[18] G. Zheng, I. Krikidis, C. Masouros, S. Timotheou, D.-A. Toumpakaris, and Z. Ding, "Rethinking the role of interference in wireless networks", *IEEE Communications Magazine*, vol. 52, no. 11, pp. 152–158, 2014.

[19] C. Masouros and E. Alsusa, "A novel transmitter-based selective-precoding technique for ds/cdma systems", in *2007 IEEE International Conference on Communications*, IEEE, 2007, pp. 2829–2834.

[20] E. Masouros Christos Alsusa, "Dynamic linear precoding for the exploitation of known interference in mimo broadcast systems", *IEEE Transactions on Wireless Communications*, vol. 8, no. 3, pp. 1396–1404, 2009.

[21] C. Masouros, "Correlation rotation linear precoding for mimo broadcast communications", *IEEE Transactions on Signal Processing*, vol. 59, no. 1, pp. 252–262, 2010.

[22] C. Masouros and G. Zheng, "Power efficient downlink beamforming optimization by exploiting interference", in *2015 IEEE Global Communications Conference (GLOBECOM)*, IEEE, 2015, pp. 1–6.

[23] ——, "Exploiting known interference as green signal power for downlink beamforming optimization", *IEEE Transactions on Signal processing*, vol. 63, no. 14, pp. 3628–3640, 2015.

[24] M. Alodeh, S. Chatzinotas, and B. Ottersten, "Energy efficient symbol-level precoding in multiuser miso channels", in *2015 IEEE 16th International Workshop on Signal Processing Advances in Wireless Communications (SPAWC)*, IEEE, 2015, pp. 36–40.

[25] ——, "Energy-efficient symbol-level precoding in multiuser miso based on relaxed detection region", *IEEE transactions on Wireless Communications*, vol. 15, no. 5, pp. 3755–3767, 2016.

[26] A. Li and C. Masouros, "Interference exploitation precoding made practical: Optimal closed-form solutions for psk modulations", *IEEE Transactions on Wireless Communications*, vol. 17, no. 11, pp. 7661–7676, 2018.

[27] K. L. Law and C. Masouros, "Constructive interference exploitation for downlink beamforming based on noise robustness and outage probability", in *2016 IEEE International Conference on Acoustics, Speech and Signal Processing (ICASSP)*, IEEE, 2016, pp. 3291–3295.

[28] ——, "Symbol error rate minimization precoding for interference exploitation", *IEEE Transactions on Communications*, vol. 66, no. 11, pp. 5718–5731, 2018.

[29] A. Li, C. Masouros, Y. Li, and B. Vucetic, "Multiplexing more streams in the mu-miso downlink by interference exploitation precoding", *arXiv preprint arXiv:1901.03844*, 2019.

[30] A. Li, C. Masouros, Y. Li, B. Vucetic, and A. L. Swindlehurst, "Interference exploitation precoding for multi-level modulations: Closed-form solutions", *arXiv preprint arXiv:1811.03289*, 2018.

[31] Y. Liu and W.-K. Ma, "Symbol-level precoding is symbol-perturbed zf when energy efficiency is sought", in *2018 IEEE International Conference on Acoustics, Speech and Signal Processing (ICASSP)*, IEEE, 2018, pp. 3869–3873.

[32] A. Li, C. Masouros, Y. Li, and B. Vucetic, "Interference exploitation precoding for multi-level modulations", in *ICASSP 2019-2019 IEEE International Conference on Acoustics, Speech and Signal Processing (ICASSP)*, IEEE, 2019, pp. 4679–4683.

[33] A. Li and C. Masouros, "Exploiting constructive mutual coupling in p2p mimo by analog-digital phase alignment", *IEEE Transactions on Wireless Communications*, vol. 16, no. 3, pp. 1948–1962, 2017.

[34] M. Alodeh, S. Chatzinotas, and B. Ottersten, "A multicast approach for constructive interference precoding in miso downlink channel", in *2014 IEEE International Symposium on Information Theory*, IEEE, 2014, pp. 2534–2538.

[35] ——, "Constructive multiuser interference in symbol level precoding for the miso downlink channel", *IEEE Transactions on Signal processing*, vol. 63, no. 9, pp. 2239–2252, 2015.

[36] M. Alodeh, S. Chatzinotas, and B. Ottersten, "Constructive interference through symbol level precoding for multi-level modulation", in *2015 IEEE Global Communications Conference (GLOBECOM)*, IEEE, 2015, pp. 1–6.

[37] M. Alodeh, S. Chatzinotas, and B. Ottersten, "Symbol-level multiuser miso precoding for multi-level adaptive modulation", *IEEE Transactions on Wireless Communications*, vol. 16, no. 8, pp. 5511–5524, 2017.

[38] A. Li and C. Masouros, "Mutual coupling exploitation for point-to-point mimo by constructive interference", in *2017 IEEE International Conference on Communications (ICC)*, IEEE, 2017, pp. 1–6.

[39] A. Kalantari, C. Tsinos, M. Soltanalian, S. Chatzinotas, W.-K. Ma, E. G. Larsson, and B. Ottersten, "m-qam precoder design for mimo directional modulation transceivers", *arXiv preprint arXiv:1702.06878*, 2017.

[40] A. Kalantari, C. Tsinos, M. Soltanalian, S. Chatzinotas, W.-K. Ma, and B. Ottersten, "Spatial peak power minimization for relaxed phase m-psk mimo directional modulation transmitter", in *2017 25th European Signal Processing Conference (EUSIPCO)*, IEEE, 2017, pp. 2011–2015.

[41] ——, "Mimo directional modulation m-qam precoding for transceivers performance enhancement", in *2017 IEEE 18th International Workshop on Signal Processing Advances in Wireless Communications (SPAWC)*, IEEE, 2017, pp. 1–5.

[42] C. Masouros, "Harvesting signal power from constructive interference in multiuser downlinks", in *Wireless Information and Power Transfer: A New Paradigm for Green Communications*, Springer, 2018, pp. 87–122.

[43] B. Wang and K. R. Liu, "Advances in cognitive radio networks: A survey", *IEEE Journal of selected topics in signal processing*, vol. 5, no. 1, pp. 5–23, 2010.

[44] T. Yucek and H. Arslan, "A survey of spectrum sensing algorithms for cognitive radio applications", *IEEE communications surveys & tutorials*, vol. 11, no. 1, pp. 116–130, 2009.

[45] E. Axell, G. Leus, E. G. Larsson, and H. V. Poor, "Spectrum sensing for cognitive radio: State-of-the-art and recent advances", *IEEE Signal processing magazine*, vol. 29, no. 3, pp. 101–116, 2012.

[46] S. K. Sharma, T. E. Bogale, S. Chatzinotas, B. Ottersten, L. B. Le, and X. Wang, "Cognitive radio techniques under practical imperfections: A survey", *IEEE Communications Surveys & Tutorials*, vol. 17, no. 4, pp. 1858–1884, 2015.

[47] I.-W. Lai, L. Zheng, C.-H. Lee, and C. W. Tan, "Beamforming duality and algorithms for weighted sum rate maximization in cognitive radio networks", *IEEE Journal on Selected Areas in Communications*, vol. 33, no. 5, pp. 832–847, 2014.

[48] G. Zheng, S. Ma, K.-K. Wong, and T.-S. Ng, "Robust beamforming in cognitive radio", *IEEE Transactions on Wireless communications*, vol. 9, no. 2, pp. 570–576, 2010.

[49] V.-D. Nguyen, H. V. Nguyen, and O.-S. Shin, "An efficient zero-forcing precoding design for cognitive mimo broadcast channels", *IEEE Communications Letters*, vol. 20, no. 8, pp. 1575–1578, 2016.

[50] R. Zhang and Y.-C. Liang, "Exploiting multi-antennas for opportunistic spectrum sharing in cognitive radio networks", *IEEE Journal of selected topics in signal processing*, vol. 2, no. 1, pp. 88–102, 2008.

[51] Y. Richter and I. Bergel, "Mmse-slnr precoding for multi-antenna cognitive radio", *IEEE transactions on signal processing*, vol. 62, no. 10, pp. 2719–2729, 2014.

[52] I. Krikidis, S. Timotheou, S. Nikolaou, G. Zheng, D. W. K. Ng, and R. Schober, "Simultaneous wireless information and power transfer in modern communication systems", *IEEE Communications Magazine*, vol. 52, no. 11, pp. 104–110, 2014.

[53] T. D. P. Perera, D. N. K. Jayakody, S. K. Sharma, S. Chatzinotas, and J. Li, "Simultaneous wireless information and power transfer (swipt): Recent advances and future challenges", *IEEE Communications Surveys & Tutorials*, vol. 20, no. 1, pp. 264–302, 2017.

[54] X. Zhou, R. Zhang, and C. K. Ho, "Wireless information and power transfer: Architecture design and rate-energy tradeoff", *IEEE Transactions on communications*, vol. 61, no. 11, pp. 4754–4767, 2013.

[55] R. Zhang and C. K. Ho, "Mimo broadcasting for simultaneous wireless information and power transfer", *IEEE Transactions on Wireless Communications*, vol. 12, no. 5, pp. 1989–2001, 2013.

[56] H. Son and B. Clerckx, "Joint beamforming design for multi-user wireless information and power transfer", *IEEE Transactions on Wireless Communications*, vol. 13, no. 11, pp. 6397–6409, 2014.

[57] J. Xu, L. Liu, and R. Zhang, "Multiuser miso beamforming for simultaneous wireless information and power transfer", *IEEE Transactions on Signal Processing*, vol. 62, no. 18, pp. 4798–4810, 2014.

[58] M. R. Khandaker and K.-K. Wong, "Swipt in miso multicasting systems", *IEEE Wireless Communications Letters*, vol. 3, no. 3, pp. 277–280, 2014.

[59] Q. Shi, L. Liu, W. Xu, and R. Zhang, "Joint transmit beamforming and receive power splitting for miso swipt systems", *IEEE Transactions on Wireless Communications*, vol. 13, no. 6, pp. 3269–3280, 2014.

[60] Y. Zou, J. Zhu, X. Wang, and L. Hanzo, "A survey on wireless security: Technical challenges, recent advances, and future trends", *Proceedings of the IEEE*, vol. 104, no. 9, pp. 1727–1765, 2016.

[61] Y.-S. Shiu, S. Y. Chang, H.-C. Wu, S. C.-H. Huang, and H.-H. Chen, "Physical layer security in wireless networks: A tutorial", *IEEE wireless Communications*, vol. 18, no. 2, pp. 66–74, 2011.

[62] A. Mukherjee, S. A. A. Fakoorian, J. Huang, and A. L. Swindlehurst, "Principles of physical layer security in multiuser wireless networks: A survey", *IEEE Communications Surveys & Tutorials*, vol. 16, no. 3, pp. 1550–1573, 2014.

[63] N. Yang, L. Wang, G. Geraci, M. Elkashlan, J. Yuan, and M. Di Renzo, "Safeguarding 5g wireless communication networks using physical layer security", *IEEE Communications Magazine*, vol. 53, no. 4, pp. 20–27, 2015.

[64] A. Wolf and E. A. Jorswieck, "Maximization of worst-case secrecy rates in mimo wiretap channels", in *2010 Conference Record of the Forty Fourth Asilomar Conference on Signals, Systems and Computers*, IEEE, 2010, pp. 290–294.

[65] Q. Li and W.-K. Ma, "Optimal and robust transmit designs for miso channel secrecy by semidefinite programming", *IEEE Transactions on Signal Processing*, vol. 59, no. 8, pp. 3799–3812, 2011.

[66] J. Huang and A. L. Swindlehurst, "Robust secure transmission in miso channels based on worst-case optimization", *IEEE Transactions on Signal Processing*, vol. 60, no. 4, pp. 1696–1707, 2011.

[67] J. E. Mazo, "Faster-than-nyquist signaling", *The Bell System Technical Journal*, vol. 54, no. 8, pp. 1451–1462, 1975.

[68] A. D. Liveris and C. N. Georghiades, "Exploiting faster-than-nyquist signaling", *IEEE Transactions on Communications*, vol. 51, no. 9, pp. 1502–1511, 2003.

[69] A. Modenini, F. Rusek, and G. Colavolpe, "Faster-than-nyquist signaling for next generation communication architectures", in *2014 22nd European Signal Processing Conference (EUSIPCO)*, IEEE, 2014, pp. 1856–1860.

[70] D. Spano, M. Alodeh, S. Chatzinotas, and B. Ottersten, "Faster-than-nyquist signaling through spatio-temporal symbol-level precoding for the multiuser miso downlink channel", *IEEE Transactions on Wireless Communications*, vol. 17, no. 9, pp. 5915–5928, 2018.

[71] M. Alodeh, D. Spano, S. Chatzinotas, and B. Ottersten, "Faster-than-nyquist spatiotemporal symbol-level precoding in the downlink of multiuser miso channels", in *2017 IEEE International Conference on Acoustics, Speech and Signal Processing (ICASSP)*, IEEE, 2017, pp. 3779–3783.

[72] D. Spano, S. Chatzinotas, and B. Ottersten, "Sequential spatia-temporal symbol-level precoding enabling faster-than-nyquist signaling for multiuser miso systems", in *2018 26th European Signal Processing Conference (EUSIPCO)*, IEEE, 2018, pp. 827–831.

[73] S. K. Mohammed and E. G. Larsson, "Single-user beamforming in large-scale MISO systems with per-antenna constant-envelope constraints: The doughnut channel", *IEEE Trans. Wireless Commun.*, vol. 11, no. 11, pp. 3992–4005, 2012, ISSN: 1536-1276. DOI: 10.1109/TWC.2012.090312.111998.

[74] ——, "Per-antenna constant envelope precoding for large multi-user MIMO systems", *IEEE Trans. Commun.*, vol. 61, no. 3, pp. 1059–1071, 2013, ISSN: 0090-6778. DOI: 10.1109/TCOMM.2013.012913.110827.

[75] F. Liu, C. Masouros, P. V. Amadori, and H. Sun, "An efficient manifold algorithm for constructive interference based constant envelope precoding", *IEEE Signal Process. Lett.*, vol. 24, no. 10, pp. 1542–1546, 2017, ISSN: 1070-9908. DOI: 10.1109/LSP.2017.2748230.

[76] S. Domouchtsidis, C. Tsinos, S. Chatzinotas, and B. Ottersten, "Constant envelope massive mimo-ofdm precoding: An improved formulation and solution", in *ICASSP 2020 - 2020 IEEE International Conference on Acoustics, Speech and Signal Processing (ICASSP)*, 2020, pp. 8956–8960.

[77] C. G. Tsinos, A. Arora, and B. Ottersten, "Constant-envelope precoding for satellite systems", in *ICASSP 2020 - 2020 IEEE International Conference on Acoustics, Speech and Signal Processing (ICASSP)*, 2020, pp. 8807–8811.

[78] H. Ochiai, "An analysis of band-limited communication systems from amplifier efficiency and distortion perspective", *IEEE Trans. Commun.*, vol. 61, no. 4, pp. 1460–1472, 2013, ISSN: 0090-6778. DOI: 10.1109/TCOMM.2013.020413.120384.

[79] A. Alkhateeb, O. E. Ayach, G. Leus, and R. W. Heath, "Channel estimation and hybrid precoding for millimeter wave cellular systems", *IEEE J. Sel. Topics Signal Process.*, vol. 8, no. 5, pp. 831–846, 2014, ISSN: 1932-4553. DOI: 10.1109/JSTSP.2014.2334278.

[80] O. E. Ayach, S. Rajagopal, S. Abu-Surra, Z. Pi, and R. W. Heath, "Spatially sparse precoding in millimeter wave MIMO systems", *IEEE Trans. Wireless Commun.*, vol. 13, no. 3, pp. 1499–1513, 2014, ISSN: 1536-1276. DOI: 10.1109/TWC.2014.011714.130846.

[81] T. E. Bogale, L. B. Le, A. Haghighat, and L. Vandendorpe, "On the number of RF chains and phase shifters, and scheduling design with hybrid analog–digital beamforming", *IEEE Trans. Wireless Commun.*, vol. 15, no. 5, pp. 3311–3326, 2016, ISSN: 1536-1276. DOI: 10.1109/TWC.2016.2519883.

[82] C. G. Tsinos, S. Maleki, S. Chatzinotas, and B. Ottersten, "On the energy-efficiency of hybrid analog-digital transceivers for single- and multi-carrier large antenna array systems", *IEEE J. Sel. Areas Commun.*, vol. 35, no. 9, pp. 1980–1995, 2017, ISSN: 0733-8716. DOI: 10.1109/JSAC.2017.2720918.

[83] S. Payami, M. Ghoraishi, and M. Dianati, "Hybrid beamforming for large antenna arrays with phase shifter selection", *IEEE Trans. Wireless Commun.*, vol. 15, no. 11, pp. 7258–7271, 2016, ISSN: 1536-1276. DOI: 10.1109/TWC.2016.2599526.

[84] A. Li and C. Masouros, "Hybrid analog-digital millimeter-wave MU-MIMO transmission with virtual path selection", *IEEE Commun. Lett.*, vol. 21, no. 2, pp. 438–441, 2017, ISSN: 1089-7798. DOI: 10.1109/LCOMM.2016.2621741.

[85] C. G. Tsinos, S. Maleki, S. Chatzinotas, and B. Ottersten, "On the energy-efficiency of hybrid analog-digital transceivers for large antenna array systems", in *IEEE International Conf. Commun. (ICC)*, 2017, pp. 1–7. DOI: 10.1109/ICC.2017.7997328.

[86] ——, "Hybrid analog-digital transceiver designs for cognitive radio millimiter wave systems", in *50th Asilomar Conf. Signals, Systems and Computers*, 2016, pp. 1785–1789. DOI: 10.1109/ACSSC.2016.7869690.

[87] S. Payami, M. Ghoraishi, M. Dianati, and M. Sellathurai, "Hybrid beamforming with a reduced number of phase shifters for massive MIMO systems", *IEEE Trans. Veh. Technol.*, vol. 67, no. 6, pp. 4843–4851, 2018, ISSN: 0018-9545. DOI: 10.1109/TVT.2018.2807921.

[88] C. G. Tsinos, S. Chatzinotas, and B. Ottersten, "Hybrid analog-digital transceiver designs for mmWave amplify-and-forward relaying systems", in *41st Int. Conf. Telecommun. Signal Process. (TSP)*, 2018, pp. 1–6. DOI: 10.1109/TSP.2018.8441203.

[89] ——, "Hybrid analog-digital transceiver designs for multi-user MIMO mmWave cognitive radio systems", *IEEE Trans. Cogn. Commun. Netw.*, pp. 1–1, 2019, ISSN: 2332-7731. DOI: 10.1109/TCCN.2019.2933423.

[90] A. Kaushik, J. Thompson, E. Vlachos, C. Tsinos, and S. Chatzinotas, "Dynamic RF chain selection for energy efficient and low complexity hybrid beamforming in millimeter wave mimo systems", *IEEE Trans. Green Commun. Netw.*, pp. 1–1, 2019, ISSN: 2473-2400. DOI: 10.1109/TGCN.2019.2931613.

[91] A. Arora, C. G. Tsinos, B. S. M. R. Rao, S. Chatzinotas, and B. Ottersten, "Hybrid transceivers design for large-scale antenna arrays using majorization-minimization algorithms", *IEEE Transactions on Signal Processing*, vol. 68, pp. 701–714, 2020.

[92] A. Kaushik, C. Tsinos, E. Vlachos, and J. Thompson, "Energy efficient adc bit allocation and hybrid combining for millimeter wave mimo systems", in *2019 IEEE Global Communications Conference (GLOBECOM)*, 2019, pp. 1–6.

[93] A. Arora, C. G. Tsinos, B. S. Mysore R, and J. Thompson, "Energy efficient adc bit allocation and hybrid combining for millimeter wave mimo systems", in *2019 IEEE Global Communications Conference (GLOBECOM)*, 2019, pp. 1–6.

[94] A. Arora, C. G. Tsinos, B. S. M. R. Rao, S. Chatzinotas, and B. Ottersten, in *International Communications Satellite Systems Conference (ICSSC'19) title= Hybrid Analog-Digital Precoding Design for Satellite Systems , year=2019, volume=, number=, pages=1-5,.*

[95] R. H. Walden, "Analog-to-digital converter survey and analysis", *IEEE J. Sel. Areas Commun.*, vol. 17, no. 4, pp. 539–550, 1999, ISSN: 0733-8716. DOI: 10.1109/49.761034.

[96] J. Mo and R. W. Heath, "Capacity analysis of one-bit quantized MIMO systems with transmitter channel state information", *IEEE Trans. Signal Process.*, vol. 63, no. 20, pp. 5498–5512, 2015, ISSN: 1053-587X. DOI: 10.1109/TSP.2015.2455527.

[97] J. Choi, J. Mo, and R. W. Heath, "Near maximum-likelihood detector and channel estimator for uplink multiuser massive MIMO systems with one-bit ADCs", *IEEE Trans. Commun.*, vol. 64, no. 5, pp. 2005–2018, 2016, ISSN: 0090-6778. DOI: 10.1109/TCOMM.2016.2545666.

[98] J. Guerreiro, R. Dinis, and P. Montezuma, "Use of 1-bit digital-to-analogue converters in massive MIMO systems", *Electron. Lett.*, vol. 52, no. 9, pp. 778–779, 2016, ISSN: 0013-5194. DOI: 10.1049/el.2015.4037.

[99] C. Studer and G. Durisi, "Quantized massive MU-MIMO-OFDM uplink", *IEEE Trans. Commun.*, vol. 64, no. 6, pp. 2387–2399, 2016, ISSN: 0090-6778. DOI: 10.1109/TCOMM.2016.2558151.

[100] A. K. Saxena, I. Fijalkow, and A. L. Swindlehurst, "Analysis of one-bit quantized precoding for the multiuser massive MIMO downlink", *IEEE Trans. Signal Process.*, vol. 65, no. 17, pp. 4624–4634, 2017, ISSN: 1053-587X. DOI: 10.1109/TSP.2017.2715006.

[101] C. Mollén, J. Choi, E. G. Larsson, and R. W. Heath, "Uplink performance of wideband massive MIMO with one-bit ADCs", *IEEE Trans. Wireless Commun.*, vol. 16, no. 1, pp. 87–100, 2017, ISSN: 1536-1276. DOI: 10.1109/TWC.2016.2619343.

[102] J. Zhang, L. Dai, Z. He, B. Ai, and O. A. Dobre, "Mixed-adc/dac multipair massive mimo relaying systems: Performance analysis and power optimization", *IEEE Trans. Commun.*, vol. 67, no. 1, pp. 140–153, 2019. DOI: 10.1109/TCOMM.2018.2869596.

[103] Z. Lu, Y. Zhang, and J. Zhang, "Quantized hybrid precoding design for millimeter-wave large-scale mimo systems", *China Commun.*, vol. 16, no. 4, pp. 130–138, 2019.

[104] J. Zhang, L. Dai, X. Li, Y. Liu, and L. Hanzo, "On low-resolution adcs in practical 5g millimeter-wave massive mimo systems", *IEEE Commun. Mag.*, vol. 56, no. 7, pp. 205–211, 2018. DOI: 10.1109/MCOM.2018.1600731.

[105] S. Jacobsson, G. Durisi, M. Coldrey, T. stein, and C. Studer, "Quantized precoding for massive MU-MIMO", *IEEE Trans. Commun.*, vol. 65, no. 11, pp. 4670–4684, 2017, ISSN: 0090-6778. DOI: 10.1109/TCOMM.2017.2723000.

[106] S. Jacobsson, G. Durisi, M. Coldrey, T. Goldstein, and C. Studer, "Nonlinear 1-bit precoding for massive MU-MIMO with higher-order modulation", in *50th Asilomar Conference on Signals, Systems and Computers*, 2016, pp. 763–767. DOI: 10.1109/ACSSC.2016.7869149.

[107] C. G. Tsinos, A. Kalantari, S. Chatzinotas, and B. Ottersten, "Symbol-level precoding with low resolution DACs for large-scale array MU-MIMO systems", in *19th IEEE Int. Workshop Signal Process. Adv. Wireless Commun. (SPAWC)*, 2018, pp. 1–5. DOI: 10.1109/SPAWC.2018.8445995.

[108] A. Li, C. Masouros, F. Liu, and A. L. Swindlehurst, "Massive MIMO 1-bit DAC transmission: A low-complexity symbol scaling approach", *IEEE Trans. Wireless Commun.*, vol. 17, no. 11, pp. 7559–7575, 2018, ISSN: 1536-1276. DOI: 10.1109/TWC.2018.2868369.

[109] C. G. Tsinos, S. Domouchtsidis, S. Chatzinotas, and B. Ottersten, "Symbol level precoding with low resolution dacs for constant envelope ofdm mu-mimo systems", *IEEE Access*, vol. 8, pp. 12 856–12 866, 2020.

[110] R. H. Walden, "Analog-to-digital converter survey and analysis", *IEEE Journal on Selected Areas in Communications*, vol. 17, no. 4, pp. 539–550, 1999.

[111] S. Jacobsson, G. Durisi, M. Coldrey, U. Gustavsson, and C. Studer, "Throughput analysis of massive mimo uplink with low-resolution adcs", *IEEE Transactions on Wireless Communications*, vol. 16, no. 6, pp. 4038–4051, 2017.

[112] ——, "One-bit massive mimo: Channel estimation and high-order modulations", in *2015 IEEE International Conference on Communication Workshop (ICCW)*, 2015, pp. 1304–1309.

[113] C. Risi, D. Persson, and E. G. Larsson, *Massive mimo with 1-bit adc*, 2014. arXiv: 1404.7736 [cs.IT].

[114] N. Liang and W. Zhang, "Mixed-adc massive mimo", *IEEE Journal on Selected Areas in Communications*, vol. 34, no. 4, pp. 983–997, 2016.

[115] J. Mo and R. W. Heath, "Capacity analysis of one-bit quantized mimo systems with transmitter channel state information", *IEEE Transactions on Signal Processing*, vol. 63, no. 20, pp. 5498–5512, 2015.

[116] J. Choi, J. Mo, and R. W. Heath, "Near maximum-likelihood detector and channel estimator for uplink multiuser massive mimo systems with one-bit adcs", *IEEE Transactions on Communications*, vol. 64, no. 5, pp. 2005–2018, 2016.

[117] C. Mollén, J. Choi, E. G. Larsson, and R. W. Heath, "Uplink performance of wideband massive mimo with one-bit adcs", *IEEE Transactions on Wireless Communications*, vol. 16, no. 1, pp. 87–100, 2017.

[118] T. Baykas, C. S. Sum, Z. Lan, J. Wang, M. A. Rahman, H. Harada, and S. Kato, "IEEE 802.15.3c: The first IEEE wireless standard for data rates over 1 Gb/s", *IEEE Commun. Mag.*, vol. 49, no. 7, pp. 114–121, 2011, ISSN: 0163-6804. DOI: 10.1109/MCOM.2011.5936164.

[119] O. E. Ayach, R. W. Heath, S. Abu-Surra, S. Rajagopal, and Z. Pi, "The capacity optimality of beam steering in large millimeter wave MIMO systems", in *IEEE 13th International Workshop on Signal Process. Advances in Wireless Commun. (SPAWC)*, 2012, pp. 100–104. DOI: 10.1109/SPAWC.2012.6292865.

[120] D. J. Love and R. W. Heath, "Equal gain transmission in multiple-input multiple-output wireless systems", *IEEE Trans. Commun.*, vol. 51, no. 7, pp. 1102–1110, 2003, ISSN: 0090-6778. DOI: 10.1109/TCOMM.2003.814195.

[121] A. Arora, C. G. Tsinos, B. Shankar Mysore R, S. Chatzinotas, and B. Ottersten, "Majorization-minimization algorithms for analog beamforming with large-scale antenna arrays", in *2019 IEEE Global Conference on Signal and Information Processing (GlobalSIP)*, 2019, pp. 1–5.

[122] S. Boyd, S. P. Boyd, and L. Vandenberghe, *Convex optimization*. Cambridge university press, 2004.

[123] C. Mollén, E. G. Larsson, and T. Eriksson, "Waveforms for the massive MIMO downlink: Amplifier efficiency, distortion, and performance", *IEEE Trans. Commun.*, vol. 64, no. 12, pp. 5050–5063, 2016, ISSN: 0090-6778. DOI: 10.1109/TCOMM.2016.2557781.

[124] S. K. Mohammed and E. G. Larsson, "Constant-envelope multi-user precoding for frequency-selective massive MIMO systems", *IEEE Wireless Commun. Lett.*, vol. 2, no. 5, pp. 547–550, 2013, ISSN: 2162-2337. DOI: 10.1109/WCL.2013.071713.130328.

[125] S. Jacobsson, O. Castañeda, C. Jeon, G. Durisi, and C. Studer, "Nonlinear precoding for phase-quantized constant-envelope massive MU-MIMO-OFDM", in *25th Int. Conf.Telecommun. (ICT)*, 2018, pp. 367–372. DOI: 10.1109/ICT.2018.8464896.

[126] J. A. Tropp and A. C. Gilbert, "Signal recovery from random measurements via orthogonal matching pursuit", *IEEE Transactions on information theory*, vol. 53, no. 12, pp. 4655–4666, 2007.

[127] S. Cui, A. J. Goldsmith, and A. Bahai, "Energy-constrained modulation optimization", *IEEE Trans. Wireless Commun.*, vol. 4, no. 5, pp. 2349–2360, 2005, ISSN: 1536-1276. DOI: 10.1109/TWC.2005.853882.

[128] D. P. Bertsekas, "Nonlinear programming", 1999.

[129] S. J. Wright, R. D. Nowak, and M. A. Figueiredo, "Sparse reconstruction by separable approximation", *IEEE Transactions on Signal Processing*, vol. 57, no. 7, pp. 2479–2493, 2009.

[130] R. Hunger, *Floating point operations in matrix-vector calculus*. Munich University of Technology, Inst. for Circuit Theory and Signal ..., 2005.

[131] J.-C. Chen, C.-K. Wen, and K.-K. Wong, "Improved constant envelope multiuser precoding for massive mimo systems", *IEEE Communications Letters*, vol. 18, no. 8, pp. 1311–1314, 2014.

[132] P. V. Amadori and C. Masouros, "Large scale antenna selection and precoding for interference exploitation", *IEEE Transactions on Communications*, vol. 65, no. 10, pp. 4529–4542, 2017.

[133] A. Kalantari, M. Soltanalian, S. Maleki, S. Chatzinotas, and B. Ottersten, "Directional modulation via symbol-level precoding: A way to enhance security", *IEEE J. Sel. Topics Signal Process.*, vol. 10, no. 8, pp. 1478–1493, 2016, ISSN: 1932-4553. DOI: 10.1109/JSTSP.2016.2600521.

[134] S. B. Weinstein, "The history of orthogonal frequency-division multiplexing [history of communications]", *IEEE Communications Magazine*, vol. 47, no. 11, pp. 26–35, 2009.

[135] S. Haykin, *Communication systems*. John Wiley & Sons, 2008.

[136] J.-F. Bao, C. Li, W.-P. Shen, J.-C. Yao, and S.-M. Guu, "Approximate gauss–newton methods for solving underdetermined nonlinear least squares problems", *Applied Numerical Mathematics*, vol. 111, pp. 92–110, 2017.

[137] L. H. Thomas, *The design of CMOS radio-frequency integrated circuits*. Cambridge University Press, 2004.

[138] Y. Nesterov, "Efficiency of coordinate descent methods on huge-scale optimization problems", *SIAM Journal on Optimization*, vol. 22, no. 2, pp. 341–362, 2012.

[139] S. Domouchtsidis, C. G. Tsinos, S. Chatzinotas, and B. Ottersten, "Symbol-level precoding for low complexity transmitter architectures in large-scale antenna array systems", *IEEE Trans. Wireless Commun.*, vol. 18, no. 2, pp. 852–863, 2019, ISSN: 1536-1276. DOI: 10.1109/TWC.2018.2885525.

[140] S. Jacobsson, G. Durisi, M. Coldrey, and C. Studer, "Massive MU-MIMO-OFDM downlink with one-bit DACs and linear precoding", in *IEEE Global Commun. Conf. (GLOBECOM)*, 2017, pp. 1–6. DOI: 10.1109/GLOCOM.2017.8254910.

[141] E. C. B. P. S. Boyd N. Parikh and J. Eckstein, "Distributed optimization and statistical learning via the alternating direction method of multipliers", *Found. Trends Mach. Learn*, vol. 3, no. 1, pp. 1–122, 2011.

[142] N. Tsagkarakis, P. P. Markopoulos, G. Sklivanitis, and D. A. Pados, "L1-norm principal-component analysis of complex data", *IEEE Transactions on Signal Processing*, vol. 66, no. 12, pp. 3256–3267, 2018.

[143] E. Telatar, "Capacity of multi-antenna gaussian channels", *European Transactions on Telecommunications*, vol. 10, no. 6, pp. 585–595, 1999. DOI: 10.1002/ett.4460100604. eprint: https://onlinelibrary.wiley.com/doi/pdf/10.1002/ett.4460100604. [Online]. Available: https://onlinelibrary.wiley.com/doi/abs/10.1002/ett.4460100604.

[144] Z. Wen, C. Yang, X. Liu, and S. Marchesini, "Alternating direction methods for classical and ptychographic phase retrieval", *Inverse Problems*, vol. 28, no. 11, p. 115 010, 2012. DOI: 10.1088/0266-5611/28/11/115010. [Online]. Available: https://doi.org/10.1088%2F0266-5611%2F28%2F11%2F115010.